Quantum Dynamics of a Driven Trapped Atom

Simon James Thwaite

A thesis
submitted in partial fulfilment
of the requirements for the degree
of
Master of Science
at
The University of Auckland

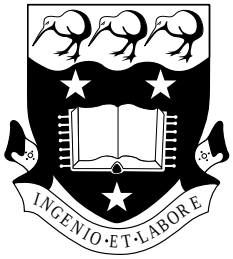

The University of Auckland
2007

Contents

Abstract

We investigate the behaviour of a harmonically trapped atom interacting with a resonant standing-wave laser field in the Lamb-Dicke limit. The laser field is treated classically, the atomic motion quantum mechanically, and the internal state of the atom as a two-level system. Spontaneous emission by the atom is neglected in order to focus on the coherent motional and internal dynamics produced by the atom-field interaction.

We solve the system numerically and characterise the motional dynamics of the atom by constructing the Q and Wigner functions for the atomic centre-of-mass state. The Q function is found to consist of two pieces, each representing a single dressed motional state of the atom. When viewed in a rotating coordinate system, the two pieces move in opposite directions on the phase plane, indicating that the atom-field interaction modifies the atomic centre-of-mass oscillation frequency by an amount that depends on the internal state of the atom. We also investigate the internal dynamics of the atom and find that the atomic excitation probability exhibits collapse and revival behaviour.

We then present an analytic diagonalisation of the system Hamiltonian by means of a Bogoliubov transformation of the trap operators. This allows the derivation of analytic expressions for the operator moments and phase-space distributions considered previously, and for the state-dependent shift of the motional oscillation frequency. It also provides a useful starting point for possible future extensions of the model.

Acknowledgements

First and foremost, I would like to thank my supervisors, Howard Carmichael and Matthew Collett, for their patient guidance, advice, and explanations throughout the course of this research. Thanks are also due to Levente Horvath for his help with aspects of the numerical solutions, and for introducing me to – and sometimes rescuing me from – Linux.

Thanks go to those fellow students and friends with whom I have spent the last two years at the University of Auckland; among others, Glen, Luke, Ian, Kent, and Alan. A special thank you goes to Matthias and Fabienne, for being great friends and colleagues. Thanks also to Chris and the Glenrowan crowd for their friendship over the past year and for providing me with a thesis-free home base for the past few months.

Finally, I would like to express my appreciation for the love and support of my family, especially my parents, without whom I would certainly not be where I am today.

Simon Thwaite
February 22, 2007.

Chapter 1

Overview

There is nothing more evocative of the subject of physics than a stylised depiction of the atom *á la* Bohr, with miniature electrons orbiting like planets around a tightly-packed cluster of spherical protons and neutrons. While the field of physics is of course far richer than this stereotype would imply, it is certainly true that the atom has played a starring role in many of the most important and influential developments in physics of the past century. It was the desire for a more complete theory of the properties of the atom and its interaction with radiation that motivated the development of the pillar of modern physics that is quantum mechanics, and the deep understanding thus obtained that led to the development of nuclear fission and the invention of the laser, achievements of such importance that their influences extend far beyond the scientific realm.

The experimental mastery over matter demonstrated by these accomplishments, however, did not extend to the isolation and manipulation of individual atoms and ions, and some two centuries after they were written, the words of the German physicist Georg Lichtenberg still rang true: "I think that it is a sad situation in all our chemistry that we are unable to suspend constituents of matter free." [48].

The breakthrough in the free suspension of constituents of matter came in the 1950s and '60s, when Wolfgang Paul and Hans Dehmelt independently developed methods of confining electrically charged particles by means of their interaction with the electromagnetic field. Their invention of what are now known as the Paul and Penning traps made possible for the first time the isolation of individual charged particles, and led to Paul and Dehmelt being awarded the 1989 Nobel Prize in Physics.

The impact that ion traps have had on physics since their introduction has been immense. In conjunction with laser cooling [1], the ability to isolate an individual particle from the environment for very long periods of time [31] has led to many achievements in precision measurement [62], precision spectroscopy [19] and the use of optical transitions as frequency standards [38]. Further, the ability to interrogate an individual quantum mechanical entity has allowed the experimental observation of such phenomena as quantum jumps between atomic states [18, 20] and the quantum

Zeno effect [68].

While research into the precision measurement aspects of trapped ions continues, the focus of the field in recent years has turned towards the topic of quantum information processing [28]. The ability to decouple trapped ions from the environment while maintaining a high level of control over their internal dynamics means that a trapped ion qubit can be accurately initialised and manipulated, while the the development of the electron shelving method of internal state detection means that the state readout can be accomplished with effectively unit efficiency. Trapped ions currently stand as one of the most promising architectures for the eventual construction of a quantum computer [29, 59, 67].

The aspect of the field of trapped ions considered in this thesis is the interaction of a single ion with a near-resonant standing-wave laser field. This model is by no means novel, having been previously studied from several different perspectives. It was first investigated in the context of laser cooling, when it was shown that aligning the trapping potential with a node of the standing wave allows the sideband cooling of the trapped ion [27, 71]. The system Hamiltonian has been shown to be equivalent to that of the Jaynes-Cummings model, both when the trap is centred at a node of the standing wave and placed at an arbitrary position [25, 70]. This equivalence leads to collapse and revival behaviour in the atomic inversion of the ion [26]. The system has also been studied in the context of quantum state engineering, and has been shown to provide the possibility of preparing exotic motional states of the trapped ion [40, 73].

Although each of these analyses focuses on a different aspect of the system, the approach common to them all is the alignment of the centre of the trapping potential with a node of the standing wave. In contrast, there has been comparatively little attention paid to the case where the trapped ion is localised about an antinode of the laser field; this latter situation is the focus of this thesis. In a similar approach to much of the work mentioned above, we consider the system in the Lamb-Dicke limit and neglect spontaneous emission by the ion in order to focus on the coherent motional and internal dynamics produced by the ion-field interaction.

There are perhaps two main motivations for an investigation of this nature. The first is a desire for a deeper scientific understanding of a system that is inherently quantum mechanical, and thus exhibits such interesting behaviour as collapses and revivals. An added attraction is the fact that the model we use is experimentally realisable, and so any novel theoretical predictions made in the course of the work could (at least in theory) be tested experimentally.

A second motivating factor is that in the Lamb-Dicke limit and the absence of spontaneous emission, the Hamiltonian is sufficiently simple to allow an analytic investigation of the system. A thorough analytic characterisation of this model and its dynamics would provide a useful knowledge base for future numerical investigation of related models.

1.1 Thesis outline

The work presented in this thesis may be broadly divided into two sections. The first section, comprising Chapter 2, contains the background material required for a complete appreciation of the investigation of the system proper, which begins in Chapter 3.

Chapter 2 presents an overview of the theoretical background associated with each component of the system. This treatment is briefer in parts than it could have been, since the majority of this theory is standard material covered in detail in many quantum mechanics and quantum optics textbooks. References to such books are provided where relevant.

Chapter 3 discusses the details of the system and the approximations inherent in the model used to describe it. The system Hamiltonian is developed and the results of the numerical solution of the system presented and discussed.

In Chapter 4, a Bogoliubov transformation is used to diagonalise the Hamiltonian and analytic expressions for operator moments and phase-space distributions are derived. The physical interpretation of the diagonalisation and its relation to the features seen in the system dynamics are discussed.

Two extensions to the original model are presented in Chapter 5. The Hamiltonian is modified to allow the trapping potential to be moved relative to the standing wave, and the effect on the system dynamics of including higher-order terms in the Lamb-Dicke parameter investigated.

The body of the thesis concludes with Chapter 6, which contains a summary of the results and discusses potential topics for future research.

Chapter 2

Background Theory

This chapter presents a summary of the theory associated with the most important aspects of the system studied in this thesis. We begin with an overview of the most commonly used ion traps and the behaviour of the ions trapped in them. After reviewing the theory of the harmonic oscillator, the interaction of an atom with the electromagnetic field is discussed, and the features of the semiclassical and quantum treatments outlined. The chapter closes with a discussion of quasi-probability distributions, which prove valuable in providing a visual representation of the state of the system.

2.1 Ion traps

The purpose of an ion trap is to confine particles to some small region of space in order that they may be observed and experimented with over a much longer period of time than would otherwise be possible. While the ability to use electric fields means that traps are simpler to realise for particles with a net electric charge, neutral particles may also be trapped (for example, by use of a magneto-optical trap [51]). The neutrality or otherwise of the trapped particle which plays a central role in this thesis is irrelevant to the results obtained, and so in keeping with current interest in the literature, we will restrict our discussion to the most common traps for charged particles.

Faced with the task of confining a charged particle, a natural reaction might be to ask whether it is possible to find an electrode configuration that produces a local minimum of the electric potential Φ at some point. The region centred on this point would act as an ion trap, as suitably charged particles would be attracted to the potential minimum and subjected to a restoring force should they try and escape.

The answer to this query is, unfortunately, in the negative. Earnshaw's theorem [42] states that a static electrode configuration can never create an extremum in the electric potential; all critical points are saddle points.[1] If we are to realise our goal

[1] The proof of this is simple: Laplace's equation states that in a charge-free region, $\nabla^2\Phi = -\nabla \cdot \mathbf{E} = 0$. Applying Gauss' Law, we find that $\int_S \mathbf{E} \cdot d\mathbf{A} = 0$, so there is no point where the

of creating an ion trap by using electromagnetic fields, we must be a little more devious in how we go about it.

Fortunately, we physicists are a wily bunch, and not one, but two methods of overcoming this problem have been devised. The first method, which forms the basis of ion traps developed by the German physicist Wolfgang Paul, sidesteps Earnshaw's theorem by using time-varying electric fields. The second involves supplementing a static electric field by a static magnetic field in such a way that the combination of fields results in a suitable trapping potential.

2.1.1 The quadrupole potential

In designing an ion trap, one of the first things we must do is choose the shape of the confining potential. This is of key importance, as the shape of the potential dictates both the behaviour of the ions in the trap and the electrode configuration required to achieve it. We would ideally like a potential which can be produced by a relatively simple electrode conformation and which gives rise to neat, predictable ion trajectories.

In view of the elegant form and tractable theory of simple harmonic motion, the shape which stands out as the sensible choice for a trapping potential is a quadratic. This is fortunate, for the potential in the neighbourhood of any equilibrium point is, to leading order, quadratic, which means that a harmonic potential is relatively easy to implement: we need simply find an electrode configuration which produces a potential minimum and keep our ions localised about this region. Conversely, it also means that any attempt at creating a higher-order trapping potential – a quartic, for example – relies critically on the precise cancellation of leading-order terms, to the extent that one slight electrode misalignment means that we will simply have discovered an expensive and complicated method of producing a harmonic potential.

For reasons which will become apparent shortly, a harmonic potential is also known as a *quadrupole potential*, and has the general form (see, for example, [33]):

$$\Phi(x, y, z) = \frac{\Phi_0}{2r_0^2}(\alpha x^2 + \beta y^2 + \gamma z^2) \tag{2.1}$$

where Φ_0 is an externally applied potential, α, β, and γ are constants which describe the structure of the field, and r_0 is a constant that depends on the physical system. The Laplace equation $\nabla^2\Phi = 0$ then imposes the requirement that

$$\alpha + \beta + \gamma = 0, \tag{2.2}$$

electric field (and therefore the force) points inwards (or outwards) from all directions. A similar argument shows the impossibility of magnetic levitation using a static configuration of permanent magnets.

which makes it clear that the potential cannot be confining in all three directions.

There are obviously an infinity of coefficient combinations which satisfy the restriction given by Eq. (2.2). However, not all of these result in unique field configurations (linearly dependent combinations describe the same field, up to an overall scale factor) and in any case, the field configurations which will prove most useful to us are the simplest ones. We can thus limit our discussion to the first two combinations of coefficients which satisfy the required restriction.

The two-dimensional quadrupole field

The simplest quadrupolar field configuration corresponds to the case of $\alpha = -\beta = 1$, $\gamma = 0$, and has the form

$$\Phi(x, y) = \frac{\Phi_0}{2r_0^2}(x^2 - y^2). \tag{2.3}$$

This field has a saddle point in the x - y plane located at the origin, and is independent of z. Charged particles will thus be trapped in one of the x- or y- directions, anti-trapped in the other, and free to move along the z-axis.

The suitability of calling it a 'quadrupole' field becomes clear when we note that this simple quadratic field can be produced by four electrodes arranged in a square of side length $\sqrt{2}r_0$. In order to maximise the area over which the potential is quadratic, the electrode surfaces should be cut to match the hyperbolic equipotential lines of Eq. (2.3); however, the shape of the field close to the origin is negligibly affected by the details of the electrode profiles, and electrodes of circular cross-section (or equivalently, point charges) produce essentially the same potential configuration in this region.

The three-dimensional quadrupole field

The next-lowest set of coefficients which satisfy Eq. (2.2) are $\alpha = \beta = 1$, $\gamma = -2$, giving rise to the field

$$\Phi(x, y, z) = \frac{\Phi_0}{2r_0^2}(x^2 + y^2 - 2z^2). \tag{2.4}$$

This potential will trap charged particles in either the x - y plane or the z-direction, and can be produced by the three-electrode configuration illustrated in Fig. 2.1. The ideal electrode shapes are again dictated by the equipotential surfaces of the field; thus the surface of the ring electrode is hyperbolic and each endcap electrode a hyperboloid of revolution about the z-axis. The distances from the electrode surfaces to the origin are related by $r_0^2 = 2z_0^2$, accounting for the factor of 2 appearing in Eq. (2.4).

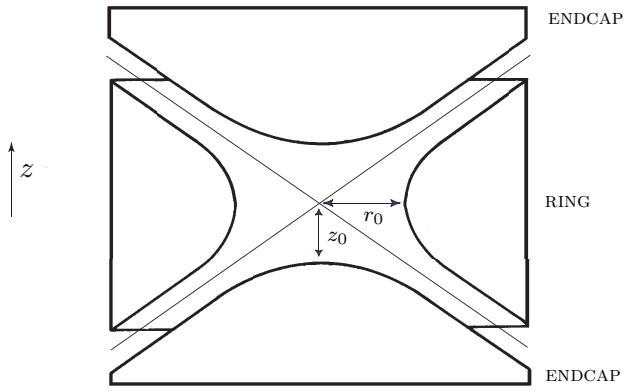

Figure 2.1: A cross-section of the (cylindrically symmetric) electrode configuration required to produce the field given by Eq. (2.4). The diagonal lines represent the asymptotes of the hyperbolic electrode surfaces.

2.1.2 The linear Paul trap

Based on the quadrupole mass filter developed for mass spectroscopy [48], the linear Paul trap uses four rod-shaped electrodes to create a two-dimensional potential of the form described by Eq. (2.3). Though capable (through a suitable choice of Φ_0) of providing radial confinement, this field is constant along the z-axis, and a separate potential is required to prevent particles escaping along the trap axis. This is provided by a pair of endcap electrodes held at a static potential U_0, creating a potential which, near the centre of the trap, is given by

$$\begin{aligned}\Phi_z(x,y,z) &= \kappa U_0 \left[z^2 - \frac{(x^2+y^2)}{2}\right] \\ &= \frac{m}{2q_0}\omega_z^2 \left[z^2 - \frac{(x^2+y^2)}{2}\right]\end{aligned} \tag{2.5}$$

where κ is a geometric factor with units of $[L]^{-2}$ and $\omega_z \equiv \sqrt{2\kappa q_0 U_0/m}$ is the axial oscillation frequency of an ion of mass m and charge q_0.

While axial confinement can be provided by a DC potential, we have already seen that a static potential applied to the rod electrodes cannot trap an ion along the x and y axes simultaneously. The linear Paul trap overcomes this problem by applying to diagonally opposite electrodes the oscillatory potential $\Phi = U_r - V_r \cos\Omega t$, where Ω is typically in the radio-frequency region ($\sim$ MHz). The other two electrodes are

held at ground. The overall potential near the centre of the trap is then given by

$$\Phi = \frac{m\omega_z^2}{2q_0}z^2 - \left[\frac{m\omega_z^2}{4q_0} - \frac{U_r - V_r\cos\Omega t}{2R^2}\right]x^2 - \left[\frac{m\omega_z^2}{4q_0} + \frac{U_r - V_r\cos\Omega t}{2R^2}\right]y^2 \tag{2.6}$$

where R is the distance from the centre of the trap to the surface of an electrode. Although at any one instant this field is only confining in two dimensions, we shall see that the effect of the time dependence is to create a potential which, on average, is harmonically trapping in all three directions.

Ion equations of motion

The equations of motion for a charged particle in the potential given by Eq. (2.6) are simple to obtain. Setting $m\ddot{\mathbf{x}} = -q_0\nabla\Phi$, we find

$$\frac{d^2z}{dt^2} = -\omega_z^2 z \tag{2.7a}$$

$$\frac{d^2x}{dt^2} = \frac{q_0}{m}\left[\kappa U_0 - \frac{U_r - V_r\cos\Omega t}{R^2}\right]x \tag{2.7b}$$

$$\frac{d^2y}{dt^2} = \frac{q_0}{m}\left[\kappa U_0 + \frac{U_r - V_r\cos\Omega t}{R^2}\right]y. \tag{2.7c}$$

The first equation describes harmonic oscillations in the z-direction at frequency ω_z, and needs no further explanation. The motion in the radial directions, however, is more complex, and it is useful to recast the equations in the form

$$\frac{d^2u_j}{d\tau^2} + [a_j - 2q_j\cos 2\tau]\,u_j = 0 \tag{2.8}$$

where $u_j = x$ or y, $\tau = \Omega t/2$, and

$$a_x = -\frac{4q_0}{m\Omega^2}\left[\kappa U_0 - \frac{U_r}{R^2}\right] \qquad q_x = \frac{-2q_0V_r}{m\Omega^2R^2} \tag{2.9a}$$

$$a_y = -\frac{4q_0}{m\Omega^2}\left[\kappa U_0 + \frac{U_r}{R^2}\right] \qquad q_y = \frac{2q_0V_r}{m\Omega^2R^2}. \tag{2.9b}$$

Note that a_j and q_j are both small ($\ll 1$). The advantage of making this change of variables is that the equations of motion now match the canonical form of a *Mathieu equation*, one of a class of differential equations with periodic coefficients [2]. Obtaining solutions for the motion of the ion is now simply an exercise in mathematics.

Floquet's theorem [3] states that the solutions to this type of equation are of the form

$$F_\beta(\tau) = e^{i\beta\tau}P(\tau) \tag{2.10}$$

where β is the characteristic exponent and $P(\tau)$ is a periodic function with the same period as the coefficients in the differential equation. In the case at hand, $P(\tau)$ has period π, and the fact that the Mathieu equation is second-order means that $F_\beta(-\tau)$ is also a valid solution. Thus we can write

$$u_j(\tau) = A_j\, e^{i\beta_j\tau} P(\tau) + B_j\, e^{-i\beta_j\tau} P(-\tau), \tag{2.11}$$

where A_j and B_j are arbitrary coefficients which could be chosen to match prescribed initial conditions.

It is clear from Eq. (2.11) that the characteristic exponent $\beta = \beta(a, q)$ determines the stability of a particular solution. If β is imaginary or complex, one of the terms in the solution grows exponentially, and the ion will be lost from the trap. Solutions which are bounded for all τ (corresponding to stable ion trajectories within the trap) require β to be purely real.

By making a Fourier expansion of $P(\tau)$, we can write a general bounded solution to the Mathieu equation as

$$u_j(\tau) = A_j \sum_{n=-\infty}^{\infty} C_{2n}\, e^{i(\beta_j+2n)\tau} + B_j \sum_{n=-\infty}^{\infty} C_{2n}\, e^{-i(\beta_j+2n)\tau}, \tag{2.12}$$

where the Fourier coefficients C_{2n} are functions of a_j and q_j. By substituting this solution into the Mathieu equation, recursion relations linking these coefficients to the characteristic exponents and the parameters a_j and q_j can be found; a little further manipulation yields continued-fraction expressions for C_{2n} and β_j, from which the solutions may be evaluated to arbitrary accuracy [4].

A first-order approximation to the ion's trajectory can be found by expanding the continued-fraction expressions to first order in a_j and second order in q_j. For the initial condition $A = B$, we find

$$u_j(t) \approx 2A_jC_0 \cos(\omega_j t)\left[1 - \frac{q_j}{2}\cos\Omega t\right] \tag{2.13}$$

where $\omega_j = \beta_j\Omega/2$, with

$$\beta_j \approx \sqrt{a_j + q_j^2/2} \;\ll 1.$$

Since β_j is small, ω_j is much smaller than Ω, and the motion of the ion comprises two distinct pieces. Superimposed on the large-amplitude, low-frequency oscillations described by the first term (known as the *secular motion* of the ion) is a high-frequency oscillation with an amplitude that is a factor of $q_j/2$ smaller. These small, fast oscillations are known as *micromotion*, and have their origin in the Fourier expansion of the periodic function $P(\tau)$. We can see from Eq. (2.12) that expanding the solution to higher orders (i.e. retaining more terms in the Fourier series) will result in the

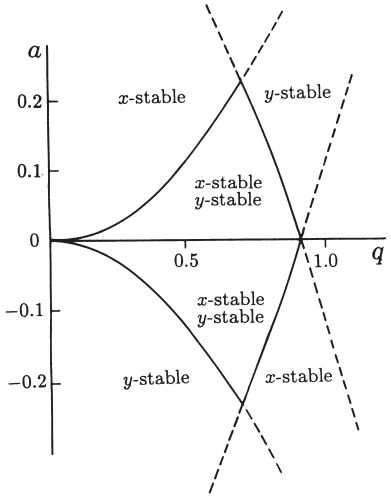

Figure 2.2: The first stability region for the linear Paul trap, taken from Ref. [33].

addition of terms with progressively higher frequencies and smaller amplitudes to the micromotion.

Since q_j is a small parameter, in most cases the micromotion is sufficiently small in comparison with the secular motion that is a reasonable approximation to neglect it altogether. This simplifies the theoretical treatment of the system enormously, for if the micromotion is neglected the ion moves as if subject to the potential

$$q_0\phi = \tfrac{1}{2}m(\omega_x^2 x^2 + \omega_y^2 y^2) \tag{2.14}$$

where the oscillation frequencies $\omega_{x,y}$ are defined above. The net result of applying a time-dependent potential to the trap electrodes is to create a *pseudo*potential which is harmonic in both the x and y directions.

A further comment on stability

As noted earlier, restricting ourselves to stable ion trajectories requires that the characteristic exponent β be real. It turns out that this is a necessary, but not sufficient, condition: not all real values of β correspond to stable solutions. This restricts the range of usable trap parameters to those corresponding to a value of β which gives a stable solution, resulting in the existence of 'stability regions' on the a - q plane. The first of these stability regions is bounded by the curves corresponding to $\beta = 0$ and $\beta = 1$, and is illustrated in Fig. 2.2.

It is exactly this feature exhibited by solutions to the Mathieu equation that makes the quadrupole mass filter so useful in mass spectroscopy. For a given ratio of U_r/V_r, stable trajectories only exist for ions which have a charge-to-mass ratio

that falls within a certain range. Ions whose charge-to-mass ratio lies outside this range have unstable trajectories, and are lost on their journey through the trap. Varying the ratio U_r/V_r allows the q_0/m ratio for which the mass filter selects to be varied, giving a relatively simple method of analysing ions produced from a sample of interest.

2.1.3 The Paul trap

Just as the two-dimensional quadrupole field lies at the heart of the linear Paul trap, the 3-D quadrupole field forms the basis for the Paul, or rf, trap. This consists of two end-cap electrodes and a ring electrode arranged as in Fig. 2.1; as for the linear case, the electrode profiles have a negligible effect on the field near the centre of the trap, and precisely shaped surfaces are not crucial to producing a quadratic field [5].

Holding the ring electrode at ground and applying the potential

$$\Phi_0 = U_r - V_r \cos \Omega t$$

to the end-cap electrodes creates the field

$$\Phi(x, y, z) = \frac{U_r - V_r \cos \Omega t}{2r_0^2}(x^2 + y^2 - 2z^2); \tag{2.15}$$

thus the equations of motion for an ion in a Paul trap are

$$\frac{d^2z}{dt^2} = \frac{2q_0}{m}\frac{U_r - V_r \cos \Omega t}{r_0^2}z \tag{2.16a}$$

$$\frac{d^2r}{dt^2} = -\frac{q_0}{m}\frac{U_r - V_r \cos \Omega t}{r_0^2}r, \tag{2.16b}$$

where $r \in \{x, y\}$. These equations can be put into the general form of the Mathieu equation (Eq. (2.8)) by defining

$$a_z = -2a_r = -\frac{8q_0U_r}{mr_0^2\Omega^2}, \qquad q_z = -2q_r = -\frac{4q_0V_r}{mr_0^2\Omega^2}. \tag{2.17}$$

Solving these equations of motion and neglecting the micromotion terms shows that the ion moves as if subject to the harmonic potential

$$q_0\phi = \tfrac{1}{2}m(\omega_r^2\rho^2 + \omega_z^2z^2) \tag{2.18}$$

where $\rho^2 = x^2 + y^2$, $\omega_j = \beta_j\,\Omega/2$, and $\beta_j^2 = a_j + q_j^2/2$ as previously.

As for the linear trap, the requirement that the ion trajectories be stable restricts the trap parameters to certain regions on the a - q plane. However, due to the factor of two between the r and z parameters, the stability zones of the three-dimensional Paul trap are not symmetric about the b-axis, as illustrated by the first stability zone shown in Fig. 2.3.

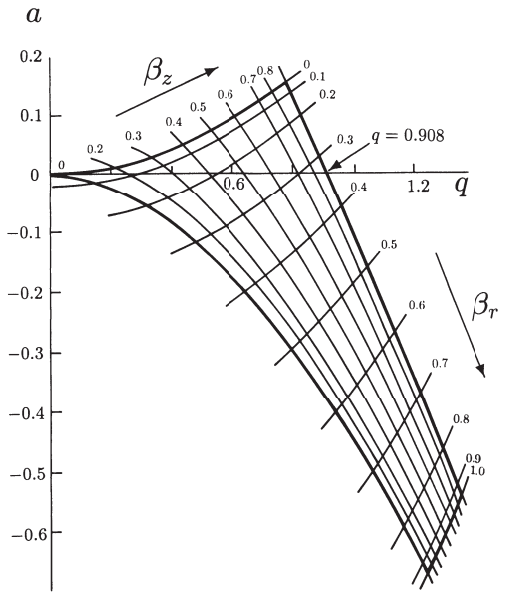

Figure 2.3: The first stability region for the three-dimensional Paul trap, taken from Ref. [33].

2.1.4 The Penning trap

The Penning trap is geometrically identical to the Paul trap, consisting of a pair of end-cap electrodes with hyperboloid surfaces separated by a hyperbolic ring electrode. The difference between the two is in the mode of operation — in place of a radiofrequency field, the Penning trap uses a static potential U_0 and a static *magnetic* field, which is usually applied in the z-direction.

In order to trap positive ions, a negative potential is normally used, giving rise to a field of the form

$$\Phi(x, y, z) = \frac{U_0}{2r_0^2}(2z^2 - x^2 - y^2). \tag{2.19}$$

Ions in this potential will be confined in the z-direction but pulled away from the centre of the trap in the radial direction, quickly hitting the ring electrode. The axial magnetic field prevents the particles from being lost in this way by forcing them into circular orbits in the x - y plane when they stray from the centre of the trap. Once away from the centre of the trap, the ions see a non-zero radially directed electric field, which, in combination with the magnetic field, gives rise to a tangential $\mathbf{E} \times \mathbf{B}$ drift. The overall motion of the ions thus consists of harmonic oscillations in the axial direction and fast orbits superimposed on a slower circular drift in the radial plane. The details of the trajectories may be found in Chapter 3 of Ref. [33].

2.2 The harmonic oscillator

Harmonic oscillations occur in any system whose Hamiltonian contains quadratic dependence on a canonical variable and the momentum conjugate to it. In a mechanical system, this describes the existence of a force which is proportional to, and directed opposite, the displacement of a body from its equilibrium position. In addition to the archetypal mechanical system of a mass connected to a spring, harmonic oscillations are observed in LC circuits, where the canonical coordinate and momentum are, respectively, the charge stored on the capacitor and the current.

The ubiquity of the harmonic oscillator in physics stems from the fact that virtually any potential is quadratic in the neighbourhood of a minimum. Consider the Taylor expansion of an arbitrary potential $V(x)$ about a local minimum at x_0:

$$V(x) \approx V(x_0) + V'(x_0)\,\delta x + \frac{V''(x_0)}{2}(\delta x)^2 + \dots \tag{2.20}$$

where $\delta x \equiv x - x_0$ is the displacement from the equilibrium position. Setting the zero point of potential energy at $V(x_0)$ and neglecting terms in $(\delta x)^3$ and higher gives

$$V(x) \approx \frac{V''(x_0)}{2}(\delta x)^2 \tag{2.21}$$

where we have used the fact that x_0 is a minimum to write $V'(x_0) = 0$. (We also assume that $V''(x_0) > 0$. If not, the critical point is either a maximum, and the system is unstable with respect to small perturbations, or a point of inflection, and the leading term in a Taylor expansion is the cubic.) For small displacements, then, the motion about *any* stable equilibrium point is harmonic! The exact meaning of 'small' will depend on the characteristics of the potential, in particular the second and higher derivatives of $V(x)$.

2.2.1 The classical harmonic oscillator

The Hamiltonian for the classical harmonic oscillator is

$$H = \frac{p^2}{2m} + \frac{m\omega^2 x^2}{2} \tag{2.22}$$

where x and p denote the coordinate and momentum respectively. They may represent physical displacement and momentum (as for a mass on a spring, or a pendulum), or may be canonical variables in the sense of Hamiltonian mechanics. The equations of motion that follow from this Hamiltonian are

$$\dot{x} = \frac{\partial H}{\partial p} = \frac{p}{m} \tag{2.23a}$$

$$\dot{p} = -\frac{\partial H}{\partial x} = -m\omega^2 x \tag{2.23b}$$

which have the familiar solutions

$$x(t) = \alpha \sin \omega t + \beta \cos \omega t \tag{2.24a}$$
$$p(t) = -m\omega(\beta \sin \omega t - \alpha \cos \omega t) \tag{2.24b}$$

where α and β are constants determined by the initial conditions.

2.2.2 The quantum harmonic oscillator

The Hamiltonian can be quantised by promoting x and p to operators

$$x \rightarrow \hat{x}$$
$$p \rightarrow \hat{p}$$

and imposing the canonical commutation relation

$$[\hat{x}, \hat{p}] = i\hbar. \tag{2.25}$$

This puts a limit on how accurately we may simultaneously know the position and momentum:

$$(\Delta\hat{x})^2(\Delta\hat{p})^2 \leq \frac{\hbar^2}{4}, \tag{2.26}$$

where $(\Delta\hat{c})^2 \equiv \langle\hat{c}^2\rangle - \langle\hat{c}\rangle^2$ is the variance of the operator $\hat{c}$.

Motivated by the fact that the Hamiltonian is the sum of two squares, we define the non-Hermitian *ladder operators*

$$\hat{a} \equiv \sqrt{\frac{m\omega}{2\hbar}}\left(\hat{x} + \frac{i\hat{p}}{m\omega}\right) \tag{2.27a}$$
$$\hat{a}^\dagger \equiv \sqrt{\frac{m\omega}{2\hbar}}\left(\hat{x} - \frac{i\hat{p}}{m\omega}\right) \tag{2.27b}$$

which obey the commutation relation

$$[\hat{a}, \hat{a}^\dagger] = 1. \tag{2.28}$$

After substituting for $\hat{x}$ and $\hat{p}$, the Hamiltonian assumes the simple form

$$\hat{H} = \hbar\omega\,(\hat{a}^\dagger\hat{a} + \tfrac{1}{2}). \tag{2.29}$$

2.2.3 Number states

The recasting of the Hamiltonian of the quantised harmonic oscillator into the form of Eq. (2.29) makes the energy eigenstates of the system simple to find. We recognise $\hat{a}^\dagger\hat{a}$ as the number operator, which can be shown to possess eigenstates with integer

eigenvalues; the eigenstates of the Hamiltonian are therefore the *number states* $|n\rangle$, with

$$\hat{a}^\dagger \hat{a}\,|n\rangle = n|n\rangle \tag{2.30a}$$
$$\hat{a}|n\rangle = \sqrt{n}\,|n-1\rangle \tag{2.30b}$$
$$\hat{a}^\dagger|n\rangle = \sqrt{n+1}\,|n+1\rangle. \tag{2.30c}$$

Thus we have

$$\hat{H}|n\rangle = \hbar\omega(n+\tfrac{1}{2})\,|n\rangle; \tag{2.31}$$

the energy spectrum of the quantised harmonic oscillator consists of a ladder of equally-spaced energy levels with energies $\frac{1}{2}\hbar\omega$, $\frac{3}{2}\hbar\omega$, $\frac{5}{2}\hbar\omega, \ldots$, etc. The time evolution of the number states amounts to multiplication by a time-dependent phase, and so the time evolution of an arbitrary state is simplified by choosing to expand it in the basis of number states:

$$\begin{aligned}|\psi(t)\rangle &= e^{-i\hat{H}t/\hbar}|\psi(0)\rangle \\ &= e^{-i\hat{H}t/\hbar}\sum_{n=0}^{\infty} c_n|n\rangle \\ &= \sum_{n=0}^{\infty} c_n\, e^{-i\omega t(n+1/2)}|n\rangle. \end{aligned}\tag{2.32}$$

The expectation values of $\hat{x}$ and $\hat{p}$ in a number state follow from Eqs. (2.30) and (2.27):

$$\langle\hat{x}\rangle_{|n\rangle} = \langle\hat{p}\rangle_{|n\rangle} = 0 \tag{2.33}$$

while their variances can be found to be

$$(\Delta\hat{x})^2 = \frac{\hbar}{m\omega}\big(n+\tfrac{1}{2}\big) \tag{2.34a}$$
$$(\Delta\hat{p})^2 = \hbar m\omega\big(n+\tfrac{1}{2}\big). \tag{2.34b}$$

We see that of the number states, the only minimum-uncertainty state (i.e. the only one which satisfies the equality in Eq. (2.26)) is the ground state $|0\rangle$.

Position-space wavefunctions

The position representation of the harmonic oscillator eigenstates can be deduced by using the equation $\hat{a}|0\rangle = 0$ to write

$$\begin{aligned} &\sqrt{\frac{m\omega}{2\hbar}}\,\langle x|\left(\hat{x}+\frac{i\hat{p}}{m\omega}\right)|0\rangle = 0 \\ \Longrightarrow\qquad &\frac{d}{dx}\langle x|0\rangle + \frac{m\omega x}{\hbar}\,\langle x|0\rangle = 0 \end{aligned}\tag{2.35}$$

where we have used the relationship

$$\langle x|\hat{p}|\psi\rangle = -i\hbar\frac{d}{dx}\langle x|\psi\rangle. \tag{2.36}$$

Equation (2.35) and the requirement that the solution be normalised give the result directly:

$$\langle x|0\rangle = \left(\frac{m\omega}{\pi\hbar}\right)^{\frac{1}{4}} e^{-\frac{m\omega}{2\hbar}x^2}; \tag{2.37}$$

the position representation of the ground state is a Gaussian centred at the origin. The squared modulus of this wavefunction has characteristic width $\sigma = \sqrt{\hbar/2m\omega}$.

The position-space wavefunctions of the higher number states can be found by repeatedly applying the raising operator to the ground state:

$$\begin{aligned}\langle x|n\rangle &= \frac{1}{\sqrt{n!}}\langle x|(\hat{a}^\dagger)^n|0\rangle \\ &= \frac{1}{\sqrt{2^n n!}}\left(\frac{m\omega}{\pi\hbar}\right)^{\frac{1}{4}}\left(\sqrt{\frac{m\omega}{\hbar}}x - \sqrt{\frac{\hbar}{m\omega}}\frac{d}{dx}\right)^n e^{-\frac{m\omega}{2\hbar}x^2}.\end{aligned} \tag{2.38}$$

To evaluate this we invoke a useful operator relation:[2]

$$z - \frac{d}{dz} = -e^{\frac{z^2}{2}}\,\frac{d}{dz}\,e^{-\frac{z^2}{2}} \tag{2.39}$$

which, through a change of variables, gives

$$\left(\sqrt{\frac{m\omega}{\hbar}}x - \sqrt{\frac{\hbar}{m\omega}}\frac{d}{dx}\right)^n = (-1)^n\left(\frac{\hbar}{m\omega}\right)^{\frac{n}{2}} e^{\frac{m\omega}{2\hbar}x^2}\,\frac{d^n}{dx^n}\,e^{-\frac{m\omega}{2\hbar}x^2}. \tag{2.40}$$

This allows us to rewrite Eq. (2.38) as

$$\begin{aligned}\langle x|n\rangle &= \frac{(-1)^n}{\sqrt{2^n n!}}\left(\frac{m\omega}{\pi\hbar}\right)^{\frac{1}{4}}\left(\frac{\hbar}{m\omega}\right)^{\frac{n}{2}} e^{\frac{m\omega}{2\hbar}x^2}\,\frac{d^n}{dx^n}\,e^{-\frac{m\omega}{\hbar}x^2} \\ &= \frac{1}{\sqrt{2^n n!}}\left(\frac{m\omega}{\pi\hbar}\right)^{\frac{1}{4}} e^{-\frac{m\omega}{2\hbar}x^2}\,H_n\left(\sqrt{\frac{m\omega}{\hbar}}x\right)\end{aligned} \tag{2.41}$$

where the Hermite polynomial $H_n(x)$ has been introduced using the definition in Eq. (A.1). The position-space wavefunctions of the number states are the Hermite polynomials multiplied by a Gaussian. The wavefunction of the n^{th} energy eigenstate crosses the x-axis n times, and the symmetry of the Hermite polynomials (see Eq. (A.3)) means that the wavefunctions are alternately even and odd, starting with the even ground state. Figure 2.4 shows the first few wavefunctions.

[2]This can be proved in a few lines of algebra: let each side act on a test function $f(z)$ and show that they give the same result.

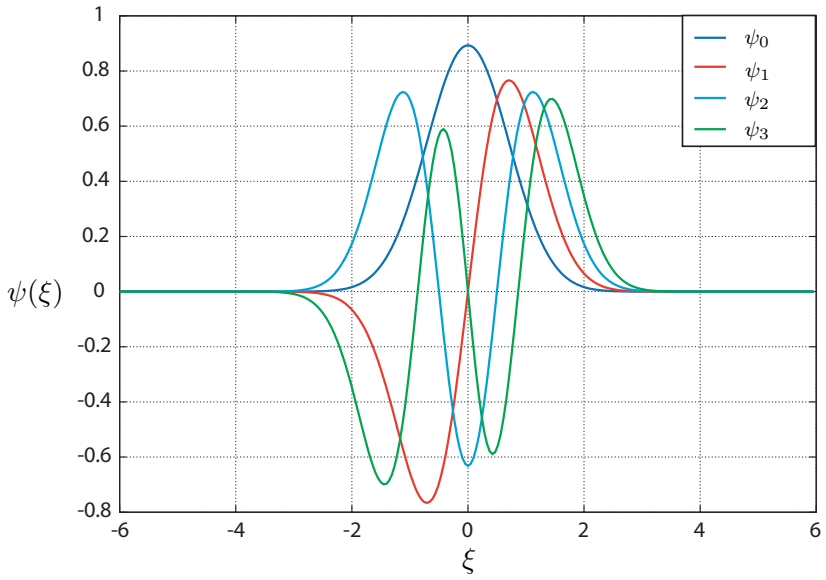

Figure 2.4: The wavefunctions of the first four energy eigenstates of the harmonic oscillator. ξ is a dimensionless position variable defined in Eq. (2.54a).

2.2.4 Coherent states

Although the number states form a very useful basis in which to expand a state, an oscillator in a number state is not a good representation of the classical case of a particle moving to and fro in a harmonic potential. Most notably, the vanishing expectation values of the position and momentum operators do not reproduce the classically expected sinusoidal oscillations in x and p. This is related to the fact that an oscillator in a number state has a well-defined amplitude but completely indeterminate phase, in contrast with our accurate knowledge of both the amplitude and the phase of the classical particle. To the extent permitted by the uncertainty principle, we would like to reproduce this knowledge in our quantised oscillator; this means sacrificing some knowledge about the amplitude in order to gain some information about the phase and motivates the introduction of the *coherent states*. These are the quantum mechanical states which most closely approximate the classical situation, and can be defined as the eigenstates of the annihilation operator:

$$\hat{a}|\alpha\rangle = \alpha|\alpha\rangle \tag{2.42}$$

where the fact that $\hat{a}$ is not Hermitian allows α to be complex. A coherent state has the number state expansion

$$|\alpha\rangle = e^{-\frac{|\alpha|^2}{2}} \sum_{n=0}^{\infty} \frac{\alpha^n}{\sqrt{n!}} |n\rangle. \tag{2.43}$$

The coherent states are complete, but not orthogonal, with

$$\hat{1} = \frac{1}{\pi}\int d^2\alpha\, |\alpha\rangle\langle\alpha| \tag{2.44}$$

$$\langle\beta|\alpha\rangle = e^{-\frac{1}{2}|\beta|^2}\, e^{-\frac{1}{2}|\alpha|^2}\, e^{\beta^*\alpha}. \tag{2.45}$$

This means that not only may a number state be expanded into coherent states, but a coherent state may be expanded into coherent states. The coherent states are therefore said to be overcomplete.

The expectation values of $\hat{x}$ and $\hat{p}$ in a coherent state are

$$\langle\hat{x}\rangle_\alpha = \sqrt{\frac{\hbar}{2m\omega}}\,(\alpha + \alpha^*) \tag{2.46a}$$

$$\langle\hat{p}\rangle_\alpha = -i\sqrt{\frac{\hbar m\omega}{2}}\,(\alpha - \alpha^*) \tag{2.46b}$$

and their variances can be found to be

$$(\Delta\hat{x})^2 = \frac{\hbar}{2m\omega} \tag{2.47a}$$

$$(\Delta\hat{p})^2 = \frac{\hbar m\omega}{2}, \tag{2.47b}$$

independent of α. The product of the variances satisfies the equality in Eq. (2.26), and so all coherent states are minimum-uncertainty states.

The time evolution of an oscillator prepared in a coherent state $|\alpha_0\rangle$ can be found by using the explicit expansion given by Eq. (2.43). Denoting by $|\psi(t)\rangle$ the state at time t, we have

$$\begin{aligned}
|\psi(t)\rangle &= e^{-i\hat{H}t/\hbar}|\alpha_0\rangle \\
&= e^{-\frac{|\alpha|^2}{2}}\, e^{-i\omega t(\hat{a}^\dagger a + \frac{1}{2})} \sum_{n=0}^{\infty} \frac{\alpha_0^n}{\sqrt{n!}}\,|n\rangle \\
&= e^{-\frac{|\alpha|^2}{2}}\, e^{-i\omega t/2} \sum_{n=0}^{\infty} \frac{e^{-in\omega t}\alpha_0^n}{\sqrt{n!}}\,|n\rangle \\
&= e^{-i\omega t/2}|\alpha_0\, e^{-i\omega t}\rangle.
\end{aligned} \tag{2.48}$$

We find that an oscillator prepared in a coherent state evolves to another coherent state of amplitude $\alpha = \alpha_0 e^{-i\omega t}$. The expectation values of the position and

momentum operators in the state $|\psi(t)\rangle$ are (cf. Eqs. (2.24))

$$\begin{aligned} x(t) &= \sqrt{\frac{\hbar}{2m\omega}}(\alpha_0\, e^{-i\omega t} + \alpha_0^*\, e^{i\omega t}) \\ &= |\alpha_0|\sqrt{\frac{2\hbar}{m\omega}}\cos(\omega t - \phi) \end{aligned} \tag{2.49a}$$

$$\begin{aligned} p(t) &= -i\sqrt{\frac{\hbar m\omega}{2}}(\alpha_0\, e^{-i\omega t} - \alpha_0^*\, e^{i\omega t}) \\ &= -|\alpha_0|\sqrt{\frac{2\hbar}{m\omega}}\sin(\omega t - \phi) \end{aligned} \tag{2.49b}$$

where the phase ϕ of the complex amplitude α_0 is set by the initial condition of the oscillator. This demonstrates that coherent states reproduce the expected oscillations in x and p.

2.2.5 Quadrature operators

It is useful to decompose the annihilation operator into its real and imaginary parts. To this end we define the quadrature operators as

$$\hat{X}_1 \equiv \frac{\hat{a} + \hat{a}^\dagger}{2} = \sqrt{\frac{m\omega}{2\hbar}}\,\hat{x} \tag{2.50a}$$

$$\hat{X}_2 \equiv \frac{\hat{a} - \hat{a}^\dagger}{2i} = \frac{1}{\sqrt{2\hbar m\omega}}\,\hat{p}. \tag{2.50b}$$

They obey the commutation relation

$$[\hat{X}_1, \hat{X}_2] = \frac{i}{2} \tag{2.51}$$

which imposes the constraint

$$(\Delta\hat{X}_1)^2(\Delta\hat{X}_2)^2 \leq \frac{1}{16}. \tag{2.52}$$

The usefulness of the quadrature operators relates to the phase-space representation of a quantum state. Instead of using axes defined by $\langle\hat{x}\rangle$ and $\langle\hat{p}\rangle$, it is convenient to use axes defined by $\langle\hat{X}_1\rangle$ and $\langle\hat{X}_2\rangle$, effectively changing to dimensionless position and momentum variables. The advantage of this simple rescaling is the disappearance of the factors of $\hbar$, m and ω that otherwise appear in the definitions of phase-space distributions.

It is also useful to generalise the quadrature operators $\hat{X}_1$ and $\hat{X}_2$ by defining the *rotated* quadrature operators $\hat{Y}_1^\phi$ and $\hat{Y}_2^\phi$:

$$\hat{Y}_1^\phi \equiv \frac{\hat{a}\,e^{-i\phi} + \hat{a}^\dagger e^{i\phi}}{2} \tag{2.53a}$$

$$\hat{Y}_2^\phi \equiv \frac{\hat{a}\,e^{-i\phi} - \hat{a}^\dagger e^{i\phi}}{2i}. \tag{2.53b}$$

The phase-space axes described by $\langle \hat{Y}_1^{\phi} \rangle$ and $\langle \hat{Y}_2^{\phi} \rangle$ are the $\langle \hat{X}_1 \rangle$ and $\langle \hat{X}_2 \rangle$ axes, rotated clockwise through an angle ϕ.

Lastly, we introduce the scaled position and momentum variables

$$\xi \equiv \langle \hat{X}_1 \rangle = \sqrt{\frac{m\omega}{2\hbar}}\, x \tag{2.54a}$$

$$\mu \equiv \langle \hat{X}_2 \rangle = \frac{1}{\sqrt{2\hbar m\omega}}\, p \tag{2.54b}$$

which are defined so that $\alpha = \xi + i\mu$.

2.2.6 The displacement operator

The displacement operator is defined as

$$D(\alpha) \equiv e^{\alpha \hat{a}^\dagger - \alpha^* \hat{a}} \tag{2.55}$$

and can be thought of as an extension to two dimensions of the familiar translation operator $e^{\frac{d}{dx}}$ (or $e^{-i\hat{p}x/\hbar}$). Its usefulness arises from the fact that a coherent state can be created by applying the displacement operator to the ground state, which can be seen explicitly:

$$\begin{aligned} D(\alpha)\,|0\rangle &= e^{\alpha \hat{a}^\dagger - \alpha^* \hat{a}} |0\rangle \\ &= e^{-\frac{1}{2}|\alpha|^2}\, e^{\alpha \hat{a}^\dagger}\, e^{-\alpha^* \hat{a}} |0\rangle \\ &= e^{-\frac{1}{2}|\alpha|^2} \sum_{n=0}^{\infty} \frac{\alpha^n}{\sqrt{n!}}\, |n\rangle \\ &= |\alpha\rangle, \end{aligned} \tag{2.56}$$

where we have used Eq. (2.30) and the coherent state expansion given by Eq. (2.43), and the Baker-Hausdorff relation [6] has been used to put $D(\alpha)$ into the form found on the second line.

The displacement operator is unitary, and its inverse amounts to an equal displacement in the opposite direction:

$$\begin{aligned} D^{-1}(\alpha) &= D^\dagger(\alpha) \\ &= D(-\alpha). \end{aligned} \tag{2.57}$$

The ladder operators are transformed by the displacement operator as

$$D^\dagger(\alpha)\, a\, D(\alpha) = \hat{a} + \alpha \tag{2.58a}$$

$$D^\dagger(\alpha)\, a^\dagger D(\alpha) = \hat{a}^\dagger + \alpha^* \tag{2.58b}$$

while the product of two displacement operators is

$$D(\beta)D(\alpha) = e^{\frac{1}{2}(\beta\alpha^* - \beta^*\alpha)}D(\beta+\alpha). \tag{2.59}$$

The prefactor $\beta\alpha^* - \beta^*\alpha$ is purely imaginary, so forming the coherent state $|\beta+\alpha\rangle$ from the ground state in one fell swoop gives the same result, up to a global phase, as displacing the coherent state $|\alpha\rangle$ by β. The phase may often be neglected, but proves important in situations such as the displacement of a superposition of states.

2.2.7 The squeezing operator

The coherent states are a collection of minimum-uncertainty states where the uncertainty is shared equally between the $\hat{X}_1$ and $\hat{X}_2$ quadratures. While the uncertainty principle sets a lower bound on the product of the quadrature variances, it says nothing about the magnitude of each individual variance. It should, therefore, be possible to create a minimum-uncertainty state with unequal quadrature variances. These are known as *squeezed states* — states in which the uncertainty in one quadrature is decreased at the expense of a greater uncertainty in the other. To describe them, we introduce the squeezing operator

$$S(\varepsilon) \equiv e^{\frac{1}{2}(\varepsilon^*\hat{a}^2 - \varepsilon\hat{a}^{\dagger 2})} \tag{2.60}$$

where ε is the squeezing parameter. The squeezing operator is unitary, and its effect can be reversed in the same way as the displacement operator:

$$\begin{aligned} S^{-1}(\varepsilon) &= S^\dagger(\varepsilon) \\ &= S(-\varepsilon). \end{aligned} \tag{2.61}$$

Action on operators

Any unitary transformation can be viewed as acting on either the operators or the states; these alternative methods applied to, for example, the time evolution operator $U(t)$, give rise to the Heisenberg and Schrödinger pictures. In studying the effects of the squeezing operator, we consider its action on the operators $\hat{a}$ and $\hat{a}^\dagger$.

The squeezing operator transforms the ladder operators as

$$S^\dagger(\varepsilon)\,\hat{a}\,S(\varepsilon) = \hat{a}\cosh|\varepsilon| - \hat{a}^\dagger e^{i\theta}\sinh|\varepsilon| \tag{2.62a}$$

$$S^\dagger(\varepsilon)\,\hat{a}^\dagger S(\varepsilon) = \hat{a}^\dagger\cosh|\varepsilon| - \hat{a}\,e^{-i\theta}\sinh|\varepsilon| \tag{2.62b}$$

where we have written the squeezing parameter as $\varepsilon = |\varepsilon|e^{i\theta}$. The effect of this transformation is most clearly seen if we consider the rotated quadrature operators defined in Eq. (2.53) for an angle $\phi = \theta/2$:

$$\hat{Y}_1^{\theta/2} \equiv \frac{\hat{a}\,e^{-i\theta/2} + \hat{a}^\dagger\,e^{i\theta/2}}{2} \tag{2.63a}$$

$$\hat{Y}_2^{\theta/2} \equiv \frac{\hat{a}\,e^{-i\theta/2} - \hat{a}^\dagger\,e^{i\theta/2}}{2i} \tag{2.63b}$$

which transform as

$$S^\dagger(\varepsilon)\,\hat{Y}_1^{\theta/2}\,S(\varepsilon) = \hat{Y}_1^{\theta/2}\,e^{-|\varepsilon|} \tag{2.64a}$$

$$S^\dagger(\varepsilon)\,\hat{Y}_2^{\theta/2}\,S(\varepsilon) = \hat{Y}_2^{\theta/2}\,e^{|\varepsilon|}. \tag{2.64b}$$

The variances of the transformed operators obey

$$\left[\Delta\big(S^\dagger(\varepsilon)\,\hat{Y}_1^{\theta/2}S(\varepsilon)\big)\right]^2 = \big(\Delta\hat{Y}_1^{\theta/2}\big)^2\,e^{-2|\varepsilon|} \tag{2.65a}$$

$$\left[\Delta\big(S^\dagger(\varepsilon)\,\hat{Y}_2^{\theta/2}S(\varepsilon)\big)\right]^2 = \big(\Delta\hat{Y}_2^{\theta/2}\big)^2\,e^{2|\varepsilon|}; \tag{2.65b}$$

the effect of the squeezing operator is to reduce the variance in one quadrature and increase it in the other, leaving the product unchanged. The size of the decrease is governed by the magnitude of the complex squeezing parameter ε, while the orientation of the quadrature axes along which the reduction in variance occurs is dictated by the phase of ε. If ε is real, the squeezing takes place along the axes of $\hat{X}_1$ and $\hat{X}_2$.

2.3 Interaction of a two-level atom with radiation

So far we have reviewed the main points of the theory of the quantised harmonic oscillator, which provides us with the means to describe the motional state of a particle held in an ion trap. The other aspect of the system which requires the development of some formalism is the description of the atom and its interaction with the incident laser beam; explicitly, we are interested in how this interaction affects the internal atomic state. The sheer size of this topic means that only a brief overview of the most relevant points can be given here; for further details and discussion the reader is referred to the exemplary text of Loudon [43].

2.3.1 The two-level atom

An atom interacting with the electromagnetic field has essentially an infinite number of energy levels between which electrons may make transitions, and so any theoretical treatment that attempts to describe the system in its entirety will be exceedingly complex. However, the only transitions which have an appreciable chance of occurring are those linking levels whose energy difference divided by $\hbar$ is comparable to the frequency of the incident field. This greatly reduces the complexity of the model, for if we assume that the properties of the incident field are such that just one atomic transition is selected for, we can ignore all atomic energy levels except the pair involved in this transition.

This two-level approximation is extremely common when considering the interaction between atoms and radiation, as it simplifies the problem to the point where it becomes analytically tractable. In addition, approximating the atom as a two-level entity makes the system mathematically equivalent to the study of a spin-$\frac{1}{2}$

system interacting with a time-varying magnetic field, a problem which has been extensively studied in the discipline of nuclear magnetic resonance.

The two-level approximation is of more than academic interest, though, as real atoms can be made to behave as essentially perfect two-level systems by the judicious selection of experimental parameters. The precise frequency and narrow bandwidth provided by laser sources allows both the selection of individual atomic transitions and the suppression of transitions to neighbouring states of similar energy. The wealth of recent results in the field of trapped ions demonstrates the impressive control exerted over the internal dynamics of an atom by experimental groups, the recent use of trapped ions as qubits being a prime example of the ability to reduce an atom to just a pair of energy levels.

The Hamiltonian of an atom in the two-level approximation is

$$\hat{H}_A = E_+|+\rangle\langle+| + E_-|-\rangle\langle-| \tag{2.66}$$

where $|\pm\rangle$ denote the ground and excited states, which have energies $E_\pm$. It is convenient to recast this Hamiltonian into a form where the energy difference between the states appears explicitly, which can be accomplished by setting the zero-point of energy midway betwen the levels. The Hamiltonian becomes

$$\hat{H}_A = \frac{\hbar\omega_A}{2}\hat{\sigma}_z \tag{2.67}$$

where $\omega_A \equiv (E_+ - E_-)/\hbar$ is the atomic transition frequency and the atomic energy operator $\hat{\sigma}_z$ is given by

$$\hat{\sigma}_z = |+\rangle\langle+| - |-\rangle\langle-|. \tag{2.68}$$

We have also used the fact that $|-\rangle\langle-| + |+\rangle\langle+| = 1$. The ground and excited atomic states now have energies $-\hbar\omega_A/2$ and $\hbar\omega_A/2$ respectively:

$$\hat{H}_A|\pm\rangle = \pm\frac{\hbar\omega_A}{2}|\pm\rangle. \tag{2.69}$$

In order to describe transitions between the ground and excited states, we introduce the atomic raising and lowering operators

$$\hat{\sigma}_+ \equiv |+\rangle\langle-| \qquad\qquad \hat{\sigma}_- \equiv |-\rangle\langle+|. \tag{2.70}$$

These operators do exactly what their names suggest:

$$\hat{\sigma}_\pm|\mp\rangle = |\pm\rangle \tag{2.71a}$$
$$\hat{\sigma}_\pm|\pm\rangle = 0 \tag{2.71b}$$

where the second line is a result of the orthogonality of the energy eigenstates.

2.3.2 Semiclassical theory

The first method of describing the interaction between an atom and the electromagnetic field involves treating the atom quantum-mechanically and the field classically, and is thus known as the semiclassical theory. It is possible to formally derive a semiclassical interaction Hamiltonian from first principles, using the invariance of the Schrödinger equation under local gauge transformations to obtain the minimal-coupling formulation of the Hamiltonian for an electron in an electromagnetic field [7]. While this is an enlightening treatment, it is more rigorous than is required here, and identical results can be obtained from a simpler, physically motivated derivation.

Consider an atom in the two-level approximation interacting with an incident electromagnetic field of frequency ω_L and wavevector $\mathbf{k}$. The electric field can be written as

$$\mathbf{E}(t) = \frac{1}{2}\left(\alpha\, e^{-i(\omega_L t - \mathbf{k}\cdot\mathbf{r})} + \alpha^* e^{i(\omega_L t - \mathbf{k}\cdot\mathbf{r})}\right)\hat{\mathbf{e}}_0 \tag{2.72}$$

where α is the complex field amplitude, $\hat{\mathbf{e}}_0$ is a unit vector denoting the polarisation direction, and $\mathbf{r}$ is the position at which the electric field is being evaluated; the factor of one-half has simply been included for later convenience. The interaction of the atom with this field is dependent on the distortion of the atomic charge distribution it produces; if the electric field is constant on the length scale of the atom, the electronic distortion is characterised by the dipole distribution. This is a good approximation at optical frequencies, where the wavelengths ($\sim 10^{-5}$ m) are several orders of magnitude larger than the typical dimensions of an atom ($\sim 10^{-10}$ m). We thus make the *dipole approximation*, neglecting the spatial variation of the electric field by evaluating Eq. (2.72) at the position of the atom, denoted by $\mathbf{r}_\mathrm{A}$; the electric field is then given by

$$\mathbf{E}(t) = \frac{1}{2}\left(\alpha\, e^{-i\omega_L t} e^{i\mathbf{k}\cdot\mathbf{r}_\mathrm{A}} + \alpha^* e^{i\omega_L t} e^{-i\mathbf{k}\cdot\mathbf{r}_\mathrm{A}}\right)\hat{\mathbf{e}}_0. \tag{2.73}$$

From classical electrostatics, we know that the interaction energy of an electric dipole of dipole moment $\mathbf{d} = q\mathbf{r}$ in a uniform electric field $\mathbf{E}$ is given by

$$U = -\mathbf{d}\cdot\mathbf{E}.$$

The dipolar interaction Hamiltonian for an atom interacting with the field described by Eq. (2.73) is thus

$$\hat{H}_I = -\frac{1}{2}\left(\alpha\, e^{-i\omega_L t} + \alpha^* e^{i\omega_L t}\right)\hat{\mathbf{e}}_0\cdot\hat{\mathbf{d}} \tag{2.74}$$

where $\hat{\mathbf{d}}$ is the atomic dipole moment operator:

$$\hat{\mathbf{d}} = -e\sum_{i=1}^{Z}\hat{\mathbf{r}}_i. \tag{2.75}$$

Here e is the electronic charge, $\hat{\mathbf{r}}_i$ is the position operator for the i^{th} electron, and the summation covers all the electrons in the atom. We now take advantage of the two-state approximation to rewrite the dipole operator as

$$\begin{aligned}\hat{\mathbf{d}} &= -e\sum_{i=1}^{Z}\sum_{m,n=\pm}|m\rangle\langle m|\hat{\mathbf{r}}_i|n\rangle\langle n| \\ &= \sum_{m,n=\pm}\boldsymbol{\mu}_{mn}|m\rangle\langle n|\end{aligned} \tag{2.76}$$

where we have defined the atomic dipole matrix elements

$$\boldsymbol{\mu}_{mn} \equiv -e\sum_{i=1}^{Z}\langle m|\hat{\mathbf{r}}_i|n\rangle.$$

A further simplification can be made if we note that the energy eigenstates cannot have a permanent dipole moment. This is due to symmetry considerations: the energy eigenstates are of either even or odd parity; no matter which, $|\psi(\mathbf{r})|^2$ is an even function, while the dipole operator is odd. The integrand $|\psi_n(\mathbf{r})|^2\sum_i\hat{\mathbf{r}}_i$ is therefore an odd function and its integral over all space is zero. The diagonal matrix elements of the dipole operator vanish and we have

$$\begin{aligned}\hat{\mathbf{d}} &= \boldsymbol{\mu}_{-+}|-\rangle\langle+| + \boldsymbol{\mu}_{+-}|+\rangle\langle-| \\ &= \boldsymbol{\mu}_{\mp}\,\hat{\sigma}_- + \boldsymbol{\mu}_{\pm}\,\hat{\sigma}_+\end{aligned} \tag{2.77}$$

where the atomic raising and lowering operators have been introduced through Eq. (2.70). Returning to the interaction Hamiltonian, we can finally write

$$H_I = -\frac{1}{2}\left(\alpha\, e^{-i\omega_L t} + \alpha^* e^{i\omega_L t}\right)\left(\mu_{\pm}\,\hat{\sigma}_+ + \mu_{\mp}\,\hat{\sigma}_-\right) \tag{2.78}$$

where $\mu_{mn} = \boldsymbol{\mu}_{mn}\cdot\hat{\mathbf{e}}_0$ and the constant $e^{\pm i\mathbf{k}\cdot\mathbf{r}_{\text{A}}}$ terms have been absorbed into the phase of α.

The Rotating-Wave Approximation

Transforming Eq. (2.78) into the interaction picture with respect to the free atomic Hamiltonian Eq. (2.67) yields

$$\tilde{H}_I = -\frac{|\mu|}{2}\left(\alpha\, e^{-i\omega_L t} + \alpha^* e^{i\omega_L t}\right)\left(\hat{\sigma}_+ e^{i(\omega_A t+\theta)} + \hat{\sigma}_- e^{-i(\omega_A t+\theta)}\right) \tag{2.79}$$

where we have written $\mu_{\pm}(=\mu_{\mp}^*) = |\mu|e^{i\theta}$. Expanding the brackets, we see two frequencies emerge: some terms oscillate at the difference frequency $\omega_L - \omega_A$, while others go as $\omega_L + \omega_A$. These two frequencies are vastly different: the first can be recognised as the detuning – typically $\sim 10^6$ Hz, but with the possibility of being as

small as zero at exact resonance – while the second is the sum of two optical frequencies and is thus $\sim 10^{15}$ Hz. On integration to find the change in a state due to this Hamiltonian these latter terms will be expected to have a much smaller contribution, and we are justified in neglecting them. We therefore make the *rotating-wave approximation* and keep only the terms proportional to $e^{\pm i(\omega_L-\omega_A)t}$, arriving at

$$\tilde{H}_I = -\frac{|\mu|}{2}\big(\alpha\,\hat{\sigma}_+\,e^{-i(\omega_L-\omega_A)t} + \alpha^*\hat{\sigma}_-e^{i(\omega_L-\omega_A)t}\big). \tag{2.80}$$

Absorbing θ, the phase of α, and the overall negative sign into the definitions of $\hat{\sigma}_\pm$, the interaction picture Hamiltonian becomes

$$\tilde{H}_I = \frac{\hbar\Omega}{2}\left(\hat{\sigma}_+e^{-i\delta t} + \hat{\sigma}_-e^{i\delta t}\right) \tag{2.81}$$

where $\delta = \omega_L - \omega_A$ is the detuning of the laser from resonance, and the Rabi frequency has been introduced as $\Omega \equiv |\alpha||\mu|/\hbar$.

Rabi Oscillations

Having presented a plausible, if not entirely rigorous, derivation of the Hamiltonian governing the dominant interaction between a two-level atom and an electromagnetic field, we now turn to the effect of this Hamiltonian on the internal state of the atom. Expanding the atomic state as

$$|\psi(t)\rangle = \tilde{c}_-\,e^{i\omega_A t/2}|-\rangle + \tilde{c}_+\,e^{-i\omega_A t/2}|+\rangle, \tag{2.82}$$

the equations of motion for the slowly-varying expansion coefficients $\tilde{c}_\pm$ are found to be

$$\dot{\tilde{c}}_- = -\frac{i\Omega}{2}\,e^{i\delta t}\,\tilde{c}_+ \tag{2.83a}$$

$$\dot{\tilde{c}}_+ = -\frac{i\Omega}{2}\,e^{-i\delta t}\,\tilde{c}_-. \tag{2.83b}$$

For the initial condition $\tilde{c}_-(0) = 1$, $\tilde{c}_+(0) = 0$ these have solutions

$$\tilde{c}_- = e^{i\delta t/2}\left[\cos\left(\frac{\Omega'}{2}t\right) - i\frac{\delta}{\Omega'}\sin\left(\frac{\Omega'}{2}t\right)\right] \tag{2.84a}$$

$$\tilde{c}_+ = -i\,e^{-i\delta t/2}\,\frac{\Omega}{\Omega'}\,\sin\left(\frac{\Omega'}{2}t\right) \tag{2.84b}$$

where $\Omega' \equiv \sqrt{\Omega^2+\delta^2}$. The probability of finding the atom in its excited state is

$$P_+ = |c_+(t)|^2 = \left(\frac{\Omega}{\Omega'}\right)^2\big[1-\cos(\Omega' t)\big]. \tag{2.85}$$

We see that the atom undergoes coherent oscillations between the ground and excited states. These are known as *Rabi oscillations*, and their amplitude and frequency depend on the magnitude of the detuning δ in comparison with the coupling strength, as measured by Ω. At exact resonance, the probability oscillates between zero and one, while for non-zero detunings the frequency of the oscillations increases and the maximum excitation probability is reduced.

Eigenstates of the interaction — the dressed atomic states

The full Hamiltonian for the interaction of an atom with the electromagnetic field is explicitly time-dependent, and thus has no eigenstates. However, the time dependence can be transformed away by moving to the interaction picture, which means that it *is* possible to find eigenstates of the system in the interaction picture. These eigenstates in the case of exact resonance ($\delta = 0$) will prove useful later, so let us solve for them now.

We can do this by using the equivalence of the algebra of the two-level atom with that of a spin-$\frac{1}{2}$ system to write $\hat{\sigma}_+ + \hat{\sigma}_- \sim \hat{\sigma}_x$. The energy eigenstates of the interacting atom are the eigenstates of the $\hat{\sigma}_x$ operator — which are not the same as the eigenstates of $\hat{\sigma}_z$ (which describes the free atom) because $\hat{\sigma}_x$ and $\hat{\sigma}_z$ do not commute. However, the eigenstates of $\hat{\sigma}_x$ can be written as linear combinations of the eigenstates of $\hat{\sigma}_z$, which motivates the definition of the upper and lower *dressed states* of the atom as

$$|U\rangle \equiv \frac{1}{\sqrt{2}}\big(|+\rangle + |-\rangle\big) \tag{2.86a}$$

$$|L\rangle \equiv \frac{1}{\sqrt{2}}\big(|+\rangle - |-\rangle\big). \tag{2.86b}$$

Rewriting the interaction term shows explicitly that the interaction is diagonal in the dressed state basis:

$$\begin{aligned}\hat{\sigma}_+ + \hat{\sigma}_- &= |+\rangle\langle -| + |-\rangle\langle +| \\ &= |U\rangle\langle U| - |L\rangle\langle L|;\end{aligned} \tag{2.87}$$

the interaction Hamiltonian Eq. (2.81) for $\delta = 0$ can thus be written as

$$\tilde{H}_I = \frac{\hbar\Omega}{2}\big(|U\rangle\langle U| - |L\rangle\langle L|\big). \tag{2.88}$$

2.3.3 Quantum theory

The semiclassical theory outlined above is both simple and successful. The assumption of a classical field is valid in many situations, and provides an understanding of the key elements of the interaction of an atom with the electromagnetic field. However, there are several aspects of the atom-field interaction which can only be understood if the electromagnetic field is treated quantum-mechanically, and so it is in this direction that we now turn.

The quantisation of the electromagnetic field is covered in detail in many textbooks [8]; to reproduce it here would take us too far afield, and so we simply sketch

the main results. The electric and magnetic field operators are expanded as

$$\hat{\mathbf{E}}(\mathbf{r},t) = \sum_{\mathbf{k}} \hat{\mathrm{e}}_{\mathbf{k}} \sqrt{\frac{\hbar\omega_{\mathbf{k}}}{2\varepsilon_0 V}} \left(\hat{a}_{\mathbf{k}}\, e^{i\mathbf{k}\cdot\mathbf{r}} + \hat{a}^{\dagger}_{\mathbf{k}}\, e^{-i\mathbf{k}\cdot\mathbf{r}} \right) \tag{2.89a}$$

$$\hat{\mathbf{B}}(\mathbf{r},t) = \sum_{\mathbf{k}} (\mathbf{k}\times\hat{\mathrm{e}}_{\mathbf{k}}) \sqrt{\frac{\hbar}{2\varepsilon_0 V\omega_{\mathbf{k}}}} \left(\hat{a}_{\mathbf{k}}\, e^{i\mathbf{k}\cdot\mathbf{r}} + \hat{a}^{\dagger}_{\mathbf{k}}\, e^{-i\mathbf{k}\cdot\mathbf{r}} \right). \tag{2.89b}$$

Here the summation is assumed to run over the polarisation (described by the polarisation unit vector $\hat{\mathrm{e}}_{\mathbf{k}}$) as well as the wavevector index, and a mode with wavevector $\mathbf{k}$ has frequency $\omega_{\mathbf{k}}$. Each mode has photon annihilation and creation operators $\hat{a}_{\mathbf{k}}$ and $\hat{a}^{\dagger}_{\mathbf{k}}$, which obey the commutation relation

$$[\hat{a}_{\mathbf{k}}, \hat{a}^{\dagger}_{\mathbf{k}'}] = \delta_{\mathbf{k},\mathbf{k}'}. \tag{2.90}$$

Upon quantisation, the classical Hamiltonian describing the energy in an electromagnetic field

$$H = \int d^3r \left[\frac{\varepsilon_0}{2}\mathbf{E}^2(\mathbf{r},t) + \frac{\mu_0}{2}\mathbf{H}^2(\mathbf{r},t) \right] \tag{2.91}$$

assumes the form

$$\hat{H} = \hbar \sum_{\mathbf{k}} \omega_{\mathbf{k}} (\hat{a}^{\dagger}_{\mathbf{k}}\hat{a}_{\mathbf{k}} + \tfrac{1}{2}) \tag{2.92}$$

and we see that each individual mode of the field behaves as a harmonic oscillator with frequency $\omega_{\mathbf{k}}$.

The Jaynes-Cummings model

The Jaynes-Cummings model describes the interaction between a two-level atom and a single near-resonant mode of the quantised electromagnetic field. First presented in 1963, it has remained important in the field of quantum optics as it is fully soluble and provides a simple, yet experimentally realisable model to which several other systems are analogous or can be simplified. A comprehensive review of the Jaynes-Cummings model and its properties is given in Ref. [57].

The Hamiltonian of the system is composed of three pieces:

$$\hat{H} = \hat{H}_A + \hat{H}_F + \hat{H}_I. \tag{2.93}$$

Here $\hat{H}_A = \hbar\omega_A\,\hat{\sigma}_z/2$ is the Hamiltonian for the free atom, $\hat{H}_F$ is the Hamiltonian for the free field, and $\hat{H}_I$ is the term describing the atom-field interaction. The Hamiltonian for the free field follows from the restriction of Eq. (2.92) to a single mode:

$$\hat{H}_F = \hbar\omega(\hat{a}^{\dagger}\hat{a} + \tfrac{1}{2}). \tag{2.94}$$

Turning to the interaction term, let us again consider the dipolar interaction Hamiltonian:

$$\hat{H}_I = -\hat{\mathbf{d}} \cdot \hat{\mathbf{E}}, \tag{2.95}$$

where $\hat{\mathbf{d}}$ is the dipole operator for the atom in the two-level approximation, as described by Eq. (2.77) and the electric field operator is given by

$$\hat{\mathbf{E}}(\mathbf{r}, t) = \sqrt{\frac{\hbar\omega}{2\varepsilon_0 V}} \left(\hat{a}\, e^{i\mathbf{k}\cdot\mathbf{r}} + \hat{a}^\dagger e^{-i\mathbf{k}\cdot\mathbf{r}} \right) \hat{\mathrm{e}}_0. \tag{2.96}$$

This is very similar to the expression for the single-mode *classical* electric field given by Eq. (2.73), with the mode operators $\hat{a}$ and $\hat{a}^\dagger$ replacing the classical field amplitudes α and α^*. Although the electric field operator is not time dependent at this point, it will gain the expected oscillatory time dependence upon transformation into the interaction picture.

We again make the dipole approximation, evaluating the electric field at the position of the atom (denoted by $\mathbf{r}_0$). The interaction Hamiltonian is therefore given by

$$\hat{H}_I = -\sqrt{\frac{\hbar\omega}{2\varepsilon_0 V}} \left(\hat{a}\, e^{i\mathbf{k}\cdot\mathbf{r}_0} + \hat{a}^\dagger e^{-i\mathbf{k}\cdot\mathbf{r}_0} \right) (\mu_\mp \hat{\sigma}_- + \mu_\pm \hat{\sigma}_+). \tag{2.97}$$

This expression contains terms of the form $\hat{a}^{(\dagger)}\hat{\sigma}_\pm$. Of these, $\hat{a}\hat{\sigma}_+$ can be interpreted as the absorption of a photon by the atom: a photon is removed from the field and the raising operator is applied to the atom. Similarly, $\hat{a}^\dagger\hat{\sigma}_-$ represents emission of a photon with simultaneous de-excitation of the atom. The remaining terms $\hat{a}\hat{\sigma}_-$ and $\hat{a}^\dagger\hat{\sigma}_+$ correspond to de-excitation of the atom with the destruction of a photon, and excitation of the atom with the emission of a photon respectively. Unlike the first two, the second two processes do not conserve energy, and thus we are justified in neglecting them to first order.

This amounts to making the rotating-wave approximation, which can be seen by converting the Hamiltonian into the interaction picture. Once again the sum and difference of the field and atomic frequencies appear, with the rapid oscillations at the sum frequency being attached to the energy-nonconserving terms $\hat{a}\hat{\sigma}_-$ and $\hat{a}^\dagger\hat{\sigma}_+$.

Having made the dipole and rotating-wave approximations, we obtain the Jaynes-Cummings Hamiltonian:

$$\hat{H} = \hbar\omega(\hat{a}^\dagger\hat{a} + \tfrac{1}{2}) + \frac{\hbar\omega_A}{2}\hat{\sigma}_z + \hbar g\,(\hat{a}\hat{\sigma}_+ + \hat{a}^\dagger\hat{\sigma}_-) \tag{2.98}$$

where the coupling constant g is defined as

$$g \equiv |\mu|\sqrt{\frac{\omega}{2\varepsilon_0 V\hbar}}. \tag{2.99}$$

Note that g is real, its phase having been absorbed into the operators $\hat{\sigma}_\pm$.

Dressed states of the JCM

The eigenstates of the free system described by the Hamiltonian $\hat{H}_A + \hat{H}_F$ are the states $|n\rangle|\pm\rangle$. However, these are not eigenstates of the full Hamiltonian given by Eq. (2.98), as can be seen explicitly:

$$\hat{H}|n\rangle|+\rangle = \left(\hbar\omega(n+\tfrac{1}{2}) + \frac{\hbar\omega_A}{2}\right)|n\rangle|+\rangle + \hbar g\sqrt{n+1}\,|n+1\rangle|-\rangle \tag{2.100a}$$

$$\hat{H}|n\rangle|-\rangle = \left(\hbar\omega(n+\tfrac{1}{2}) - \frac{\hbar\omega_A}{2}\right)|n\rangle|-\rangle + \hbar g\sqrt{n}\,|n-1\rangle|+\rangle; \tag{2.100b}$$

the terms $\hat{a}\hat{\sigma}_+$ and $\hat{a}^\dagger\hat{\sigma}_-$ couple the states $|n\rangle|+\rangle$ and $|n+1\rangle|-\rangle$. The only exception to this pairing is the state $|0\rangle|-\rangle$, which has energy $-\hbar\omega_A/2$ and is the ground state of both the free and the interacting system.

Equations (2.100) suggest that the excited states of the interacting system are linear combinations of $|n\rangle|+\rangle$ and $|n+1\rangle|-\rangle$. They can be found by solving the eigenvalue equation

$$\hat{H}|E_n\rangle = E_n|E_n\rangle \tag{2.101}$$

where

$$|E_n\rangle = a_n|n\rangle|+\rangle + b_n|n+1\rangle|-\rangle. \tag{2.102}$$

Taking for simplicity the case of exact resonance ($\omega = \omega_A$), we find the dressed states of the system to be

$$|U_n\rangle = \frac{1}{\sqrt{2}}\big(|n\rangle|+\rangle + |n+1\rangle|-\rangle\big) \tag{2.103a}$$

$$|L_n\rangle = \frac{1}{\sqrt{2}}\big(|n\rangle|+\rangle - |n+1\rangle|-\rangle\big) \tag{2.103b}$$

with energies

$$E_n^U = \hbar\omega(n+\tfrac{1}{2}) + \hbar g\sqrt{n+1} \tag{2.104a}$$

$$E_n^L = \hbar\omega(n+\tfrac{1}{2}) - \hbar g\sqrt{n+1}. \tag{2.104b}$$

In contrast to the eigenstates of the non-interacting system $|n\rangle|\pm\rangle$, the dressed states described by Eq. (2.103) cannot be factorised into an atomic state multiplied by a field state. In the presence of an interaction, neither the atom nor the field possess energy eigenstates individually; the eigenstates belong to the coupled atom-field system.

Collapse and Revival Phenomena

Having developed a quantum-mechanical model of the atom-field interaction, it is time to investigate the behaviour of a system governed by it. We expect the dynamics to be richer than those of the semiclassical situation, since quantising the field has provided us with an extra degree of freedom: in addition to the atomic state, we can now select different states in which to prepare the field. We will see that the choice of different field states results in quite different predictions for the internal dynamics of the atom.

We assume that the atom is prepared in the ground state, and write the initial state of the system as

$$|\psi\rangle = c_0|0\rangle|-\rangle + \sum_{n=0}^{\infty} d_n|n+1\rangle|-\rangle. \tag{2.105}$$

The time evolution of $|\psi\rangle$ can be found by rewriting $|n+1\rangle|-\rangle$ in terms of $|U_n\rangle$ and $|L_n\rangle$, which evolve trivally. We find that at some later time t, the state is given by

$$|\psi(t)\rangle = c_0|0\rangle|-\rangle + \sum_{n=0}^{\infty} d_n\, e^{-i\omega t(n+1)}\big[\cos(\kappa_n t)|n+1\rangle|-\rangle - i\sin(\kappa_n t)|n\rangle|+\rangle\big], \tag{2.106}$$

where $\kappa_n \equiv g\sqrt{n+1}$. If the field is prepared in the number state $|m\rangle$, the atomic excitation probability is

$$P_+(t) = \frac{1}{2}\big[1 - \cos(2g\sqrt{m}t)\big] \tag{2.107}$$

which shows the expected Rabi oscillations at a frequency $\Omega = 2g\sqrt{m}$.

Let us instead consider a field prepared in a coherent state of amplitude α_0. The expansion coefficients d_n are then given by Eq. (2.43), and we find for the excitation probability

$$P_+(t) = \frac{e^{-|\alpha_0|^2}}{2} \sum_{m=0}^{\infty} \frac{|\alpha_0|^{2m}}{m!}\big[1 - \cos(2g\sqrt{m}t)\big] \tag{2.108}$$

The probability of finding the atom in the excited state is given by the sum of many oscillations at different frequencies. For short times, the individual oscillations interfere constructively and the excitation probability shows Rabi oscillations. As time passes, the individual oscillations begin to dephase, the Rabi oscillations 'wash out' and the excitation probability stabilises at some approximately steady-state value (0.5 for the resonant case).

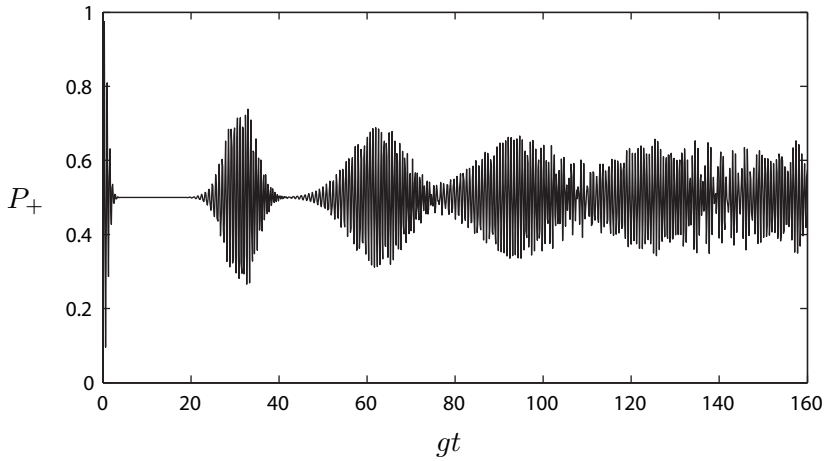

Figure 2.5: The behaviour of the atomic excitation probability in the Jaynes-Cummings model (Eq. (2.108)) for an initial coherent state of amplitude $\alpha_0 = 5$.

Up to this point, we have gained no information through quantising the field; the same predictions can be made from the semiclassical model by noting that a coherent state has some uncertainty in the electric field amplitude. For a classical field this is effected by replacing the electric field amplitude by a statistical distribution with mean α_0. Averaging over the resultant Rabi oscillations shows that the atomic excitation probability undergoes a similar collapse to a steady-state value.

What happens next, however, is a unique prediction of the Jaynes-Cummings model. The quantisation of the field means that the excitation probability Eq. (2.108) is not the average over a distribution of continuously-varying frequencies, but a sum over a range of discrete frequencies. After some sufficiently long time, the individual terms rephase and oscillations reappear in the excitation probability – the atomic excitation undergoes a *revival*. While the collapse can be understood using a classical field, the revival is due to the existence of discrete energy levels of the field and so is a purely quantum phenomenon.

2.3.4 The anharmonic oscillator

Though the Jaynes-Cummings model provides the best-known example of collapse and revival behaviour, it is not the only system which contains this feature. Collapses and revivals also occur in the anharmonic oscillator, albeit in a slightly different form.

The anharmonic oscillator has Hamiltonian

$$\hat{H} = \hat{H}_0 + \frac{g}{\hbar\omega}\,\hat{H}_0^2 \tag{2.109}$$

where $\hat{H}_0 = \hbar\omega\,\hat{a}^\dagger\hat{a}$ is the free Hamiltonian for a harmonic oscillator. Among other things, this Hamiltonian can be used to describe the transmission of an optical field state through an amplitude-dispersive medium [32, 72]. If we expand the state vector $|\psi\rangle$ as

$$|\psi\rangle = \sum_n c_n|n\rangle, \tag{2.110}$$

we find that the state at some later time t is given by

$$\begin{aligned}|\psi(t)\rangle &= e^{-igt(\hat{a}^\dagger\hat{a})^2}\sum_n c_n|n\rangle \\ &= \sum_n c_n(t)|n\rangle\end{aligned} \tag{2.111}$$

where $c_n(t) = c_n\,e^{-igtn^2}$. The expansion coefficients are therefore periodic with a period of $t = 2\pi/(gn^2)$.

This periodic evolution of the expansion coefficients is what gives rise to the collapse and revival behaviour in the model. Since n^2 is always an integer, each expansion cofficient returns to its original value c_n whenever $gt = 2k\pi$ $(k = 0, 1, 2\ldots)$, and so the entire state vector is periodic with period $2\pi/g$.

The key point of difference between the collapse and revival behaiour of the anharmonic oscillator and the Jaynes-Cummings model is the extent to which the original state is reproduced. Equation (2.106) shows that the oscillation frequencies appearing in the Jaynes-Cummings model are irrational and thus incommensurate. This means that the individual oscillations do not exactly rephase, a fact which is reflected in the decay of the amplitude and quality of the revivals seen in Fig. 2.5. In contrast, the oscillation frequencies appearing in Eq. (2.111) are rational; the coefficients thus rephase perfectly, and the state continues to recur completely forever.

2.4 Phase-space distributions

The typical method of visualising the state of a classical dynamical system is through the use of phase-space. In this formalism, the state of the system is represented by a point (or more generally, a probability distribution) that lives in a space spanned by canonical coordinate and momentum axes. As the system evolves in time, the distribution moves through the phase-space along a trajectory governed by the system Hamiltonian.

A natural question to ask is whether a similar formalism can be used to describe the state of a quantum mechanical system. The answer turns out to be yes, with one important caveat. The central object in the phase space representation of a classical system is a probability distribution in the canonical coordinate and momentum. In

quantum mechanics, however, these observables are represented by non-commuting operators, and so we may have a probability distribution for the coordinate, or for the momentum, but never for the two at once. The phase-space representations that have been developed for quantum systems are therefore commonly known as *pseudo-* or *quasi*-probability distributions. Although they act similarly to true probability distributions in many respects, in some cases they may take on negative values or become highly singular.

2.4.1 The Q function

The Q function can be defined as the Fourier transform of the antinormally-ordered characteristic function:

$$Q(\alpha,\alpha^*) \equiv \frac{1}{\pi^2}\int_{-\infty}^{\infty} d^2z\,\chi_A(z,z^*)\,e^{-iz^*\alpha^*}e^{-iz\alpha}, \tag{2.112}$$

where $\chi_A(z,z^*)$ is defined as

$$\chi_A(z,z^*) = \mathrm{tr}\big(\hat{\rho}\,e^{iz\hat{a}}e^{az^*\hat{a}^\dagger}\big). \tag{2.113}$$

It is proportional to the coherent state diagonal matrix element of the density operator $\hat{\rho}$:

$$Q(\alpha,\alpha^*) = \frac{1}{\pi}\langle\alpha|\hat{\rho}|\alpha\rangle. \tag{2.114}$$

The Q function is positive definite and normalised such that

$$\int_{-\infty}^{\infty} d^2\alpha\,Q(\alpha,\alpha^*) = 1. \tag{2.115}$$

Integrating the Q function against powers of the phase-space variables α and α^* gives the average of the same powers of the operators $\hat{a}$ and $\hat{a}^\dagger$, with the operators written in antinormal order ($\hat{a}$ to the left of $\hat{a}^\dagger$):

$$\int_{-\infty}^{\infty} d^2\alpha\,\alpha^m\alpha^{*n}\,Q(\alpha,\alpha^*) = \mathrm{tr}\left(\hat{\rho}\,\hat{a}^m\hat{a}^{\dagger n}\right). \tag{2.116}$$

where $\hat{\rho}$ is the density operator for the system.

Number state

The Q function for a number state can be found by using the expansion given by Eq. (2.43):

$$\begin{aligned} Q_{|n\rangle}(\alpha,\alpha^*) &= \frac{1}{\pi}|\langle\alpha|n\rangle|^2 \\ &= \frac{1}{\pi n!}|\alpha|^{2n}e^{-|\alpha|^2}. \end{aligned} \tag{2.117}$$

This function is radially symmetric with a peak at $|\alpha| = \sqrt{n}$, reflecting the precisely defined amplitude and completely indeterminate phase of a number state. Figure 2.6 shows the Q function for the number state $|n = 2\rangle$.

Coherent state

The Q function for a coherent state $|\alpha_0\rangle$ follows easily from the overlap between coherent states (Eq. (2.45)):

$$\begin{aligned} Q_{|\alpha_0\rangle}(\alpha,\alpha^*) &= \frac{1}{\pi}|\langle\alpha|\alpha_0\rangle|^2 \\ &= \frac{1}{\pi}\,e^{-(\xi-\xi_0)^2}e^{-(\mu-\mu_0)^2}, \end{aligned} \tag{2.118}$$

where $\xi_{(0)}$ and $\mu_{(0)}$ are the real and imaginary parts of $\alpha_{(0)}$. The Q function for a coherent state is a two-dimensional Gaussian centred at (ξ_0,μ_0); the unit variance in each direction reflects the equal uncertainties in the $\hat{X}_1$ and $\hat{X}_2$ quadratures.

2.4.2 The Wigner function

The Wigner function can be defined as the Fourier transform of the symmetrically-ordered characteristic function:

$$W(\alpha,\alpha^*) \equiv \frac{1}{\pi^2}\int_{-\infty}^{\infty} d^2z\,\chi_S(z,z^*)\,e^{-iz^*\alpha^*}e^{-iz\alpha}, \tag{2.119}$$

where $\chi_S(z,z^*)$ is defined as

$$\chi_S(z,z^*) = \mathrm{tr}\left[\hat{\rho}\,e^{i(z\hat{a}+z^*\hat{a}^\dagger)}\right]. \tag{2.120}$$

Integrating the Wigner function against powers of the phase-space variables α and α^* gives the average of all possible combinations of the same powers of the operators $\hat{a}$ and $\hat{a}^\dagger$, for example

$$\int_{-\infty}^{\infty} d^2\alpha\,\alpha\alpha^*\,W(\alpha,\alpha^*) = \frac{1}{2}\left[\langle\hat{a}^\dagger\hat{a}\rangle + \langle\hat{a}\hat{a}^\dagger\rangle\right] \tag{2.121a}$$

$$\int_{-\infty}^{\infty} d^2\alpha\,\alpha^2\alpha^*\,W(\alpha,\alpha^*) = \frac{1}{3}\left[\langle\hat{a}^\dagger\hat{a}^2\rangle + \langle\hat{a}\hat{a}^\dagger\hat{a}\rangle + \langle\hat{a}^2\hat{a}^\dagger\rangle\right]. \tag{2.121b}$$

An alternative definition of the Wigner function involves the Fourier transform of shifted position-space wavefunctions [9]:

$$W(x,p) \equiv \frac{1}{2\pi\hbar}\int_{-\infty}^{\infty} dy\,\langle x+y/2|\hat{\rho}|x-y/2\rangle\,e^{-ipy/\hbar} \tag{2.122}$$

where x and p are the standard position and momentum variables.

Number state

The Wigner function for a number state is

$$W_{|n\rangle}(\xi,\mu) = \frac{2}{\pi}\,(-1)^n e^{-2(\xi^2+\mu^2)}L_n\big(4(\mu^2+\xi^2)\big) \tag{2.123}$$

where $L_n(x)$ is a Laguerre polynomial. Like the Q function, the Wigner function for a number state is symmetric with respect to phase. The Wigner function for a number state is negative in places (see Fig. 2.6), which reflects the fact that a number state is not a classical state.

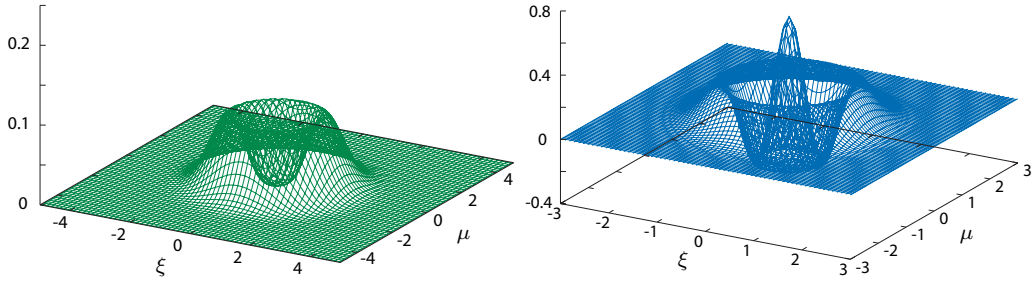

Figure 2.6: A comparison of the Q (left) and Wigner (right) functions for the number state $|n = 2\rangle$.

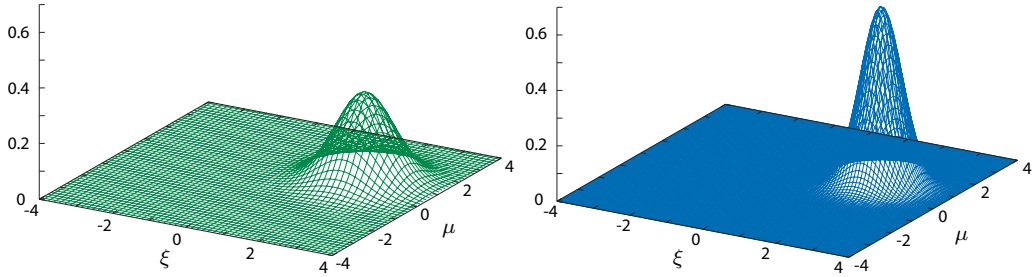

Figure 2.7: A comparison of the Q (left) and Wigner (right) functions for the coherent state $|\alpha_0 = 2 + i\rangle$.

Coherent state

The Wigner function for a coherent state is

$$W_{|\alpha_0\rangle}(\xi, \mu) = \frac{2}{\pi} e^{-2(\xi-\xi_0)^2} e^{-2(\mu-\mu_0)^2}. \tag{2.124}$$

This describes a two-dimensional Gaussian centred at (ξ_0, μ_0), similar to the Q function for a coherent state. However, the Wigner function is narrower than the Q function – the variance in each direction is smaller by a factor of two.

This difference in variance is related to the structure of the antinormally- and symmetrically-ordered characteristic functions. If the $\hat{a}$ and $\hat{a}^\dagger$ operators in one of the functions are reordered such that a direct comparison can be made, it becomes clear that χ_A is narrower than χ_S, and so has a broader Fourier transform.

The Q and Wigner functions are also related by the fact that the Q function for a given state can be obtained by taking the convolution of the relevant Wigner function with a Gaussian. The Q function for a coherent state is therefore broader and shorter than the corresponding Wigner function, as can be seen from the comparison in Fig. 2.7.

Chapter 3

A Numerical Investigation of the System Dynamics

Having laid in place the theoretical background associated with each of its individual components, we are now in a position to begin our analysis of the system at hand. The first section of this chapter introduces the formalism used to describe the system and discusses the validity of the approximations made, while the second outlines the behaviour of various quantities of interest obtained from the numerical solution of the system.

3.1 System outline

Illustrated in Fig. 3.1, the system consists of a harmonically trapped atom[1] interacting with a resonant standing-wave electromagnetic field. We treat the electromagnetic field classically, the motion of the atom quantum mechanically, and the internal state of the atom as a two-level system.

3.1.1 State description

The state vector of the system can be written as

$$|\psi(t)\rangle = |\phi_+(t)\rangle|+\rangle + |\phi_-(t)\rangle|-\rangle \tag{3.1}$$

where $|\phi_\pm(t)\rangle$ describe the centre-of-mass of the atom and $|\pm\rangle$ are the atomic energy eigenstates.[2] The centre-of-mass wavepackets can be expanded in the number-state

[1] While the net charge of the trapped particle will dictate exactly how the trapping is implemented, it has no bearing on the results obtained; 'atom' should thus be interpreted as being synonymous with 'ion' for the remainder of this thesis.

[2] Since the motional and internal states belong to different Hilbert spaces, to be entirely correct we should write $|\psi(t)\rangle = |\phi_+(t)\rangle \otimes |+\rangle + |\phi_-(t)\rangle \otimes |-\rangle$, where $\otimes$ denotes the tensor product. In the same manner, that the operators only act on that piece of the state in the Hilbert space to which they belong could be made explicit by writing, for example, $\hat{a}^\dagger = \hat{a}^\dagger \otimes \hat{\mathbb{1}}_\mathrm{A}$, where $\hat{\mathbb{1}}_\mathrm{A}$ is the identity operator for the internal state of the atom. As physicists, however, we are allowed to be less than rigorous at times, and we shall leave such pedantry behind the scenes.

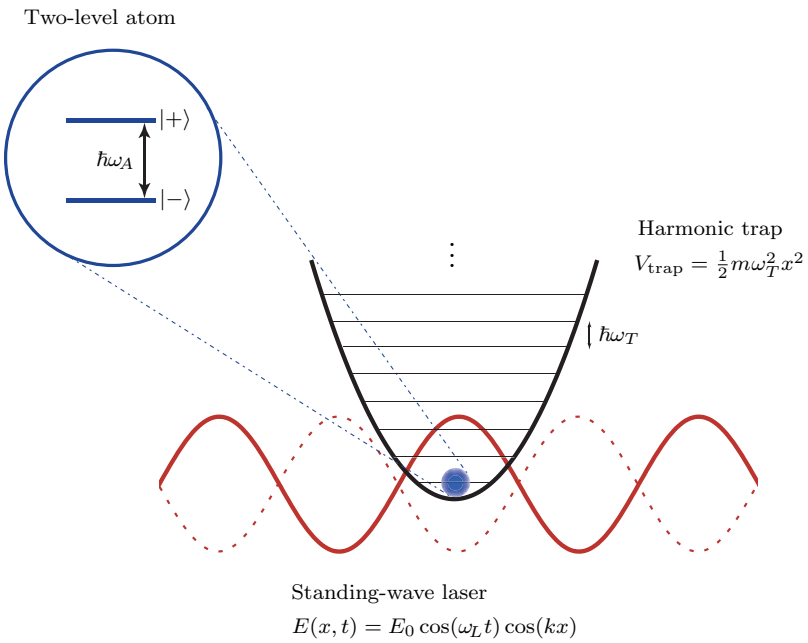

Figure 3.1: The system studied in this thesis.

basis as

$$|\phi_{\pm}(t)\rangle = \sum_n c_n^{\pm}(t)\,|n\rangle. \tag{3.2}$$

3.1.2 System Hamiltonian

The Hamiltonian of the system can be written as

$$\hat{H} = \hat{H}_T + \hat{H}_A + H_F + \hat{H}_I \tag{3.3}$$

where $\hat{H}_T$ and $\hat{H}_A$ describe the motional and internal states, respectively, of the trapped atom, H_F describes the free electromagnetic field, and $\hat{H}_I$ describes the atom-field interaction.

The centre-of-mass motion of the atom.

The atom is assumed to be confined to move in one dimension only, with coordinate x. Since the confining potential of an ion trap is well approximated by a quadratic potential (see §2.1), the Hamiltonian for the atomic motion is that of a quantised harmonic oscillator, as discussed in §2.2.2:

$$\hat{H}_T = \hbar\omega_T\,(\hat{a}^\dagger\hat{a} + \tfrac{1}{2}). \tag{3.4}$$

Here ω_T is the trap frequency, and $\hat{a}$ ($\hat{a}^\dagger$) is a phonon annihilation (creation) operator which acts to lower (raise) the motional state of the centre-of-mass of the atom.

The internal state of the atom.

The atom is treated as a two-level system and spontaneous emission is neglected. Making these approximations, the Hamiltonian describing the internal state of the atom is given by

$$\hat{H}_A = \frac{\hbar\omega_A}{2}\hat{\sigma}_z \tag{3.5}$$

where ω_A is the atomic transition frequency, and $\hat{\sigma}_z$ is the atomic energy operator in the two-level approximation.

The free electromagnetic field.

Treating the electromagnetic field classically means its Hamiltonian is a classical function which commutes with all other pieces of the system Hamiltonian. It can therefore be ignored, as the only effect it has on the system dynamics is to multiply the states by a (fundamentally unobservable) global phase.

The atom-field interaction.

The atom-field interaction is described by a semiclassical interaction Hamiltonian, which may be obtained by following a similar procedure to that outlined in §2.3.2. The sole point of difference is the inclusion of an additional factor of $\cos k\hat{x}$, which accounts for the standing-wave configuration of the electromagnetic field. Note that the choice of a cosine corresponds to aligning the centre of the harmonic trap with an antinode of the standing wave, an assumption which will be lifted in Chapter 5. We find

$$\hat{H}_I = \frac{\hbar\Omega}{2}\left(\hat{\sigma}_+ e^{-i\omega_L t} + \hat{\sigma}_- e^{i\omega_L t}\right)\cos k\hat{x}, \tag{3.6}$$

where ω_L and $k = \omega_L/c$ are the frequency and wavenumber of the electromagnetic field.

We have obtained the Hamiltonian for our system, but there remains one further simplification which must be made before we set about analysing it. The cosine of an operator is not a pleasant thing to work with, and we will not get very far in our investigation of the Hamiltonian if this term is allowed to remain in its present form. We thus replace the cosine by its Taylor expansion:

$$\begin{aligned}\cos k\hat{x} &= 1 - \frac{(k\hat{x})^2}{2} + \frac{(k\hat{x})^4}{24} - \dots \\ &= 1 - \frac{\eta_{\mathrm{LD}}^2}{2}(\hat{a} + \hat{a}^\dagger)^2 + \frac{\eta_{\mathrm{LD}}^4}{24}(\hat{a} + \hat{a}^\dagger)^4 - \dots .\end{aligned} \tag{3.7}$$

where in the second line we have introduced the *Lamb-Dicke parameter*:

$$\eta_{\mathrm{LD}} \equiv k\sqrt{\frac{\hbar}{2m\omega_T}} = 2\pi\frac{x_0}{\lambda}. \tag{3.8}$$

Here $x_0 \equiv \left(\langle 0|\hat{x}^2|0\rangle\right)^{1/2} = \sqrt{\hbar/2m\omega_T}$ is the spread of the ground-state wavefunction of the atomic centre-of-mass. The Lamb-Dicke parameter measures the ratio of this spread to the wavelength of the incident laser, providing a quantitative measure of how tightly the particle is trapped.

Of particular interest to the field of trapped ions is the strong trapping limit, where the ion is confined to an area which is small in comparison with the wavelength of the exciting radiation. This corresponds to $\eta_{\rm LD} \ll 1$, a regime known as the Lamb-Dicke limit.

The reason for the importance of this limit is essentially twofold. Experimentally, we find that it is only in the strong trapping regime that the Doppler-induced sidebands present in the absorption spectrum of the trapped ion are sufficiently clearly resolved to allow sideband cooling on a dipole transition [10]. From a theoretical point of view, the system Hamiltonian of a trapped ion interacting with a laser invariably contains some sort of power series in $\eta_{\rm LD}$, the truncation of which at low order simplifies things greatly.

Returning to the Hamiltonian, we take the Lamb-Dicke limit and neglect terms of order $\eta_{\rm LD}^4$ and higher. We arrive at

$$\hat{H} = \hbar\omega_T(\hat{a}^\dagger\hat{a} + \tfrac{1}{2}) + \frac{\hbar\omega_A}{2}\hat{\sigma}_z + \frac{\hbar\Omega}{2}\left(\hat{\sigma}_+ e^{-i\omega_L t} + \hat{\sigma}_- e^{i\omega_L t}\right)\left[1 - \chi(\hat{a} + \hat{a}^\dagger)^2\right] \quad (3.9)$$

where, for the sake of notational simplicity, we have defined

$$\chi \equiv \eta_{\rm LD}^2/2. \quad (3.10)$$

This is the Hamiltonian which we shall use to investigate the system illustrated in Fig. 3.1.

3.1.3 Validity of approximations

Before we continue, it is worthwhile reviewing and commenting on the validity of the approximations that have been made in obtaining the Hamiltonian appearing in Eq. (3.9).

The centre-of-mass motion of the atom.
A classical treatment of the atomic motion would require that the energy associated with the motion be large in comparison with the spacing of the energy levels of the trap: a condition only fulfilled when the atom is high in the trapping potential. Treating the atomic motion quantum-mechanically lifts this restriction, extending the scope of the model to include occupation of the very lowest states of the trap.

On the other hand, the expansion of the cosine is only valid when the argument is small – that is, $k\hat{x} \ll 1$. Assuming a coherent state of real amplitude α_0, this corresponds to

$$\chi \alpha_0^2 \ll 0.25 \tag{3.11}$$

which gives some idea of how highly the motional state of the atom may be excited before the cosine approximation becomes a poor one.

Illustrations of system dynamics in this chapter are typically shown for two cases. One of these has a comparatively large value of $\chi\alpha_0^2$ ($= 0.16$) which means that the Lamb-Dicke approximation is not strictly justified. Nevertheless, it is interesting to observe this case, as the features appearing in the dynamics are more clearly visible. The second case typically has $\chi\alpha^2 = 0.04$, and is in a regime where the Lamb-Dicke approximation is justified. These plots are intended to show that the features are still present in the dynamics, although they may be more difficult to observe.

Numeric solutions of the system in the absence of the Lamb-Dicke approximation are presented in Chapter 5, which also includes a discussion of the size of the errors introduced by the approximation.

The internal dynamics of the atom.

Our treatment of the internal dynamics of the atom contains two key assumptions: that the atom may be represented by a two-level system and that spontaneous emission by the atom can be neglected.

In contrast with the Lamb-Dicke approximation, which limits the range of applicability of the results, or the dipole and rotating-wave approximations, which are justified simply by virtue of the fact that we treat an optical frequency transition, the validity of these approximations depends heavily on our ability to engineer the corresponding experimental situation – namely, an effectively two-state system with a negligible spontaneous emission rate.

As it would happen, the ability to prepare systems with these characteristics has steadily approached perfection over the past decade [41, 52], primarily because these are the exact conditions required for experiments concerned with the trapped-ion implementation of quantum information processing [28, 58]. The binary nature of a qubit mandates the use of a two-level system, while the ability to perform a useful number of bit operations before decoherence becomes a problem requires that the time between spontaneous emission events be far longer than the time scale characterising the coherent dynamics of the ion [11].

Impressive experimental achievements in this area indicate that the preparation of such systems is sufficiently common that our approximations are justifiable. While the exact method by which the requisite conditions are attained depends on

the details of the experiment, the basic premises are simple enough to mention here. An atom can be made to behave as a two-level system by choosing the properties of the incident light such that all transitions except the desired one are sufficiently detuned or forbidden that they may be neglected, while the suppression of spontaneous emission is most commonly achieved in one of two ways, which are outlined briefly in §3.1.4.

The atom-field interaction.
In the course of deriving the semiclassical atom-field interaction Hamiltonian, the dipole and rotating-wave approximations were made. Though the use of these approximations is both common and well established in the field of quantum optics, it is worth confirming their validity in the case at hand.

The dipole approximation assumes that the incident electromagnetic field is of sufficiently long wavelength that its magnitude does not vary appreciably over the width of the atom.[3] In the current system, the incident field is assumed to be in the optical region ($\lambda \sim 10^{-6}$ m), while the size of the trapped atom is characterised by the Bohr radius ($\sim 5 \times 10^{-11}$ m). Even allowing for some variation in the species of atom and transition frequency used, these length scales differ by 3 – 5 orders of magnitude, making it clear that the dipole approximation is justified.

When the rotating-wave approximation (RWA) was made, the terms oscillating at the sum frequency $\omega_A + \omega_L$ were discarded on the basis that their contribution upon integration would be negligible. While this captures the essence of the justification for the RWA, the more accurate criterion for discarding these terms is that the frequency at which they oscillate is large *in comparison with all other frequencies appearing in the system.* In the current system, the terms with which $\omega_L + \omega_A$ must be compared are the laser detuning (typically $\sim$ MHz), the Rabi frequency (10 kHz – 50 MHz), and the trap frequency (1 – 50 MHz). Noting that these terms are all at least seven orders of magnitude below the optical frequency range ($\sim 10^{14}$ Hz) to which ω_L and ω_A belong confirms that the RWA is valid for the system at hand.

3.1.4 Experimental realisation

Lest we be accused of having our heads in the theoretical clouds, let us briefly outline a possible experimental realisation of this model.

A single ion held in a Paul trap (either linear or 3D) is the simplest realisation of the harmonically trapped atom. The one-dimensional model outlined here could be implemented by 'freezing out' the motion in the other two dimensions by making the trapping potential strongly asymmetric and cooling the ion to the ground state of the oscillator, while the standing-wave potential could be provided by a single

[3] Note that this is different from the Lamb-Dicke approximation, which deals with the amplitude of oscillation of the atom, not the size of the atom itself.

retro-reflected laser beam.

The choice of which atomic levels to use for the 'excited' and 'ground' states is limited somewhat by the requirement that spontaneous emission be negligible (that it take place on a much longer time scale than the internal and motional dynamics of the atom). This effectively rules out the use of an excited state possessing a dipole-allowed transition, leaving us with two ways of implementing the required two-level system:

a) Use a Raman transition to link two stable states (for example, two magnetic sublevels). Although an extra laser is required, this method has the advantage of being able to use states with extremely long lifetimes.

b) Use levels linked by a dipole-forbidden transition. Many quadrupole transitions have lifetimes of the order of seconds, easily long enough to observe the atom dynamics taking place on the μs – ms time scale.

Both of these methods have been used to implement qubits with trapped ions; for examples see Refs. [45] and [55] respectively.

It is worth noting that we may also borrow from experiments involving qubits an efficient technique for ascertaining the internal state of the atom. This assumes the existence of a dipole-allowed transition linking one of the two states (say $|-\rangle$) with a third state (call it $|\text{aux}\rangle$). The atomic state readout is accomplished by irradiating the atom with a laser tuned to the $|-\rangle \rightarrow |\text{aux}\rangle$ transition frequency. Observation of a clear fluorescence signal (which could be $\gtrsim 10^6$ counts s^{-1}) indicates that the atom was initially in $|-\rangle$, while a lack of fluorescence indicates that the atom was initially in $|+\rangle$. This is known as the 'electron shelving' technique [18, 47], and due to its high efficiency ($\geq 90\%$), has become the standard method of state detection in trapped ion experiments [64].

3.2 Numerical solutions

We begin our investigation of the system with a numeric simulation. Our starting point is the Schrödinger equation:

$$\frac{d|\psi(t)\rangle}{dt} = \frac{1}{i\hbar}\hat{H}\,|\psi(t)\rangle \tag{3.12}$$

where the state $|\psi(t)\rangle$ and the Hamiltonian $\hat{H}$ are given by Eq. (3.1) and Eq. (3.9) respectively. In order to remove the rapid evolution produced by the free Hamiltonian, we transform into the interaction picture by defining the state

$$|\psi(t)\rangle_I \equiv e^{i\hat{H}_0 t/\hbar}\,|\psi(t)\rangle \tag{3.13}$$

where $\hat{H}_0 = \hat{H}_T + \hat{H}_A$. The time evolution of $|\psi(t)\rangle_I$ is given by the interaction-picture Schrödinger equation

$$\frac{d|\psi(t)\rangle_I}{dt} = \frac{1}{i\hbar}\tilde{H}_I(t)\,|\psi(t)\rangle_I \tag{3.14}$$

where

$$\tilde{H}_I \equiv e^{i\hat{H}_0 t/\hbar}\,\hat{H}_I\,e^{-i\hat{H}_0 t/\hbar}. \tag{3.15}$$

Carrying out these transformations, we find

$$|\psi_\pm(t)\rangle_I = \sum_n \tilde{c}_n^+(t)\,|n\rangle|+\rangle + \tilde{c}_n^-(t)|n\rangle|-\rangle \tag{3.16}$$

and

$$\tilde{H}_I = \frac{\hbar\Omega}{2}\left(\hat{\sigma}_+ e^{-i\Delta t} + \hat{\sigma}_- e^{i\Delta t}\right)\left[1 - \chi\left(\hat{a}e^{-i\omega_T t} + \hat{a}^\dagger e^{i\omega_T t}\right)^2\right], \tag{3.17}$$

where to describe the state we have introduced the slowly-varying expansion coefficients

$$\tilde{c}_n^\pm(t) \equiv c_n^\pm(t)\,e^{i[\omega_T(n+\frac{1}{2})\pm\omega_A/2]t} \tag{3.18}$$

and $\Delta \equiv \omega_L - \omega_A$ is the detuning of the laser from resonance with the atomic transition frequency. For the remainder of the thesis we will assume the laser is tuned to exact resonance.

Equations of motion for the expansion coefficients $\tilde{c}_n^\pm$ follow from Eq. (3.14) and the orthogonality of the basis states. We find

$$\begin{aligned}\frac{d\tilde{c}_n^\pm}{dt} = \frac{i\Omega}{2}\Big\{&e^{i2\omega_T t}\sqrt{n(n-1)}\chi\,\tilde{c}_{n-2}^\mp - [1-(2n+1)\chi]\,\tilde{c}_n^\mp \\ &+e^{-i2\omega_T t}\sqrt{(n+1)(n+2)}\chi\,\tilde{c}_{n+2}^\mp\Big\}.\end{aligned} \tag{3.19}$$

As seen earlier, the choice of atomic basis states means that the equations of motion for $\tilde{c}^\pm$ are coupled together. If necessary, they could be decoupled by constructing suitable linear combinations of $\tilde{c}^+$ and $\tilde{c}^-$, effectively moving to the dressed-state basis discussed in §2.3.2.

As is often the case, the numeric solution of these equations is facilitated by recasting them into dimensionless units. To this end, we work with the scaled time $\tau \equiv \omega_T t$; the parameters that govern the atom-field interaction are then χ and the ratio Ω/ω_T. It is the dependence of the system dynamics on these two parameters that we wish to investigate.

We select as an initial state a coherent motional state of amplitude α_0, with the atom in the ground state, i.e.

$$c_n^-(0) = e^{-\frac{1}{2}|\alpha_0|^2} \frac{\alpha_0^n}{\sqrt{n!}} \tag{3.20a}$$

$$c_n^+(0) = 0. \tag{3.20b}$$

Details of the numerical solution of the system and relevant sections of computer code are presented in Appendix E.

3.2.1 Complex amplitude of the oscillator

In order to analyse the effect of the atom-field interaction it is convenient to remove the free evolution of the oscillator by working in a rotating coordinate system. This is accomplished by evaluating the expectation value of the Schrödinger-picture operator $\hat{a}$ with respect to the interaction-picture states $|\psi(t)\rangle_I$. We find

$$\begin{aligned} \langle \hat{a} \rangle_I(t) &= {}_I\langle \psi(t)| \hat{a} |\psi(t)\rangle_I \\ &= \sum_{n=0} \sqrt{n+1} \left[(\tilde{c}_{n+1}^+)^* \tilde{c}_n^+ + (\tilde{c}_{n+1}^-)^* \tilde{c}_n^- \right] \end{aligned} \tag{3.21}$$

where the second line follows on substitution of the state expansion given by Eq. (3.16). Figure 3.2 shows the motion of $\langle \hat{a} \rangle$ on the phase plane for various values of the system parameters.

Starting from α_0, $\langle \hat{a} \rangle_I$ oscillates from one side of the phase plane to the other, tracing out a series of bounces as it goes. The bounces have frequency

$$\omega_{\text{bounce}} \simeq 2$$

and an amplitude proportional to $\chi\Omega/\omega_T$. The excursions across the phase plane have frequency

$$\omega_{\text{rev}} \simeq \frac{\chi\Omega}{\omega_T}$$

and precess anticlockwise around the origin, so that the extrema of the trajectory move around the circumference of a circle of radius $|\alpha_0|$. The frequency of this precession is

$$\omega_{\text{prec}} \simeq \frac{\chi^2\Omega^2}{2\omega_T^2}.$$

The origin of these frequencies will become clear when the Hamiltonian is analytically diagonalised in Chapter 4, but we can make here some preliminary comments on their form. Consider transforming the Hamiltonian Eq. (3.9) into the interaction picture and neglecting the terms in $\hat{a}^2$ and $\hat{a}^{\dagger 2}$; the interaction then contains only a term in $\hat{a}^\dagger\hat{a}$ and a constant. If we use the atomic dressed states to write

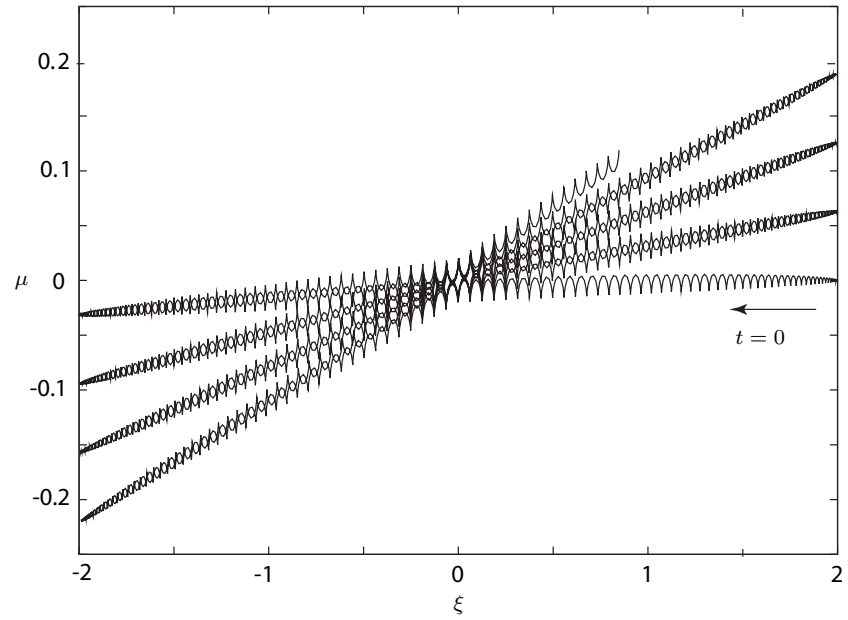

(a) $\chi = 0.01$, $\Omega/\omega_T = 1$, $\tau = 0 - 2400$.

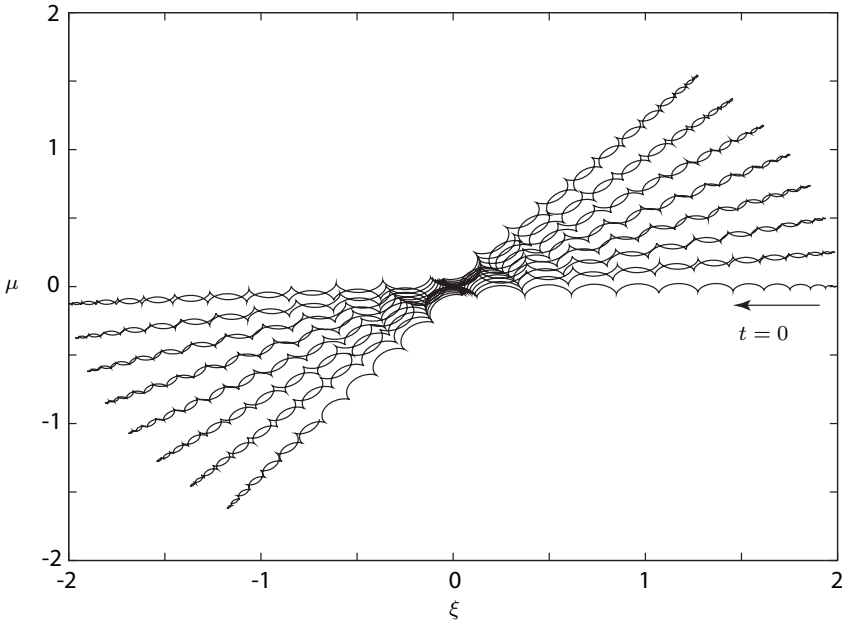

(b) $\chi = 0.04$, $\Omega/\omega_T = 1$, $\tau = 0 - 1200$.

Figure 3.2: The motion of $\langle \hat{a} \rangle$ on the phase plane for two choices of parameters; note the difference in y-axis scales between the two figures. The initial coherent state was $|\alpha_0 = 2\rangle$ in each case.

the interaction in a diagonal form, the term in $\hat{a}^\dagger\hat{a}$ combines with the free oscillator term and modifies the oscillation frequency by an amount $\pm\chi\Omega$, dependent on the internal state of the atom. The combination of the two pieces of $\langle\hat{a}\rangle$ (which move in opposite directions in the rotating frame) gives rise to the back-and-forth motion of $\langle\hat{a}\rangle$ on the phase plane. The precession frequency, however, cannot be explained by this simple approach, which suggests that the precession of $\langle\hat{a}\rangle$ is linked to the quadratic terms in $\hat{a}$ and $\hat{a}^\dagger$.

3.2.2 Average phonon number

The average occupation level of the trap is given by the expectation value of the number operator:

$$\begin{aligned}\langle\hat{a}^\dagger\hat{a}\rangle &= \langle\psi(t)|\hat{a}^\dagger\hat{a}|\psi(t)\rangle \\ &= \sum_n n\left(|c_n^+|^2 + |c_n^-|^2\right). \end{aligned} \tag{3.22}$$

Figure 3.3 shows examples of the behaviour of $\langle\hat{a}^\dagger\hat{a}\rangle$ over time. We see that the effect of the atom-field interaction is to introduce a periodic variation in the mean phonon number about the expected value of $|\alpha_0|^2$. The variation consists of a high-frequency oscillation modulated by a low-frequency envelope, the magnitude of which is proportional to $\chi\Omega/\omega_T$. The high-frequency oscillations have frequency 2, while the envelope has frequency $2\chi\Omega/\omega_T$.

The variation in the average phonon number cannot be explained by the simple interpretation of the Hamiltonian used above. This suggests that, like the precession of $\langle\hat{a}\rangle$, it is caused by the quadratic terms in $\hat{a}$ and $\hat{a}^\dagger$.

3.2.3 Atomic excitation probability

The probability of finding the atom in the excited state is given by the expectation value of the operator $\hat{\sigma}_+\hat{\sigma}_-$:

$$\begin{aligned}\langle\hat{\sigma}_+\hat{\sigma}_-\rangle &= \langle\psi(t)|\hat{\sigma}_+\hat{\sigma}_-|\psi(t)\rangle \\ &= \sum_n |c_n^+|^2. \end{aligned} \tag{3.23}$$

This is equal to the norm of $|\phi_+(t)\rangle$. As a consequence of the coupling of the atomic states by the interaction Hamiltonian, the norm of each motional state does not remain constant in time, but rather gives the probability of finding the atom in the corresponding internal state;

$$\langle\phi_\pm(t)|\phi_\pm(t)\rangle = \sum_n |c_n^\pm(t)|^2 = P_\pm(t).$$

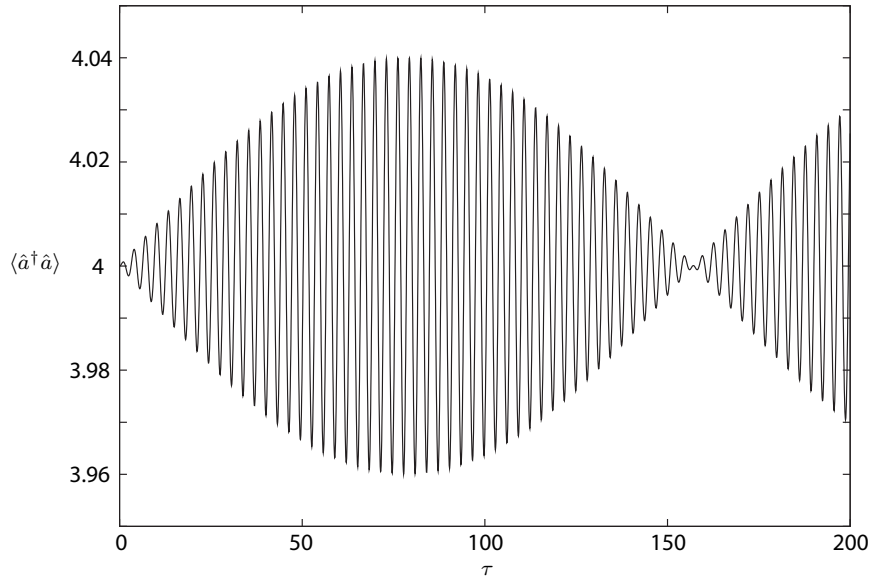

(a) $\chi = 0.01$, $\Omega/\omega_T = 1$.

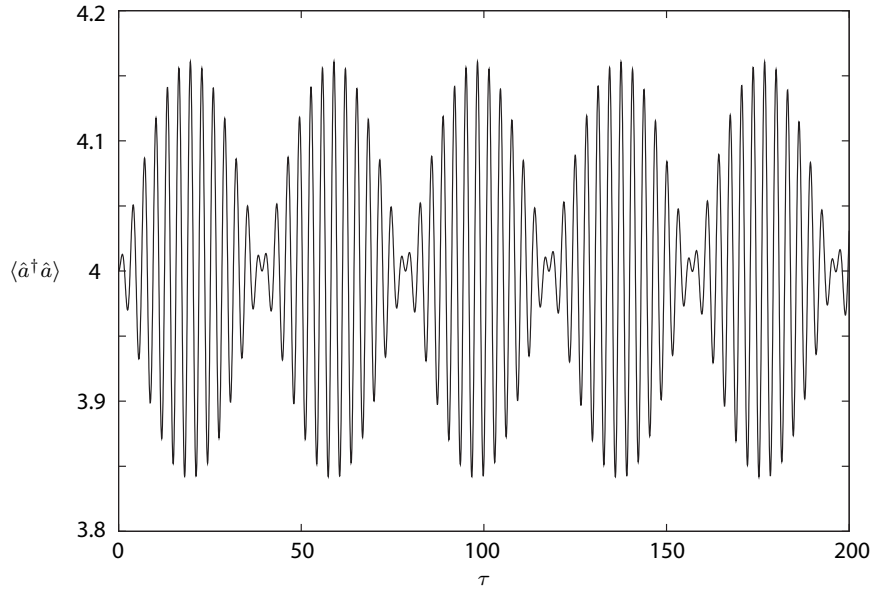

(b) $\chi = 0.04$, $\Omega/\omega_T = 1$.

Figure 3.3: The average phonon number vs. time for two values of χ, for an initial coherent state of amplitude $\alpha_0 = 2$. The frequency and amplitude of the oscillations about the expected value of $|\alpha_0|^2 = 4$ increase significantly when χ is increased.

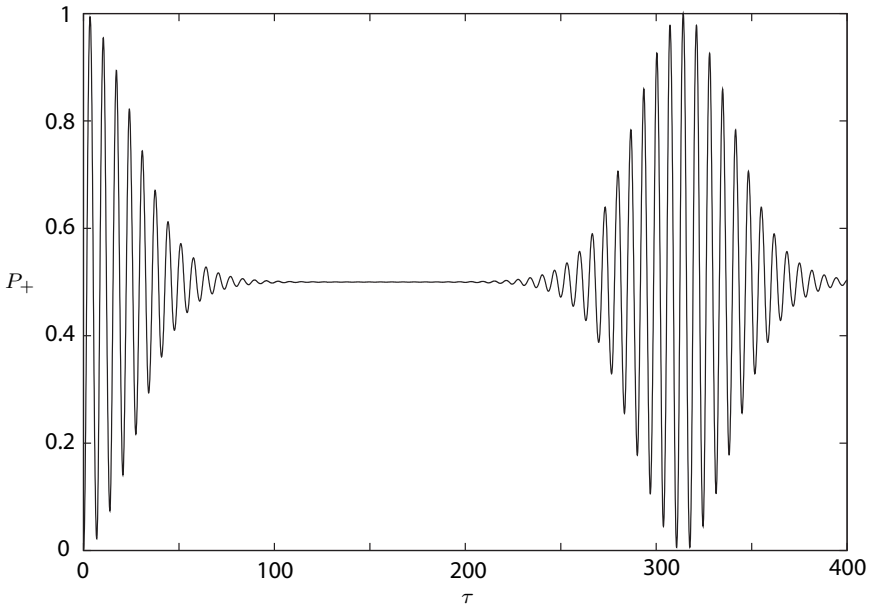

(a) $\chi = 0.01$, $\Omega/\omega_T = 1$.

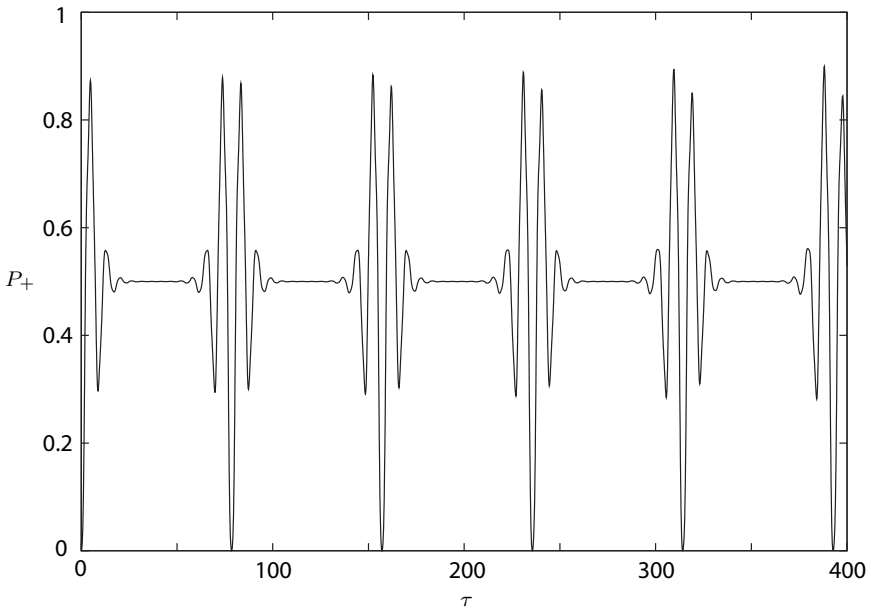

(b) $\chi = 0.04$, $\Omega/\omega_T = 1$.

Figure 3.4: The probability of finding the atom in the excited state as a function of the dimensionless time τ. As χ is increased, the revivals become more frequent and more abrupt.

As illustrated by the plots in Figure 3.4, the atomic excitation probability shows collapse and revival behaviour. The revivals are complete, and recur periodically with frequency

$$\omega_{\rm rev} \simeq \frac{\chi\Omega}{\omega_T};$$

each revival coincides with the arrival of $\langle\hat{a}\rangle$ at an extremum of its trajectory. In the limit $\chi \to 0$ (for finite Ω/ω_T) the time between revivals becomes infinite and the behaviour of the excitation probability reduces to the usual Rabi cycling.

3.2.4 Motional state Q function

Constructing the Q function for the motional state gives a better understanding of the behaviour of the operator moments, as well as providing a visual representation of the dynamics of the centre-of-mass of the atom. It is given by

$$Q_{\rm CM}(\alpha,\alpha^*) = \frac{1}{\pi}\langle\alpha|\hat{\rho}_{\rm CM}|\alpha\rangle$$

where $\hat{\rho}_{\rm CM}$ is the reduced density operator, obtained by taking the trace of the system density operator over the internal atomic states:

$$\begin{aligned}\hat{\rho}_{\rm CM} = {\rm tr}_{\rm A}(\hat{\rho}) &= \langle+|\hat{\rho}|+\rangle + \langle-|\hat{\rho}|-\rangle \\ &= |\phi_+\rangle\langle\phi_+| + |\phi_-\rangle\langle\phi_-|. \end{aligned} \tag{3.24}$$

The Q function is thus the sum of two terms:

$$\begin{aligned}Q^{\pm}_{\rm CM}(\alpha,\alpha^*) &= \frac{1}{\pi}|\langle\alpha|\phi_+\rangle|^2 + \frac{1}{\pi}|\langle\alpha|\phi_-\rangle|^2 \\ &\equiv Q^{+}_{\rm CM}(\alpha,\alpha^*) + Q^{-}_{\rm CM}(\alpha,\alpha^*). \end{aligned} \tag{3.25}$$

The explicit form of each term can be found by expanding the coherent and motional states in the number state basis; thus

$$Q^{\pm}_{\rm CM}(\alpha,\alpha^*) = \frac{e^{-|\alpha|^2}}{\pi}\left|\sum_n \frac{\tilde{c}^{\pm}_n(\alpha^*)^n}{\sqrt{n!}}\right|^2. \tag{3.26}$$

Figure 3.5 illustrates the time evolution of the Q function. Owing to the choice of initial state, the Q function starts off as a two-dimensional Gaussian centred at (ξ_0,μ_0). It then splits into two pieces, which rotate about the origin in opposite directions and eventually meet to form a single peak on the opposite side of the phase plane; their recombination coincides with the appearance of the first revival in the atomic excitation probability. This behaviour continues *ad infinitum*, with two collisions occurring for every complete circuit performed by each piece of the Q function.

The points at which these collisions occur do not remain stationary, but move gradually anticlockwise about the origin in the same manner as the trajectory of $\langle\hat{a}\rangle$. While we can do no more now than observe the existence of this precession and make an empirical estimate of its frequency, the analytic solutions presented in the next chapter will shed some light on its cause.

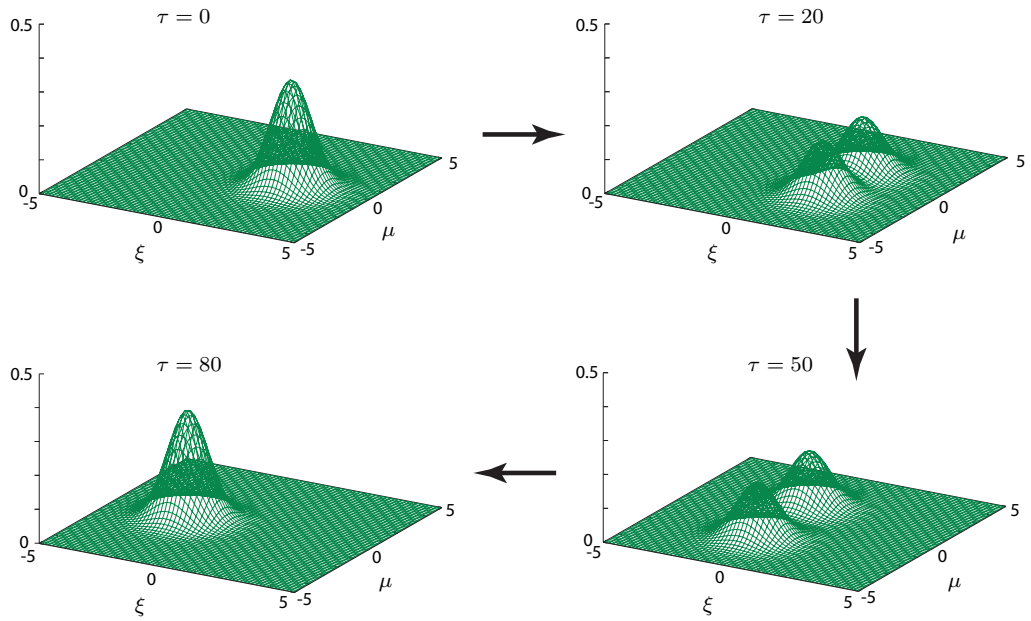

Figure 3.5: The motional state Q function for $\chi = 0.04$, $\Omega/\omega_T = 1$. This figure is representative of the Q function for a wide range of values of χ; the only difference is the time scale on which the dynamics occur. The rotation and precession slow down significantly as χ is reduced, and disappear for $\chi = 0$.

3.2.5 Motional state Wigner function

The Wigner function for the centre-of-mass state of the atom is most easily evaluated from its definition as the Fourier transform of the product of shifted wave functions. While there exist other methods of calculating the Wigner function, the rapid evaluation of Fourier transforms offered by the various incarnations of the Fast Fourier Transform (FFT) algorithm make this method highly efficient.

Working from the definition given by Eq. (2.122), we make a change of variables to the dimensionless position and momentum defined by Eq. (2.54):

$$\xi = \sqrt{\frac{m\omega}{2\hbar}}\, x \qquad \mu = \frac{1}{\sqrt{2\hbar m\omega}}\, p \tag{3.27}$$

and further define a dimensionless Fourier transform variable

$$\zeta \equiv \frac{1}{\pi}\sqrt{\frac{m\omega}{2\hbar}}\, y. \tag{3.28}$$

Substituting the reduced density operator according to Eq. (3.24) and noting that the phase-space volume transforms as

$$d\xi\, d\mu = \frac{1}{2\hbar}\, dx\, dp, \tag{3.29}$$

we find that the Wigner function is given by

$$W_{\mathrm{CM}}(\xi,\mu) = W^{+}_{\mathrm{CM}}(\xi,\mu) + W^{-}_{\mathrm{CM}}(\xi,\mu) \tag{3.30}$$

where

$$W^{\pm}_{\mathrm{CM}}(\xi,\mu) = \int_{-\infty}^{\infty} e^{-i2\pi\mu\zeta}\, \psi^{*}_{\pm}(\xi - \pi\zeta/2)\, \psi_{\pm}(\xi + \pi\zeta/2)\, d\zeta. \tag{3.31}$$

Here $\psi_{\pm}(\xi)$ are the wave functions of the atomic centre-of-mass states $|\phi_{\pm}\rangle$. The method used to calculate the Wigner function is discussed in Appendix E.3.

Since the Q function for a coherent state is simply a broadened version of the Wigner function, the behaviour of the two in the system at hand are essentially identical. Figure 3.6 illustrates the behaviour of the Wigner function.

The behaviour of the sum of the two pieces of the Wigner function is rather mundane, but an interesting feature appears when we look at each piece individually. As illustrated in Fig. 3.7, the individual Wigner function W^{-}_{CM} consists of two lumps corresponding to the two dressed motional states *and* a set of interference fringes between them. The presence of interference fringes shows that the system is in a coherent superposition of the two dressed motional states. This is consistent with the finding that the atomic centre-of-mass state collapses into a 'Schrödinger

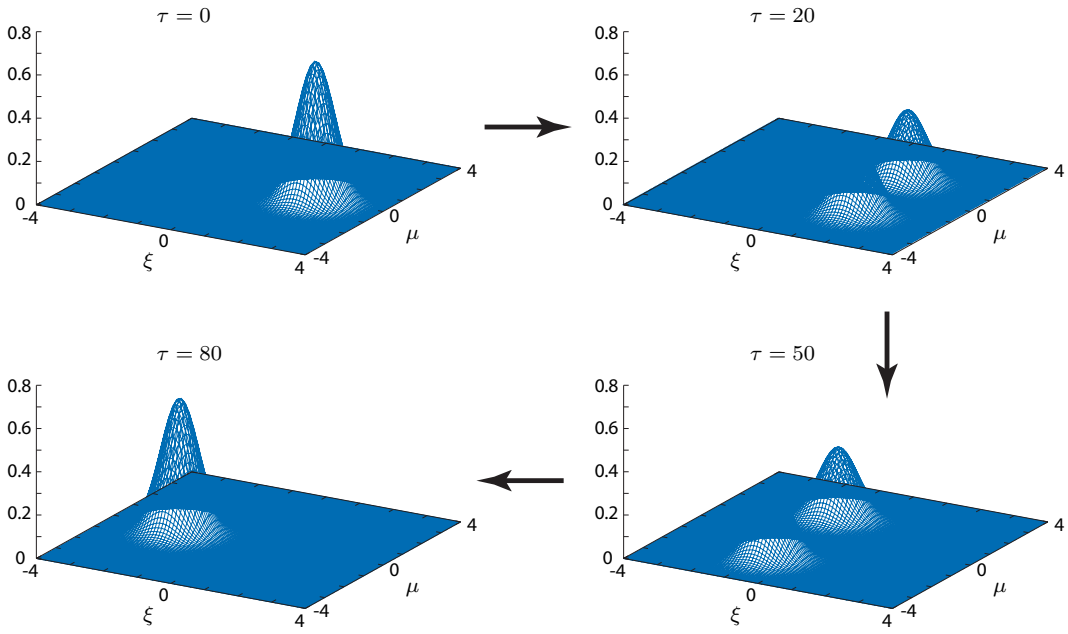

Figure 3.6: The motional state Wigner function for $\chi = 0.04$, $\Omega/\omega_T = 1$. The dynamics of the Wigner function are essentially identical to that of the Q function.

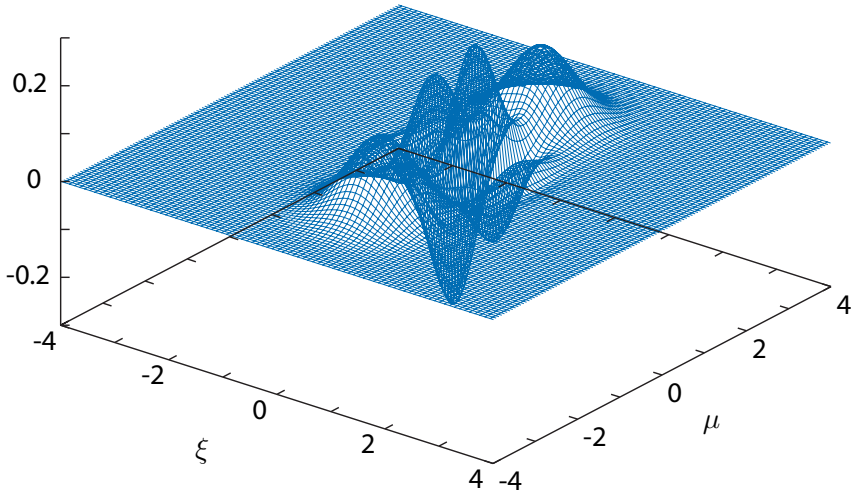

Figure 3.7: The Wigner function W^{-}_{CM} for $\chi = 0.04$, $\Omega/\omega_T = 1$, $\tau = 36$.

cat' state (that is, a superposition of two coherent states) after a measurement is made on the internal state of the atom [40].

The other piece of the Wigner function W^{+}_{CM} is identical, except that the interference fringes are π out of phase. When the two pieces are summed (the trace over the internal atom state taken), the interference fringes present in each piece precisely cancel out, leaving the Wigner function looking as it does in Fig. 3.6.

Chapter 4

An Analytic Approach to the System

While the numeric solutions presented in the previous chapter provide a valuable overview of the system dynamics, the insight they provide as to the cause of the behaviour is limited. With a view to achieving a deeper understanding, we therefore turn to an analytic investigation of the Hamiltonian.

The first section of this chapter outlines how the system Hamiltonian can be put into a diagonal form by a Bogoliubov transformation. This makes possible the derivation of analytic expressions for operator moments and phase space distributions, which are presented in the second part of the chapter.

4.1 Diagonalisation of the Hamiltonian

The starting point in our quest for analytic solutions is the Schrödinger picture Hamiltonian discussed in §3.1.2:

$$\hat{H} = \hbar\omega_T(\hat{a}^\dagger\hat{a} + \tfrac{1}{2}) + \frac{\hbar\omega_A}{2}\hat{\sigma}_z + \frac{\hbar\Omega}{2}\left(\hat{\sigma}_+ e^{-i\omega_A t} + \hat{\sigma}_- e^{i\omega_A t}\right)\left[1 - \chi(\hat{a} + \hat{a}^\dagger)^2\right],$$

where we have assumed that the laser is tuned to resonance with the atomic transition. In order to remove the time dependence from the interaction term, we make the transformation

$$\tilde{H} = e^{i\hat{H}_A t/\hbar}\,\hat{H}\,e^{-i\hat{H}_A t/\hbar} - \hat{H}_A \tag{4.1}$$

where $\hat{H}_A = \frac{1}{2}\hbar\omega_A\hat{\sigma}_z$ is the free Hamiltonian for the internal state of the atom; in this way we move into the interaction picture with respect to the internal atomic states only. We find

$$\tilde{H} = \hbar\omega_T(\hat{a}^\dagger\hat{a} + \tfrac{1}{2}) + \frac{\hbar\Omega}{2}(\hat{\sigma}_+ + \hat{\sigma}_-)\left[1 - \chi(\hat{a} + \hat{a}^\dagger)^2\right]. \tag{4.2}$$

4.1.1 A change of basis

To diagonalise the system Hamiltonian it is convenient to work in an atomic basis in which the interaction term is diagonal. This motivates a switch from the energy eigenstates $|\pm\rangle$ to the dressed atomic states discussed in §2.3.2:

$$|U\rangle \equiv \frac{1}{\sqrt{2}}\big(|+\rangle + |-\rangle\big) \tag{4.3a}$$

$$|L\rangle \equiv \frac{1}{\sqrt{2}}\big(|+\rangle - |-\rangle\big). \tag{4.3b}$$

In this basis the system state vector can be written as

$$|\psi(t)\rangle = \frac{1}{\sqrt{2}}\big(|\phi_U(t)\rangle|U\rangle + |\phi_L(t)\rangle|L\rangle\big), \tag{4.4}$$

where $|\phi_i(t)\rangle$ ($i \in \{U, L\}$) are the dressed motional states:

$$|\phi_U(t)\rangle \equiv |\phi_+(t)\rangle + |\phi_-(t)\rangle \tag{4.5a}$$

$$|\phi_L(t)\rangle \equiv |\phi_+(t)\rangle - |\phi_-(t)\rangle. \tag{4.5b}$$

4.1.2 $\tilde{H}$ separates into two pieces

Rewriting the Hamiltonian (Eq. (4.2)) in the dressed state basis gives

$$\begin{aligned}
\tilde{H} &= \hbar\omega_T(\hat{a}^\dagger\hat{a} + \tfrac{1}{2}) + \frac{\hbar\Omega}{2}\big(|U\rangle\langle U| - |L\rangle\langle L|\big)\left[1 - \chi(\hat{a} + \hat{a}^\dagger)^2\right] \\
&= \left[\hbar\big(\omega_T - \chi\Omega\big)(\hat{a}^\dagger\hat{a} + \tfrac{1}{2}) - \frac{\hbar\chi\Omega}{2}\left(\hat{a}^2 + \hat{a}^{\dagger 2}\right) + \frac{\hbar\Omega}{2}\right]|U\rangle\langle U| \\
&\quad + \left[\hbar\big(\omega_T + \chi\Omega\big)(\hat{a}^\dagger\hat{a} + \tfrac{1}{2}) + \frac{\hbar\chi\Omega}{2}\left(\hat{a}^2 + \hat{a}^{\dagger 2}\right) - \frac{\hbar\Omega}{2}\right]|L\rangle\langle L| \\
&\equiv \hat{H}_U \otimes |U\rangle\langle U| + \hat{H}_L \otimes |L\rangle\langle L|,
\end{aligned} \tag{4.6}$$

where we have used the fact that the Hamiltonian for the free centre-of-mass motion is multiplied by the identity operator in the internal-state space, which can be written as $|U\rangle\langle U| + |L\rangle\langle L|$. On the last line, the tensor product has been written explicitly to make it clear that the $\hat{H}_i$ act on the motional states while $|i\rangle\langle i|$ act on the internal states.

This separation of the Hamiltonian into two distinct pieces is a key step in obtaining analytic solutions, as it means that the motional dressed states evolve independently rather than being coupled together. This can be seen by considering the time evolution of the overall state:

$$\begin{aligned}
i\hbar\frac{d}{dt}\big(|\phi_U(t)\rangle|U\rangle + |\phi_L(t)\rangle|L\rangle\big) &= \tilde{H}\big(|\phi_U(t)\rangle|U\rangle + |\phi_L(t)\rangle|L\rangle\big) \\
&= \hat{H}_U|\phi_U(t)\rangle|U\rangle + \hat{H}_L|\phi_L(t)\rangle|L\rangle.
\end{aligned} \tag{4.7}$$

Multiplying from the left by $\langle i|$ gives the equation of motion for each motional state,

$$i\hbar\frac{d}{dt}|\phi_i(t)\rangle = \hat{H}_i|\phi_i(t)\rangle, \tag{4.8}$$

which may be straightforwardly integrated to give

$$|\phi_i(t)\rangle = e^{-i\hat{H}_i t/\hbar}|\phi_i(0)\rangle. \tag{4.9}$$

It is clear from this equation that the norm of each dressed motional state is constant. This contrasts with the behaviour of the norm of $|\phi_\pm\rangle$, which represents the probability to find the atom in the corresponding internal state and therefore oscillates between zero and one. It is interesting to note that

$$\langle\phi_U(t)|\phi_U(t)\rangle = \text{const.} = 1 + 2\text{Re}\big\{\langle\phi_+(t)|\phi_-(t)\rangle\big\} \tag{4.10a}$$
$$\langle\phi_L(t)|\phi_L(t)\rangle = \text{const.} = 1 - 2\text{Re}\big\{\langle\phi_+(t)|\phi_-(t)\rangle\big\} \tag{4.10b}$$

and so although the norm of $|\phi_\pm\rangle$ changes, the real part of the overlap $\langle\phi_+|\phi_-\rangle$ remains constant.

For the initial condition of a coherent motional state and an unexcited atom (Eq. 3.20) we find that

$$|\phi_U(0)\rangle = |\alpha_0\rangle, \qquad |\phi_L(0)\rangle = -|\alpha_0\rangle \tag{4.11}$$

so that each motional state is normalised to unity,

$$\langle\phi_i(t)|\phi_i(t)\rangle = \langle\phi_i(0)|\phi_i(0)\rangle = 1. \tag{4.12}$$

4.1.3 Diagonalising $\hat{H}_U$ and $\hat{H}_L$

Consider the two pieces of the system Hamiltonian defined in Eq. (4.6):

$$\hat{H}_U = \hbar(\omega_T - \chi\Omega)\big(\hat{a}^\dagger\hat{a} + \tfrac{1}{2}\big) - \frac{\hbar\chi\Omega}{2}\left(\hat{a}^2 + \hat{a}^{\dagger 2}\right) + \frac{\hbar\Omega}{2} \tag{4.13a}$$
$$\hat{H}_L = \hbar(\omega_T + \chi\Omega)\big(\hat{a}^\dagger\hat{a} + \tfrac{1}{2}\big) + \frac{\hbar\chi\Omega}{2}\left(\hat{a}^2 + \hat{a}^{\dagger 2}\right) - \frac{\hbar\Omega}{2}. \tag{4.13b}$$

In addition to a term describing the free oscillator, each piece of the Hamiltonian contains an interaction which is quadratic in $\hat{a}$ and $\hat{a}^\dagger$. Hamiltonians of this form appear in quantum optics in the analysis of squeezed light, and can be generated from a free oscillator Hamiltonian by applying a squeezing transformation (Eqs. (2.62)) to $\hat{a}$ and $\hat{a}^\dagger$. Consequently, $\hat{H}_U$ and $\hat{H}_L$ can be put into a diagonal form by making a Bogoliubov transformation of the system operators.

The details of the diagonalisation procedure are presented in Appendix D, and we shall simply state the results here. We introduce new operators $\hat{c}_i$ and $\hat{c}_i^\dagger$, defined as

$$\begin{pmatrix} \hat{c}_i \\ \hat{c}_i^\dagger \end{pmatrix} = \frac{1}{\sqrt{1-\eta_i^2}} \begin{pmatrix} 1 & -\eta_i \\ -\eta_i & 1 \end{pmatrix} \begin{pmatrix} \hat{a} \\ \hat{a}^\dagger \end{pmatrix} \tag{4.14}$$

where

$$\eta_i = \frac{-1+\sqrt{1-4g_i^2}}{2g_i} \tag{4.15a}$$

$$g_U = -\frac{\chi\Omega}{2(\omega_T - \chi\Omega)}, \qquad g_L = \frac{\chi\Omega}{2(\omega_T + \chi\Omega)}. \tag{4.15b}$$

These new operators are the result of the transformation

$$\hat{c}_i^{(\dagger)} = S^\dagger(\xi_i)\, \hat{a}^{(\dagger)} S(\xi_i) \tag{4.16}$$

where $S(x)$ is the squeezing operator and $\xi_i = \tanh^{-1}\eta_i$.

When written in terms of $\hat{c}$ and $\hat{c}^\dagger$ the two pieces of the system Hamiltonian become

$$\hat{H}_U = \hbar\omega_U(\hat{c}_U^\dagger \hat{c}_U + \tfrac{1}{2}) + \frac{\hbar\Omega}{2} \tag{4.17a}$$

$$\hat{H}_L = \hbar\omega_L(\hat{c}_L^\dagger \hat{c}_L + \tfrac{1}{2}) - \frac{\hbar\Omega}{2} \tag{4.17b}$$

where ω_U and ω_L are effective mode frequencies, given by

$$\omega_U = \omega_T\sqrt{1-2\frac{\chi\Omega}{\omega_T}} \tag{4.18a}$$

$$\omega_L = \omega_T\sqrt{1+2\frac{\chi\Omega}{\omega_T}}. \tag{4.18b}$$

The physical interpretation of this diagonalisation is that the atom-field interaction makes the oscillation frequency of the centre-of-mass of the atom *dependent on its internal state*. The magnitude of the frequency shift is governed by the strength of the interaction relative to the free evolution, as measured by the ratio $\chi\Omega/\omega_T$.

The dependence of the oscillation frequency on the internal state of the atom is the central result of the analytic solution, and the root cause of the interesting dynamics seen in the previous chapter. To see this, we note that the Rabi and trap frequencies are typically of similar magnitude, while working in the Lamb-Dicke regime means that χ is small; $\chi\Omega/\omega_T$ is therefore a small parameter, and the

oscillation frequencies can be expanded as a series:

$$\omega_U = \omega_T - \chi\Omega - \frac{(\chi\Omega)^2}{2\omega_T} - \frac{(\chi\Omega)^3}{6\omega_T^2} - \cdots \tag{4.19a}$$

$$\omega_L = \omega_T + \chi\Omega - \frac{(\chi\Omega)^2}{2\omega_T} + \frac{(\chi\Omega)^3}{6\omega_T^2} - \cdots . \tag{4.19b}$$

From these we define the sum and difference frequencies

$$\omega_+ \equiv \frac{\omega_L + \omega_U}{2} \approx \omega_T - \frac{\chi^2\Omega^2}{2\omega_T} \tag{4.20a}$$

$$\omega_- \equiv \frac{\omega_L - \omega_U}{2} \approx \chi\Omega + \frac{\chi^3\Omega^3}{6\omega_T^2}, \tag{4.20b}$$

the relevance of which becomes clear when we recall the approximate frequencies appearing in the numeric solutions of $\langle\hat{a}\rangle$ and P_+:

$$\omega_{\text{bounce}} \approx 2, \qquad \omega_{\text{rev}} \approx \frac{\chi\Omega}{\omega_T}, \qquad \omega_{\text{prec}} \approx \frac{\chi^2\Omega^2}{2\omega_T^2}. \tag{4.21}$$

We see that, up to a factor of ω_T, which reflects the fact that the numeric solutions were evaluated with respect to the scaled time $\tau \equiv \omega_T t$, the empirically-obtained bounce, revival and precession frequencies are first-order approximations to $\omega_T + \omega_+$, ω_- and $\omega_T - \omega_+$, respectively.

We are now in a position to derive analytic expressions for the operator moments and phase-space distributions investigated numerically in the previous chapter.

4.2 Operator moments

The analytic expressions for the operator moments turn out to be fairly complicated, and to extract the key features of the solutions it is a good idea to make some approximations. We can use the fact that $\chi\Omega \ll \omega_T$ to write

$$\eta_U = -\eta_L \approx \frac{\chi\Omega}{2\omega_T} \equiv \eta, \qquad \eta_i^2 \approx 0. \tag{4.22}$$

4.2.1 Complex amplitude of the oscillator

The expectation value of $\hat{a}$ is given by

$$\begin{aligned}\langle\hat{a}\rangle &= \langle\psi(t)|\hat{a}|\psi(t)\rangle \\ &= \frac{1}{2}\big[\langle\phi_L(t)|\hat{a}|\phi_L(t)\rangle + \langle\phi_U(t)|\hat{a}|\phi_U(t)\rangle\big] \\ &\equiv \frac{1}{2}\big[\langle\hat{a}\rangle_L + \langle\hat{a}\rangle_U\big],\end{aligned} \tag{4.23}$$

where we have expanded the state $|\psi(t)\rangle$ according to Eq. (4.4) and used the orthogonality of the atomic dressed states. To evaluate each term on the right hand side, we invert the transformation described by Eq. (4.14) and write $\hat{a}$ in terms of $\hat{c}$ and $\hat{c}^\dagger$:

$$\langle \hat{a} \rangle_i = \frac{1}{\sqrt{1-\eta_i^2}} \left[\langle \phi_i(t) | \hat{c}_i | \phi_i(t) \rangle + \eta_i \langle \phi_i(t) | \hat{c}_i^\dagger | \phi_i(t) \rangle \right]. \tag{4.24}$$

This is a useful step because the time evolution operators that take $|\phi_i(0)\rangle$ to $|\phi_i(t)\rangle$ (see Eq. (4.9)) act simply on $\hat{c}$ and $\hat{c}^\dagger$, transforming them according to

$$e^{i\omega_i t\, \hat{c}_i^\dagger \hat{c}_i}\, \hat{c}_i\, e^{-i\omega_i t\, \hat{c}_i^\dagger \hat{c}_i} = \hat{c}_i\, e^{-i\omega_i t}. \tag{4.25}$$

Applying the initial conditions (Eq. (4.11)) and transforming back to $\hat{a}$ and $\hat{a}^\dagger$, we can evaluate Eq. (4.23) to find

$$\begin{aligned} \langle \hat{a} \rangle = \frac{1}{2} \Bigg[& \frac{1}{1-\eta_U^2} \left(\alpha_0 (e^{-i\omega_U t} - \eta_U^2 e^{i\omega_U t}) + 2i\eta_U \alpha_0^* \sin \omega_U t \right) \\ & + \frac{1}{1-\eta_L^2} \left(\alpha_0 (e^{-i\omega_L t} - \eta_L^2 e^{i\omega_L t}) + 2i\eta_L \alpha_0^* \sin \omega_L t \right) \Bigg] \end{aligned} \tag{4.26}$$

In order to compare this analytic solution with the numeric solution discussed earlier, we must remove the free evolution by multiplying by $e^{i\omega_T t}$. Assuming for simplicity a real value of α_0 and applying the approximations of Eq. (4.22), we find

$$\begin{aligned} \mathrm{Re}\left\{ \langle \hat{a} \rangle e^{i\omega_T t} \right\} \approx\ & \alpha_0 \cos(\omega_{\mathrm{rev}} t) \cos(\omega_{\mathrm{prec}} t) \\ & - \alpha_0 \eta \sin(\omega_{\mathrm{rev}} t) \left[\sin(\omega_{\mathrm{prec}} t) + \sin(\omega_{\mathrm{bounce}} t) \right] \qquad (4.27a) \\ \mathrm{Im}\left\{ \langle \hat{a} \rangle e^{i\omega_T t} \right\} \approx\ & \alpha_0 \cos(\omega_{\mathrm{rev}} t) \sin(\omega_{\mathrm{prec}} t) \\ & + \alpha_0 \eta \sin(\omega_{\mathrm{rev}} t) \left[\cos(\omega_{\mathrm{prec}} t) + \cos(\omega_{\mathrm{bounce}} t) \right]. \qquad (4.27b) \end{aligned}$$

where we have introduced the frequencies (ordered from largest to smallest)

$$\omega_{\mathrm{bounce}} \equiv \omega_T + \frac{\omega_L + \omega_U}{2} \tag{4.28a}$$

$$\omega_{\mathrm{rev}} \equiv \frac{\omega_L - \omega_U}{2} \tag{4.28b}$$

$$\omega_{\mathrm{prec}} \equiv \omega_T - \frac{\omega_L + \omega_U}{2}. \tag{4.28c}$$

The first term of the solution given by Eqs. (4.27) describes the gross motion of $\langle \hat{a} \rangle$, consisting of an oscillatory term representing the back and forth motion multiplied by a slowly-varying term describing the precession. The second piece describes a high-frequency oscillation, which represents the bounces traced out by $\langle \hat{a} \rangle$ as it moves from one side of the phase plane to the other; the amplitude of these bounces changes on both the revival and precession time scales.

4.2.2 Average phonon number

In finding the mean occupation level of the trap, it turns out to be convenient to work with $\hat{a}^\dagger\hat{a}+\frac{1}{2}$ rather than with $\hat{a}^\dagger\hat{a}$, as the structure of the Bogoliubov transformation means that the former is marginally simpler when written in terms of $\hat{c}$ and $\hat{c}^\dagger$. We find

$$\begin{aligned}\langle\hat{a}^\dagger\hat{a}+\tfrac{1}{2}\rangle &= \langle\psi(t)|\hat{a}^\dagger\hat{a}+\tfrac{1}{2}|\psi(t)\rangle \\ &= \frac{1}{2}\Big[\langle\hat{a}^\dagger\hat{a}+\tfrac{1}{2}\rangle_U + \langle\hat{a}^\dagger\hat{a}+\tfrac{1}{2}\rangle_L\Big]. \end{aligned} \tag{4.29}$$

The technique used to evaluate each term is identical to that used in the calculation of $\langle\hat{a}\rangle_i$; only the algebra is a little messier. We arrive at

$$\begin{aligned}\langle\hat{a}^\dagger\hat{a}+\tfrac{1}{2}\rangle_i = \frac{1}{\left(1-\eta_i^2\right)^2}\Big\{&\left[|\alpha_0|^2+\tfrac{1}{2}\right]\left[(1+\eta_i^2)^2-4\eta_i^2\cos 2\omega_i t\right] \\ &-4|\alpha_0|^2\eta_i\sin\omega_i t\left[\eta_i^2\sin(\omega_i t+2\phi_0)+\sin(\omega_i t-2\phi_0)\right]\Big\}\end{aligned} \tag{4.30}$$

where the amplitude of the initial coherent state has been written as $\alpha_0 = |\alpha_0|\,e^{i\phi_0}$.

After making the approximations of Eq. (4.22) we find

$$\langle\hat{a}^\dagger\hat{a}\rangle = |\alpha_0|^2\left\{1-\frac{\chi\Omega}{\omega_T}\sin(2\omega_+ t)\sin(2\omega_- t)\right\}. \tag{4.31}$$

The interpretation of this solution is straightforward; superimposed on the constant $|\alpha_0|^2$ term is a high-frequency oscillation with a slowly-varying amplitude. This is precisely the behaviour seen in the numeric solutions in §3.2.2.

4.2.3 Atomic excitation probability

The atomic excitation probability is given by

$$\begin{aligned}P_+(t) &= \langle\phi_+(t)|\phi_+(t)\rangle \\ &= \frac{1}{4}\sum_{i,j=U,L}\langle\phi_i(t)|\phi_j(t)\rangle \\ &= \frac{1}{2}\Big[1+\mathrm{Re}\big\{\langle\phi_U(t)|\phi_L(t)\rangle\big\}\Big]\end{aligned} \tag{4.32}$$

where the normalisation of the dressed motional states has been used. The probability of finding the atom in the excited state depends on the overlap of the dressed motional states.

To evaluate this overlap we use Eq. (4.9) to write

$$\begin{aligned}|\phi_i(t)\rangle &= e^{\mp i\Omega t/2}\,e^{-i\omega_i t(\hat{c}_i^\dagger\hat{c}_i+\frac{1}{2})}|\phi_i(0)\rangle \\ &= e^{\mp i\Omega t/2}\,S^\dagger(\xi_i)\,e^{-i\omega_i t(\hat{a}^\dagger\hat{a}+\frac{1}{2})}S(\xi_i)|\phi_i(0)\rangle,\end{aligned} \tag{4.33}$$

where the second line follows because the squeezing operator is unitary. Equation (4.33) in conjunction with the initial conditions gives

$$\begin{aligned}\langle\phi_U(t)|\phi_L(t)\rangle = -e^{i\Omega t}\langle\alpha_0|S^\dagger(\xi_U)\, e^{i\omega_U t(\hat{a}^\dagger\hat{a}+\frac{1}{2})}S(\xi_U)\\ \times S^\dagger(\xi_L)e^{-i\omega_L t(\hat{a}^\dagger\hat{a}+\frac{1}{2})}S(\xi_L)|\alpha_0\rangle.\end{aligned} \tag{4.34}$$

In theory, there is nothing preventing us from evaluating this expression by the same operator reordering process used to evaluate the Q function in §4.3.1 – it has twice as many terms, but a very similar structure. In practice, however, we find that the quantity of algebra scales in such a way that a two-fold increase in the number of terms leads to a calculation which is several orders of magnitude messier.

Fortunately, we can evaluate the overlap by a somewhat simpler method. Inserting the identity as an integral over coherent states (see Eq. (2.44)) between $S(\xi_U)$ and $S^\dagger(\xi_L)$ in Eq. (4.34) puts the overlap into the form

$$\begin{aligned}\langle\phi_U(t)|\phi_L(t)\rangle = -\frac{1}{\pi}\, e^{i\Omega t}\int d^2\beta\, \langle\alpha_0|S^\dagger(\xi_U)\, e^{i\omega_U t(\hat{a}^\dagger\hat{a}+\frac{1}{2})}S(\xi_U)|\beta\rangle\\ \times \langle\beta|S^\dagger(\xi_L)e^{-i\omega_L t(\hat{a}^\dagger\hat{a}+\frac{1}{2})}S(\xi_L)|\alpha_0\rangle.\end{aligned}$$

The advantage this provides is that each term on the right hand side has exactly the same form as one arising in the calculation of the Q-function (see Eq. (4.38)), saving us a lot of operator reordering. The obvious disadvantage is that we have to carry out the integration over β. However, the trade turns out to be worthwhile, since although the algebra is messy, the integrals are Gaussian and can be readily evaluated.

After rather a lot of algebra, we arrive at

$$\langle\phi_U(t)|\phi_L(t)\rangle = e^{i\Omega t}\frac{C_0}{\sqrt{ab}}\exp\left[-\frac{\left(\alpha_0^* e^{-i\omega_U t}\lambda_U - \alpha_0 e^{i\omega_L t}\lambda_L\right)^2}{4+2\eta_L(1-\lambda_L)+2\eta_U(1-\lambda_U)}\right]\exp\left[\frac{c^2}{4b}\right] \tag{4.35}$$

where

$$\begin{aligned}C_0 &= \sqrt{\lambda_U\lambda_L}\, e^{i(\omega_L-\omega_U)t/2}\exp\left[-|\alpha_0|^2+\alpha_0^{*2}\frac{\eta_U}{2}(1-\lambda_U)+\alpha_0^2\frac{\eta_L}{2}(1-\lambda_L)\right]\\ a &\equiv 1+\frac{\eta_L}{2}(1-\lambda_L)+\frac{\eta_U}{2}(1-\lambda_U)\\ b &\equiv 1-\frac{\eta_L}{2}(1-\lambda_L)-\frac{\eta_U}{2}(1-\lambda_U)+\frac{\left(\eta_U(1-\lambda_U)-\eta_L(1-\lambda_L)\right)^2}{4+2\eta_L(1-\lambda_L)+2\eta_U(1-\lambda_U)}\end{aligned}$$

and

$$\begin{aligned}c = {}& \alpha_0^* e^{-i\omega_U t}\lambda_U + \alpha_0 e^{i\omega_L t}\lambda_L\\ & - \frac{\left(\eta_U(1-\lambda_U)-\eta_L(1-\lambda_L)\right)\left(\alpha_0^* e^{-i\omega_U t}\lambda_U - \alpha_0 e^{i\omega_L t}\lambda_L\right)}{2+\eta_L(1-\lambda_L)+\eta_U(1-\lambda_U)}\end{aligned}$$

with

$$\lambda_L \equiv \frac{1-\eta_L^2}{e^{2i\omega_L t}-\eta_L^2}, \qquad \lambda_U \equiv \frac{1-\eta_U^2}{e^{-2i\omega_U t}-\eta_U^2}.$$

This formula is fairly impenetrable; even taking $\eta_i^2 = 0$ does not simplify it enough to permit a straightforward interpretation. We must simply be content with stating that it reproduces the collapse and revival behaviour seen in the numeric solutions.

4.3 Phase-space distributions

4.3.1 The Q function

Recall that the Q function for the motional state is given by

$$Q_{\mathrm{CM}}(\alpha,\alpha^*) = \frac{1}{\pi}\langle\alpha|\hat{\rho}_{\mathrm{CM}}|\alpha\rangle \tag{4.36}$$

where $\hat{\rho}_{\mathrm{CM}}$ is the reduced density operator obtained by tracing over the internal states of the atom. In the dressed state basis

$$\hat{\rho}_{\mathrm{CM}} = \frac{1}{2}\big[|\phi_U(t)\rangle\langle\phi_U(t)| + |\phi_L(t)\rangle\langle\phi_L(t)|\big],$$

and we find

$$Q_{\mathrm{CM}}(\alpha,\alpha^*) = \frac{1}{2\pi}\big(Q^U_{\mathrm{CM}}(\alpha,\alpha^*) + Q^L_{\mathrm{CM}}(\alpha,\alpha^*)\big) \tag{4.37}$$

where

$$\begin{aligned} Q^i_{\mathrm{CM}}(\alpha,\alpha^*) &= |\langle\alpha|\phi_i(t)\rangle|^2 \\ &= |\langle\alpha|e^{-i\hat{H}_i t/\hbar}|\alpha_0\rangle|^2. \end{aligned} \tag{4.38}$$

The two pieces of the Q function correspond to the two peaks seen in the numeric solutions (see Fig. 3.5), each peak being due to a single dressed motional state of the atom.

In order to evaluate each piece of the Q function we need to rearrange the exponential appearing in Eq. (4.38) so that all the $\hat{a}$ operators appear to the right of the $\hat{a}^\dagger$ operators – that is, we must put the time-evolution operator into its *normally ordered* form. We begin by writing the Hamiltonian in terms of $\hat{a}$ and $\hat{a}^\dagger$:

$$\begin{aligned} e^{-i\hat{H}_i t/\hbar} &= e^{-i\omega_i t(\hat{c}_i^\dagger\hat{c}_i+\frac{1}{2})} \\ &= e^{-i\omega_i t S^\dagger(\xi_i)(\hat{a}^\dagger\hat{a}+\frac{1}{2})S(\xi_i)} \\ &= S^\dagger(\xi_i)e^{-i\omega_i t(\hat{a}^\dagger\hat{a}+\frac{1}{2})}S(\xi_i), \end{aligned} \tag{4.39}$$

where the last line follows because the squeezing operator is unitary, and we have dropped the phase factor produced by the $\pm\hbar\Omega/2$ terms in the Hamiltonian because they contribute nothing to the magnitude of the expression. Writing the squeezing operators out explicitly, we have

$$e^{-i\hat{H}_i t/\hbar} = \exp\left[-\frac{\xi_i}{2}(\hat{a}^2 - \hat{a}^{\dagger 2})\right] \exp\left[-i\omega_i t(\hat{a}^\dagger \hat{a} + \tfrac{1}{2})\right] \exp\left[\frac{\xi_i}{2}(\hat{a}^2 - \hat{a}^{\dagger 2})\right]. \quad (4.40)$$

To proceed any further, we need to unravel the squeezing operators and move the resulting terms in $\hat{a}$ and $\hat{a}^\dagger$ to the correct side of the central exponential. To this end, we state several useful operator ordering relationships; firstly

$$\begin{aligned}\exp\left[\kappa(\hat{a}^2 - \hat{a}^{\dagger 2})\right] = \exp\left[-\frac{\tanh 2\kappa}{2}\hat{a}^{\dagger 2}\right] \exp\left[-(\hat{a}^\dagger \hat{a} + \tfrac{1}{2})\ln(\cosh 2\kappa)\right] \\ \times \exp\left[\frac{\tanh 2\kappa}{2}\hat{a}^2\right], \end{aligned} \quad (4.41)$$

secondly

$$\begin{aligned}\exp\left[\kappa \hat{a}^2\right] \exp\left[\lambda \hat{a}^{\dagger 2}\right] = \exp\left[\frac{2\lambda}{1-4\kappa\lambda}\hat{a}^{\dagger 2}\right] \exp\left[-\ln(1-4\kappa\lambda)(\hat{a}^\dagger \hat{a} + \tfrac{1}{2})\right] \\ \times \exp\left[-\frac{2\kappa}{1-4\kappa\lambda}\hat{a}^2\right], \end{aligned} \quad (4.42)$$

and finally

$$\exp\left[\beta\, \hat{a}^\dagger \hat{a}\right] = :\exp\left[(e^\beta - 1)\, \hat{a}^\dagger \hat{a}\right]: \quad (4.43)$$

where $:f(\hat{a}, \hat{a}^\dagger):$ indicates the normally-ordered form of $f(\hat{a}, \hat{a}^\dagger)$. These relationships are proved in Appendix B.

Returning to Eq. (4.40), we decompose the squeezing operators and find

$$\begin{aligned} e^{-i\hat{H}_i t/\hbar} = \exp\left[\frac{\eta_i}{2}\hat{a}^{\dagger 2}\right] \exp\left[-\ln(\cosh \xi_i)\left(\hat{a}^\dagger \hat{a} + \tfrac{1}{2}\right)\right] \exp\left[-\frac{\eta_i}{2}\hat{a}^2\right] \\ \times \exp\left[-i\omega_i t\left(\hat{a}^\dagger \hat{a} + \tfrac{1}{2}\right)\right] \\ \times \exp\left[-\frac{\eta_i}{2}\hat{a}^{\dagger 2}\right] \exp\left[-\ln(\cosh \xi_i)\left(\hat{a}^\dagger \hat{a} + \tfrac{1}{2}\right)\right] \exp\left[\frac{\eta_i}{2}\hat{a}^2\right]. \end{aligned} \quad (4.44)$$

Moving the exponentials of $\hat{a}^2$ and $\hat{a}^{\dagger 2}$ to the right and left respectively and normally-

ordering the central exponential, we arrive at

$$\begin{aligned} e^{-i\hat{H}_i t/\hbar} = \; & e^{-i\omega_i t/2} \frac{1}{\cosh\xi_i \sqrt{1-\eta_i^2 e^{-2i\omega_i t}}} \\ & \times \exp\left[\frac{\eta_i}{2}\left(1-\frac{1}{\cosh^2\xi_i(e^{2i\omega_i t}-\eta_i^2)}\right)\hat{a}^{\dagger 2}\right] \\ & \times :\exp\left[-\hat{a}^\dagger\hat{a}\left(1-\frac{e^{-i\omega_i t}}{\cosh^2\xi_i\left(1-\eta_i^2 e^{-2i\omega_i t}\right)}\right)\right]: \\ & \times \exp\left[\frac{\eta_i}{2}\left(1-\frac{1}{\cosh^2\xi_i(e^{2i\omega_i t}-\eta_i^2)}\right)\hat{a}^2\right]. \end{aligned} \tag{4.45}$$

The matrix element in Eq. (4.38) can now be evaluated by acting the annihilation operators to the right and the creation operators to the left. We obtain for each piece of the Q function

$$Q^i_{\rm CM}(\alpha,\alpha^*) = e^{-|\alpha-\alpha_0|^2}|q_i|^2 \tag{4.46}$$

with

$$\begin{aligned} q_i = & \sqrt{\frac{1-\eta_i^2}{1-\eta_i^2\, e^{-2i\omega_i t}}}\, \exp\left[\frac{\eta_i}{2}\left(1-\frac{1-\eta_i^2}{e^{2i\omega_i t}-\eta_i^2}\right)\left(\alpha^{*2}+\alpha_0^2\right)\right] \\ & \times \exp\left[-\alpha_0\alpha^*\left(1-\frac{e^{i\omega_i t}(1-\eta_i^2)}{e^{2i\omega_i t}-\eta_i^2}\right)\right], \end{aligned}$$

where we have used the fact that

$$\cosh\xi_i = \cosh(\tanh^{-1}\eta_i) = \frac{1}{\sqrt{1-\eta_i^2}}.$$

We need not understand the details of Eq. (4.46) to be able to explain the behaviour of the Q function seen in Fig. 3.5. The two peaks, each corresponding to a single dressed motional state, rotate around the origin with different frequencies. $Q^U_{\rm CM}$ moves at a slightly lower frequency than ω_T, while $Q^L_{\rm CM}$ moves at a slightly higher frequency. Working in the interaction picture corresponds to observing the motion from a reference frame rotating at ω_T; from this frame the peaks appear to move in opposite directions, meeting periodically on alternating sides of the phase plane. The precession of this meeting point about the origin is due to the fact that ω_U and ω_L are not symmetrically placed about ω_T; the margin separating ω_U from ω_T is greater than the margin separating ω_L from ω_T (see Eqs. (4.19)). However, the difference is small, appearing only at second order in $\chi\Omega/\omega_T$.

4.3.2 The Wigner function

Substituting the reduced density operator into the definition of the Wigner function (Eq. (2.119)) gives

$$W_{\rm CM}(\alpha,\alpha^*) = \frac{1}{2}\big(W^U_{\rm CM}(\alpha,\alpha^*) + W^L_{\rm CM}(\alpha,\alpha^*)\big) \tag{4.47}$$

where

$$W^i_{\rm CM}(\alpha,\alpha^*) = \frac{1}{\pi^2}\int d^2z\, \langle\phi_i(t)|e^{iz^*\hat{a}^\dagger + iz\hat{a}}|\phi_i(t)\rangle\, e^{-iz^*\alpha^*}e^{-iz\alpha}. \tag{4.48}$$

The first step in evaluating this expression is to calculate the matrix element which appears in the integrand. This can be written as

$$\begin{aligned}\langle\phi_i(t)|e^{iz^*\hat{a}^\dagger + iz\hat{a}}|\phi_i(t)\rangle = e^{-\frac{1}{2}|z|^2}\langle\alpha_0|S^\dagger(\xi_i)\,e^{i\omega_i t(\hat{a}^\dagger\hat{a}+\frac{1}{2})}S(\xi_i)\,e^{iz^*\hat{a}^\dagger} \\ \times\; e^{iz\hat{a}}\,S^\dagger(\xi_i)e^{-i\omega_i t(\hat{a}^\dagger\hat{a}+\frac{1}{2})}S(\xi_i)|\alpha_0\rangle\end{aligned} \tag{4.49}$$

and can be evaluated by using the squeezing and time-evolution operators to transform the $\hat{a}$ and $\hat{a}^\dagger$ operators which appear in the central exponentials. Making the first transformation, we find

$$\begin{aligned}&\langle\phi_i(t)|e^{iz^*\hat{a}^\dagger + iz\hat{a}}|\phi_i(t)\rangle \\ &\quad= \; e^{-\frac{1}{2}|z|^2}\langle\alpha_0|S^\dagger(\xi_i)e^{i\omega_i t(\hat{a}^\dagger\hat{a}+\frac{1}{2})}\exp\left[\frac{iz^*}{\sqrt{1-\eta_i^2}}(\hat{a}^\dagger+\eta_i\hat{a})\right] \\ &\qquad\times\exp\left[\frac{iz}{\sqrt{1-\eta_i^2}}(\hat{a}+\eta_i\hat{a}^\dagger)\right]e^{-i\omega_i t(\hat{a}^\dagger\hat{a}+\frac{1}{2})}S(\xi_i)|\alpha_0\rangle.\end{aligned} \tag{4.50}$$

Regrouping the central terms gives

$$\begin{aligned}&\langle\phi_i(t)|e^{iz^*\hat{a}^\dagger + iz\hat{a}}|\phi_i(t)\rangle \\ &\quad= \; \exp\left[-\frac{\eta_i(z^2+z^{*2})}{2(1-\eta_i^2)}\right]\exp\left[-\frac{|z|^2}{2}\left(\frac{1+\eta_i^2}{1-\eta_i^2}\right)\right] \\ &\qquad\times\langle\alpha_0|S^\dagger(\xi_i)e^{i\omega_i t(\hat{a}^\dagger\hat{a}+\frac{1}{2})}\exp\left[\frac{i(z^*+\eta_i z)}{\sqrt{1-\eta_i^2}}\,\hat{a}^\dagger\right] \\ &\qquad\times\exp\left[\frac{i(z+\eta_i z^*)}{\sqrt{1-\eta_i^2}}\,\hat{a}\right]e^{-i\omega_i t(\hat{a}^\dagger\hat{a}+\frac{1}{2})}S(\xi_i)|\alpha_0\rangle.\end{aligned} \tag{4.51}$$

Evaluating the remaining transformations and applying $\hat{a}$ and $\hat{a}^\dagger$ to the states, we arrive at

$$\begin{aligned}
&\langle\phi_i(t)|e^{iz^*\hat{a}^\dagger+iz\hat{a}}|\phi_i(t)\rangle \\
&\quad= \exp\left[-\frac{\eta_i(z^2+z^{*2})}{2(1-\eta_i^2)}\right]\exp\left[-\frac{|z|^2}{2}\left(\frac{1+\eta_i^2}{1-\eta_i^2}\right)\right]\exp\left[\frac{\eta_i(z^*+\eta_i z)^2 e^{2i\omega_i t}}{2(1-\eta_i^2)^2}\right] \\
&\qquad\times\exp\left[\frac{\eta_i(z+\eta_i z^*)^2}{2(1-\eta_i^2)^2}e^{-2i\omega_i t}\right]\exp\left[-\eta_i^2\frac{(z^*+\eta_i z)(z+\eta_i z^*)}{(1-\eta_i^2)^2}\right] \\
&\qquad\times\exp\left[\frac{i\alpha_0}{1-\eta_i^2}\left(e^{-i\omega_i t}(z+\eta_i z^*)-\eta_i e^{i\omega_i t}(z^*+\eta_i z)\right)\right] \\
&\qquad\times\exp\left[\frac{i\alpha_0^*}{1-\eta_i^2}\left(e^{i\omega_i t}(z^*+\eta_i z)-\eta_i e^{-i\omega_i t}(z+\eta_i z^*)\right)\right]. \qquad (4.52)
\end{aligned}$$

As for the Q function, carrying out the integration proves to be messy but straightforward. We eventually find

$$W^i_{\mathrm{CM}}(\alpha,\alpha^*)=\frac{1}{\pi\sqrt{ab}}\exp\left[\frac{d^2}{4b}\right]\exp\left[\frac{c^2}{4a}\right] \qquad (4.53)$$

with

$$\begin{aligned}
a=&\ \frac{1}{2(1-\eta_i^2)^2}\left[(1-\eta_i^2)^2-4\eta_i(1-\eta_i)^2\sin^2\omega_i t\right] \\
b=&\ \frac{1}{2(1-\eta_i^2)^2}\left[(1-\eta_i^2)^2+4\eta_i(1+\eta_i)^2\sin^2\omega_i t\right] \\
&-\frac{2\eta_i^2\sin^2 2\omega_i t}{(1-\eta_i^2)^2-4\eta_i(1-\eta_i)^2\sin^2\omega_i t} \\
c=&\ \alpha-\alpha^*+\frac{\alpha_0^*}{1-\eta_i^2}\left[e^{i\omega_i t}-\eta_i^2 e^{-i\omega_i t}-2i\eta_i\sin\omega_i t\right] \\
&-\frac{\alpha_0}{1-\eta_i^2}\left[e^{-i\omega_i t}-\eta_i^2 e^{i\omega_i t}+2i\eta_i\sin\omega_i t\right]
\end{aligned}$$

and

$$\begin{aligned}
d=&\ -i(\alpha+\alpha^*+D+D^*) \\
&+\frac{2\eta_i\sin(2\omega_i t)(1-\eta_i^2)}{(1-\eta_i^2)^2-4\eta_i(1-\eta_i)^2\sin^2\omega_i t}\left[\alpha-\alpha^*-D+D^*\right]
\end{aligned}$$

where

$$D=\frac{\alpha_0}{1-\eta_i^2}\left(e^{-i\omega_i t}-\eta_i^2 e^{i\omega_i t}-2i\eta_i\sin\omega_i t\right).$$

The behaviour of the Wigner function is similar to that of the Q-function, with two peaks corresponding to the two motional dressed states rotating in opposite directions about the origin.

4.4 Summary

The most important points of this chapter can be summarised as follows.

- By switching to the atomic dressed state basis, the Hamiltonian can be separated into two pieces, each of which governs the evolution of an individual motional state. The pieces each have the form of a squeezing Hamiltonian, and can be diagonalised by making a Bogoliubov transformation of the $\hat{a}$ and $\hat{a}^\dagger$ operators.
- The atom-field interaction makes the frequency of oscillation different for each motional dressed state – one oscillates at a slightly higher frequency than ω_T, the other at a slightly lower frequency. This state-dependent frequency shift is the cause of the behaviour seen in the numerical solutions.
- Diagonalising the two pieces of the Hamiltonian makes it possible to find analytic expressions for various quantities of interest. While some of these are fairly convoluted, they reproduce the numerical solutions seen in the previous chapter.

Chapter 5

Extending the Model

The model analysed in this thesis is a fairly simple one, and it may easily be extended in a number of ways. This chapter presents the results of two such extensions. In the first section, the analytic solutions derived in the previous chapter are extended to include an arbitrary trap position on the standing wave, while the second section investigates the effect of retaining in the Hamiltonian the previously discarded higher order terms in χ.

5.1 Varying the trap position

The analysis of the system up to this point has assumed that the minimum of the trapping potential is aligned with an antinode of the standing wave. This restriction can be lifted by making the replacement

$$\cos k\hat{x} \to \cos(k\hat{x} + \delta), \tag{5.1}$$

where δ describes the offset of the trap centre from an antinode of the standing wave. The symmetry of the situation means we need only consider values of δ between zero (the trap is aligned with an antinode) and $\pi/2$ (the trap is aligned with a node); values of δ outside this range give solutions which are identical up to a phase factor of π.

Making this replacement, the system Hamiltonian in the Schrödinger picture is given by (cf. Eq. (3.9))

$$\hat{H} = \hbar\omega_T(\hat{a}^\dagger\hat{a} + \tfrac{1}{2}) + \frac{\hbar\omega_A}{2}\hat{\sigma}_z + \frac{\hbar\Omega}{2}\left(\hat{\sigma}_+ e^{-i\omega_A t} + \hat{\sigma}_- e^{i\omega_A t}\right)\cos(k\hat{x} + \delta), \tag{5.2}$$

where we have assumed that the laser is tuned to resonance with the atomic transition. Transforming to the atomic interaction picture and the dressed-state basis, the Hamiltonian becomes

$$\tilde{H} = \hbar\omega_T(\hat{a}^\dagger\hat{a} + \tfrac{1}{2}) + \frac{\hbar\Omega}{2}\big(|U\rangle\langle U - |L\rangle\langle L|\big)\cos(k\hat{x} + \delta). \tag{5.3}$$

We expand the cosine as

$$\cos(k\hat{x} + \delta) = \cos k\hat{x} \cos\delta - \sin k\hat{x} \sin\delta \tag{5.4}$$

and assume that $k\hat{x}$ is sufficiently small that $\cos k\hat{x}$ and $\sin k\hat{x}$ can be replaced by their Taylor expansions to lowest order (i.e., $1 - (k\hat{x})^2/2$ and $k\hat{x}$, respectively) to arrive at

$$\tilde{H} = \hat{H}_U \otimes |U\rangle\langle U| + \hat{H}_L \otimes |L\rangle\langle L| \tag{5.5}$$

with (cf. Eqs. (4.13))

$$\begin{aligned}\hat{H}_U = {} & \hbar\left(\omega_T - \chi\Omega\cos\delta\right)\left(\hat{a}^\dagger\hat{a} + \tfrac{1}{2}\right) - \hbar\sqrt{\frac{\chi}{2}}\Omega\sin\delta\,\left(\hat{a} + \hat{a}^\dagger\right) \\ & - \frac{\hbar\chi\Omega}{2}\cos\delta\left(\hat{a}^2 + \hat{a}^{\dagger 2}\right) + \frac{\hbar\Omega}{2}\cos\delta \end{aligned} \tag{5.6a}$$

$$\begin{aligned}\hat{H}_L = {} & \hbar\left(\omega_T + \chi\Omega\cos\delta\right)\left(\hat{a}^\dagger\hat{a} + \tfrac{1}{2}\right) + \hbar\sqrt{\frac{\chi}{2}}\Omega\sin\delta\,\left(\hat{a} + \hat{a}^\dagger\right) \\ & + \frac{\hbar\chi\Omega}{2}\cos\delta\left(\hat{a}^2 + \hat{a}^{\dagger 2}\right) - \frac{\hbar\Omega}{2}\cos\delta. \end{aligned} \tag{5.6b}$$

The effect of a nonzero value of δ is to introduce into each piece of the Hamiltonian a term in $\hat{a} + \hat{a}^\dagger$.

Just as a Hamiltonian containing a quadratic interaction term can be produced by making a squeezing transformation on $\hat{a}$ and $\hat{a}^\dagger$, a Hamiltonian with an interaction term linear in $\hat{a}$ and $\hat{a}^\dagger$ is the result of transforming a free oscillator Hamiltonian by the unitary displacement operator $D(\alpha)$. Hamiltonians of this type can therefore be diagonalised by defining new operators which are related to $\hat{a}$ and $\hat{a}^\dagger$ through a displacement transformation (Eqs. (2.58)).

In the case at hand, $\hat{H}_U$ and $\hat{H}_L$ contain both a displacement and a squeezing term, and so we define

$$\begin{pmatrix}\hat{c}_i \\ \hat{c}_i^\dagger\end{pmatrix} = \frac{1}{\sqrt{1-\eta_i^2}}\left[\begin{pmatrix}1 & -\eta_i \\ -\eta_i & 1\end{pmatrix}\begin{pmatrix}\hat{a} \\ \hat{a}^\dagger\end{pmatrix} + (1-\eta_i)\kappa_i\right], \tag{5.7}$$

which corresponds to making the transformation

$$\hat{c}_i = D^\dagger(\kappa_i)S^\dagger(\xi_i)\,\hat{a}\,S(\xi_i)D(\kappa_i) \tag{5.8a}$$

$$\hat{c}_i^\dagger = D^\dagger(\kappa_i)S^\dagger(\xi_i)\,\hat{a}^\dagger\,S(\xi_i)D(\kappa_i) \tag{5.8b}$$

with $\xi_i = \tanh^{-1}\eta_i$. If we set

$$\kappa_i = \frac{\lambda_i}{1+2g_i}, \qquad \eta_i = \frac{-1+\sqrt{1-4g_i^2}}{2g_i} \tag{5.9a}$$

with

$$\lambda_U = -\sqrt{\frac{\chi}{2}}\frac{\Omega\sin\delta}{\omega_T - \chi\Omega\cos\delta}, \qquad \lambda_L = \sqrt{\frac{\chi}{2}}\frac{\Omega\sin\delta}{\omega_T + \chi\Omega\cos\delta} \tag{5.9b}$$

$$g_U = -\frac{\chi\Omega\cos\delta}{2(\omega_T - \chi\Omega\cos\delta)}, \qquad g_L = \frac{\chi\Omega\cos\delta}{2(\omega_T + \chi\Omega\cos\delta)} \tag{5.9c}$$

$\hat{H}_U$ and $\hat{H}_L$ become

$$\hat{H}_U = \hbar\omega_U\big(\hat{c}_U^\dagger\hat{c}_U + \tfrac{1}{2}\big) - \frac{\hbar\chi\Omega^2\sin^2\delta}{2(\omega_T - 2\chi\Omega\cos\delta)} + \frac{\hbar\Omega}{2}\cos\delta \tag{5.10a}$$

$$\hat{H}_L = \hbar\omega_L\big(\hat{c}_L^\dagger\hat{c}_L + \tfrac{1}{2}\big) - \frac{\hbar\chi\Omega^2\sin^2\delta}{2(\omega_T + 2\chi\Omega\cos\delta)} - \frac{\hbar\Omega}{2}\cos\delta \tag{5.10b}$$

where the effective mode frequencies are given by

$$\omega_U = \omega_T\sqrt{1 - 2\frac{\chi\Omega\cos\delta}{\omega_T}} \tag{5.11a}$$

$$\omega_L = \omega_T\sqrt{1 + 2\frac{\chi\Omega\cos\delta}{\omega_T}}. \tag{5.11b}$$

We see that the state-dependent frequency shift becomes progressively smaller as the trap is moved away from the antinode, disappearing completely when the trap reaches a node. Since this frequency shift is the cause of much of the interesting behaviour seen in the past two chapters, we expect the system dynamics to become somewhat more mundane as δ is increased from zero.

5.1.1 Complex oscillator amplitude

The expectation value of $\hat{a}$ can be evaluated in the same way as in §4.2.1, the only difference being that the relationship between $\hat{c}^{(\dagger)}$ and $\hat{a}^{(\dagger)}$ is now given by Eq. (5.7). We find

$$\langle\hat{a}\rangle_i = \frac{1}{1-\eta_i^2}\Big[(\alpha_0+\kappa_i)\big(e^{-i\omega_i t} - \eta_i^2 e^{i\omega_i t}\big) + 2i\eta_i(\alpha_0^* + \kappa_i)\sin\omega_i t\Big] - \kappa_i. \tag{5.12}$$

Figure 5.1 shows the motion of $\langle\hat{a}\rangle$ on the phase plane for several values of δ. As δ increases, the movement across the phase plane and the precession of $\langle\hat{a}\rangle$ become progressively slower, the trajectories become more open, and the bounces become smaller and more irregular. All of these features disappear as $\delta \to \pi/2$, consistent with the observation that $\omega_i \to \omega_T$ and $\eta_i \to 0$.

We can gain some understanding of the system at $\delta = \pi/2$ by considering $\langle\hat{a}\rangle_U$ and $\langle\hat{a}\rangle_L$ separately. Assuming a real value of α_0 and writing $\kappa \equiv \kappa_L = -\kappa_U$, we find from Eq. (5.12)

$$\langle\hat{a}\rangle_U = (\alpha_0 - \kappa)e^{-i\omega_T t} + \kappa \tag{5.13a}$$

$$\langle\hat{a}\rangle_L = (\alpha_0 + \kappa)e^{-i\omega_T t} - \kappa. \tag{5.13b}$$

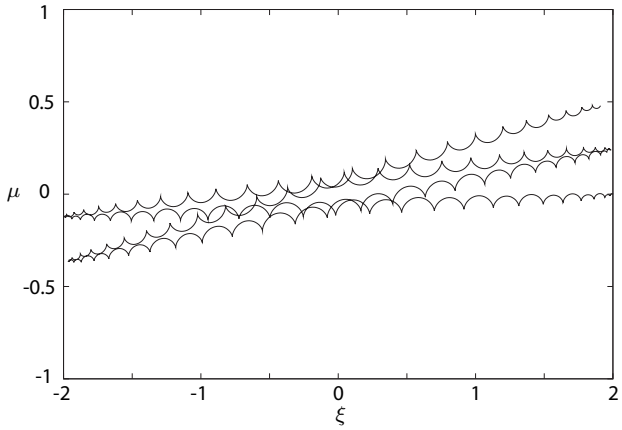

(a) $\delta = \pi/12$

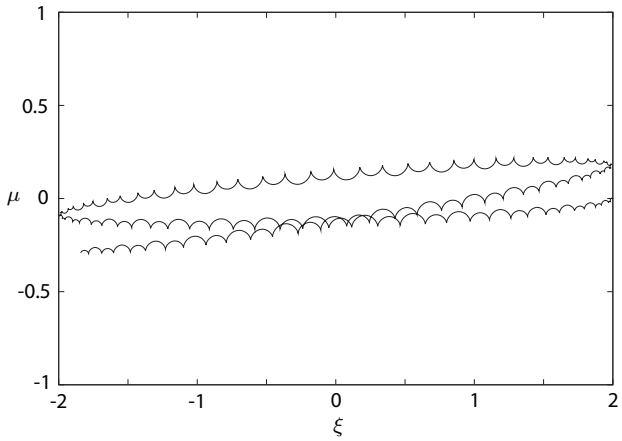

(b) $\delta = \pi/4$

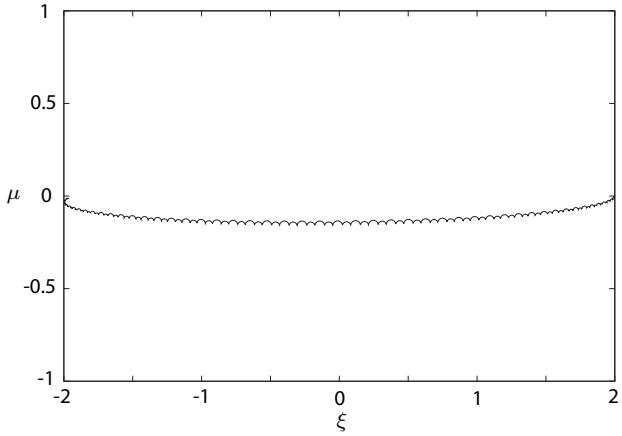

(c) $\delta = 5\pi/12$

Figure 5.1: The changing behaviour of $\langle \hat{a} \rangle$ as the trap is moved away from a node of the standing wave. As δ is increased from zero, the trajectories become more open, and the motion across the phase plane slows down. Parameters are $\chi = 0.04$, $\Omega/\omega_T = 1$, $\tau = 0 - 320$.

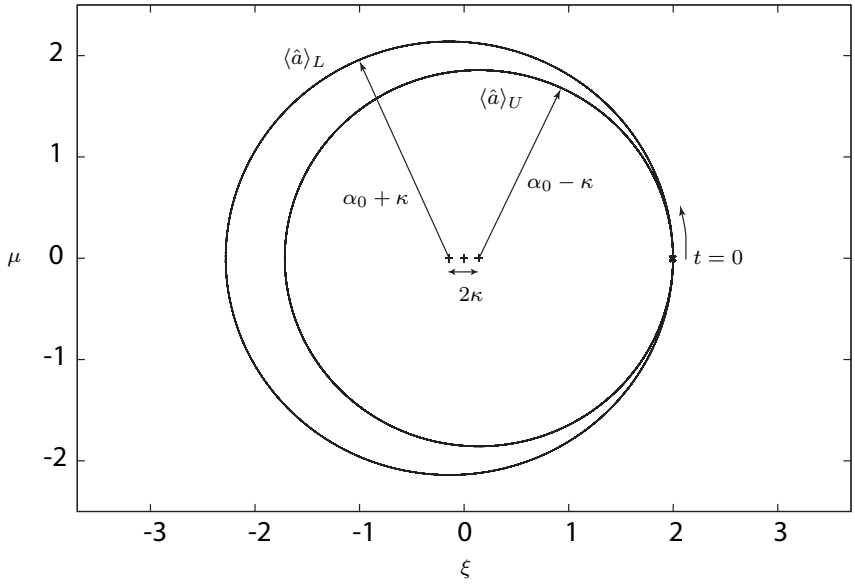

Figure 5.2: The motion of $\langle\hat{a}\rangle_U$ and $\langle\hat{a}\rangle_L$ on the phase plane for $\delta = \pi/2$, $\chi = 0.04$, $\Omega/\omega_T = 1$. The amplitude of oscillation of the trapped atom depends on its internal state.

These solutions are illustrated in Figure 5.2. $\langle\hat{a}\rangle_U$ and $\langle\hat{a}\rangle_L$ each move with frequency ω_T around a circle, just as would be expected for a free oscillator. However, the presence of the interaction term causes both the radius and the origin of the circles to differ: $\langle\hat{a}\rangle_U$ traces out a circle of radius $\alpha_0-\kappa$ centred at κ, while $\langle\hat{a}\rangle_L$ moves around a circle of radius $\alpha_0+\kappa$ centred at $-\kappa$. Aligning the trap with a node rather than an antinode of the standing wave has effectively replaced the state-dependent frequency shift by a state-dependent trap origin and oscillation amplitude.

5.1.2 Average phonon number

The expectation value $\langle \hat{a}^\dagger \hat{a} + \frac{1}{2} \rangle$ can be evaluated by the same method as used in §4.2.2. We find

$$\begin{aligned}
\langle \hat{a}^\dagger \hat{a} + \tfrac{1}{2} \rangle_i =& \big(|\alpha_0|^2 + \tfrac{1}{2}\big) \left[\frac{(1+\eta_i^2)^2}{(1-\eta_i^2)^2} - \frac{4\eta_i^2}{(1-\eta_i^2)^2} \cos 2\omega_i t \right] \\
&+ \alpha_0 \left[\frac{(1+\eta_i^2)(1-\eta_i)^2\kappa_i}{(1-\eta_i^2)^2} - \frac{(1+\eta_i)\kappa_i}{(1-\eta_i^2)} \big(e^{-i\omega_i t} - \eta_i\, e^{i\omega_i t} \big) \right. \\
&\qquad \left. + \frac{2\kappa_i(1-\eta_i)\eta_i}{(1-\eta_i^2)^2} \big(e^{-2i\omega_i t} - \eta_i\, e^{2i\omega_i t} \big) \right] \\
&+ \alpha_0^* \left[\frac{(1+\eta_i^2)(1-\eta_i)^2\kappa_i}{(1-\eta_i^2)^2} - \frac{(1+\eta_i)\kappa_i}{(1-\eta_i^2)} \big(e^{i\omega_i t} - \eta_i e^{-i\omega_i t} \big) \right. \\
&\qquad \left. + \frac{2\kappa_i(1-\eta_i)\eta_i}{(1-\eta_i^2)^2} \big(e^{2i\omega_i t} - \eta_i e^{-2i\omega_i t} \big) \right] \\
&+ \alpha_0^2 \left[\frac{\eta_i}{(1-\eta_i^2)^2} \big(e^{-2i\omega_i t} + \eta_i^2 e^{2i\omega_i t} \big) - \frac{\eta_i(1+\eta_i^2)}{(1-\eta_i^2)^2} \right] \\
&+ \alpha_0^{*2} \left[\frac{\eta_i}{(1-\eta_i^2)^2} \big(e^{2i\omega_i t} + \eta_i^2 e^{-2i\omega_i t} \big) - \frac{\eta_i(1+\eta_i^2)}{(1-\eta_i^2)^2} \right] \\
&+ \kappa_i^2 \left[1 + \frac{(1+\eta_i^2)(1-\eta_i)^2}{(1-\eta_i^2)^2} - 2\cos\omega_i t + \frac{2\eta_i(1-\eta_i)^2}{(1-\eta_i^2)^2} \cos 2\omega_i t \right].
\end{aligned} \tag{5.14}$$

Figure 5.3 illustrates how the average phonon number changes with increasing δ. The periodic modulation about the average value of $|\alpha_0|^2$ disappears, replaced by an oscillation of unit frequency with a slowly-varying amplitude. For $\delta = \pi/2$ we find

$$\langle \hat{a}^\dagger \hat{a} + \tfrac{1}{2} \rangle = |\alpha_0|^2 + \tfrac{1}{2} + 4\kappa^2 (1 - \cos \omega_T t). \tag{5.15}$$

The behaviour seen here is simply understood if we consider the different amplitudes of oscillation of the motional dressed states. If α_0 is real, at $\omega_T t = \pi$ the upper and lower dressed states are coherent states centred on $-(\alpha_0 - 2\kappa)$ and $-(\alpha_0 + 2\kappa)$ respectively. Although these are equidistant from the point $-\alpha_0$, where they would both be in the absence of any interaction, the dependence of $\langle \hat{a}^\dagger \hat{a} + \frac{1}{2} \rangle$ on the *square* of the amplitude produces the extra term appearing in Eq. (5.15).

5.1.3 Atomic excitation probability

Recall that the probability of finding the atom in its excited state is given by

$$P_+(t) = \frac{1}{2} \Big[1 + \mathrm{Re} \big\{ \langle \phi_U(t) | \phi_L(t) \rangle \big\} \Big].$$

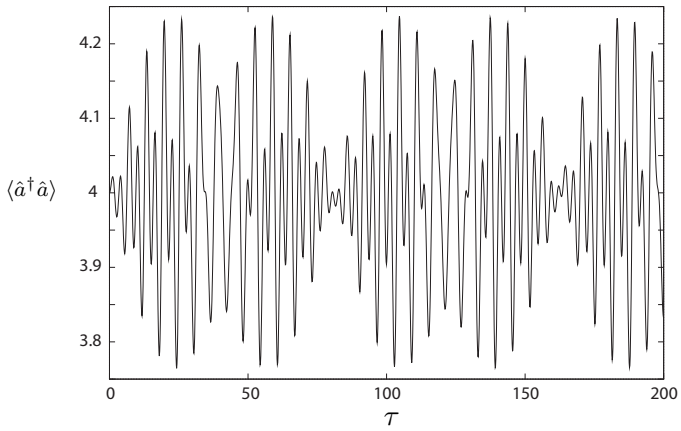

(a) $\delta = \pi/12$

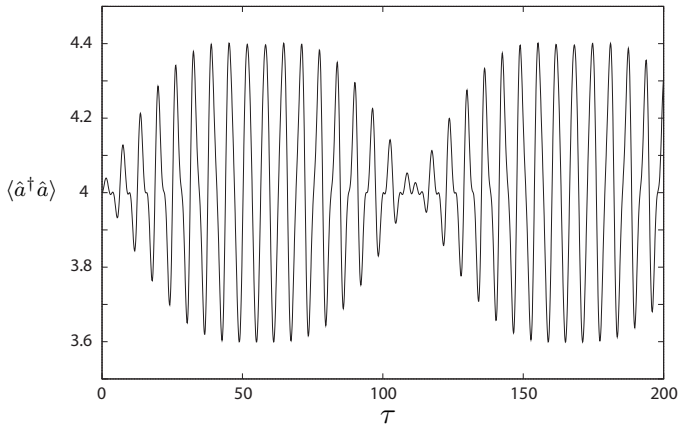

(b) $\delta = \pi/4$

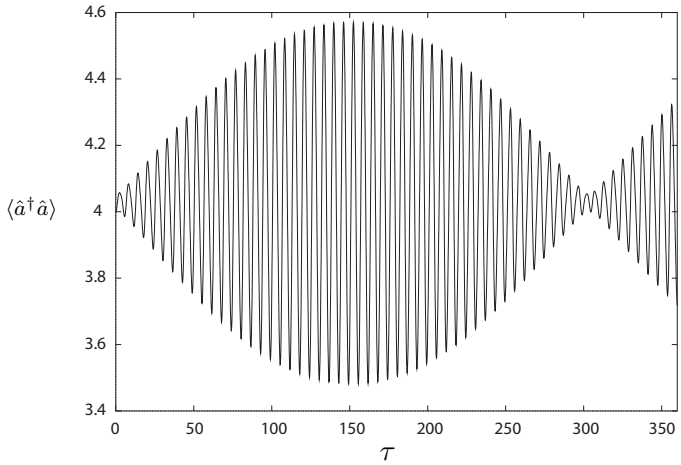

(c) $\delta = 5\pi/12$

Figure 5.3: The behaviour of the average phonon number with increasing δ. The parameters are $\chi = 0.04$, $\Omega/\omega_T = 1$.

Extracting the time-evolution operator from each state and using Eq. (5.10) to write each piece of the Hamiltonian in its diagonal form, we find

$$\begin{aligned}\langle\phi_U(t)|\phi_L(t)\rangle = -\langle\alpha_0|D^\dagger(\kappa_U)S^\dagger(\xi_U)\, e^{i\omega_U t(\hat{a}^\dagger\hat{a}+\frac{1}{2})}S(\xi_U)D(\kappa_U) \\ \times D^\dagger(\kappa_L)S^\dagger(\xi_L)e^{-i\omega_L t(\hat{a}^\dagger\hat{a}+\frac{1}{2})}S(\xi_L)D(\kappa_L)|\alpha_0\rangle \\ \times \exp\left[i\Omega t\cos\delta\left(1-\frac{2\chi^2\Omega^2\sin^2\delta}{\omega_T^2-4\chi^2\Omega^2\cos^2\delta}\right)\right].\end{aligned} \tag{5.16}$$

Following the procedure used in §4.2.3, we insert the identity as an expansion over coherent states at the end of the first line. The displacement operator $D(\kappa_U)$ can then be acted on the coherent state $|\beta\rangle$ by noting that

$$\begin{aligned}D(\kappa_U)\,|\beta\rangle &= D(\kappa_U)D(\beta)|0\rangle \\ &= D(\beta+\kappa_U)\exp\left[\frac{1}{2}(\beta^*\kappa_U-\beta\kappa_U^*)\right]|0\rangle \\ &= \exp\left[\frac{\kappa_U}{2}(\beta^*-\beta)\right]|\beta+\kappa_U\rangle,\end{aligned} \tag{5.17}$$

where Eq. (2.59) has been used to combine the two displacement operators, and we have used the fact that κ_U is real. In a similar fashion, the $D^\dagger(\kappa_L)$ operator can be acted to the left, and thus we arrive at

$$\begin{aligned}\langle\phi_U(t)|\phi_L(t)\rangle = -\frac{1}{\pi}\int d^2\beta\,\langle\alpha_0+\kappa_U|S^\dagger(\xi_U)e^{i\omega_U t(\hat{a}^\dagger\hat{a}+\frac{1}{2})}S(\xi_U)|\beta+\kappa_U\rangle \\ \times\langle\beta+\kappa_L|S^\dagger(\xi_L)e^{i\omega_L t(\hat{a}^\dagger\hat{a}+\frac{1}{2})}S(\xi_L)|\alpha_0+\kappa_L\rangle \\ \times\exp\left[\frac{(\kappa_U-\kappa_L)}{2}(\alpha_0-\alpha_0^*)\right]\exp\left[\frac{(\kappa_U-\kappa_L)}{2}(\beta^*-\beta)\right] \\ \times\exp\left[i\Omega t\cos\delta\left(1-\frac{2\chi^2\Omega^2\sin^2\delta}{\omega_T^2-4\chi^2\Omega^2\cos^2\delta}\right)\right].\end{aligned} \tag{5.18}$$

The matrix elements that remain on the right-hand side are of the same form as those which appear in the calculation of the Q function, and can be evaluated by making use of Eq. (4.45). The last task is to perform the integration over β, which once again proves to be straightforward but messy. We eventually arrive at

$$\begin{aligned}\langle\phi_U(t)|\phi_L(t)\rangle = \frac{C_0}{\sqrt{pr}}\exp\left[\frac{q^2}{4p}\right]\exp\left[\frac{(\kappa_U-\kappa_L)}{2}(\alpha_0-\alpha_0^*)\right] \\ \times\exp\left[i\Omega t\cos\delta\left(1-\frac{2\chi^2\Omega^2\sin^2\delta}{\omega_T^2-4\chi^2\Omega^2\cos^2\delta}\right)\right] \\ \times\exp\left[\frac{-\left[A_U-A_L^*\right]^2}{4+2\eta_U(1-\varepsilon_U)+2\eta_L(1-\varepsilon_L^*)}\right]\end{aligned}$$

with

$$\begin{aligned} C_0 = {} & e^{i(\omega_L-\omega_U)t/2}\sqrt{\varepsilon_U\varepsilon_L^*}\,\exp\left[\kappa_U^2\frac{\eta_U}{2}(1-\varepsilon_U)+\kappa_L^2\frac{\eta_L}{2}(1-\varepsilon_L^*)\right] \\ & \times\exp\left[\frac{(\alpha_0^*+\kappa_U)^2\eta_U}{2}(1-\varepsilon_U)+\frac{(\alpha_0+\kappa_L)^2\eta_L}{2}(1-\varepsilon_L^*)-|\alpha_0|^2\right] \\ & \times\exp\left[-\kappa_U(\alpha_0^*+\kappa_U)(1-e^{-i\omega_U t}\varepsilon_U)-\kappa_L(\alpha_0+\kappa_L)(1-e^{i\omega_L t}\varepsilon_L^*)\right] \end{aligned}$$

$$p = 1-\frac{\eta_U}{2}(1-\varepsilon_U)-\frac{\eta_U}{2}(1-\varepsilon_L^*)+\frac{\left[\eta_U(1-\varepsilon_U)-\eta_L(1-\varepsilon_L^*)\right]^2}{4+2\eta_U(1-\varepsilon_U)+2\eta_L(1-\varepsilon_L^*)}$$

and

$$q = A_U+A_L^*-\frac{\big(\eta_U(1-\varepsilon_U)-\eta_L(1-\varepsilon_L^*)\big)\big(A_U-A_L^*\big)}{2+\eta_U(1-\varepsilon_U)+\eta_L(1-\varepsilon_L^*)}$$

$$r = 1+\frac{\eta_U}{2}(1-\varepsilon_U)+\frac{\eta_L}{2}(1-\varepsilon_L^*)$$

where

$$A_i = \kappa_i\left[\eta_i(1-\varepsilon_i)-(1-e^{-i\omega_i t}\varepsilon_i)\right]+\alpha_0^*\varepsilon_i\,e^{-i\omega_i t},$$

$$\varepsilon_i = \frac{1-\eta_i^2}{e^{-2i\omega_i t}-\eta_i^2}.$$

The behaviour of the atomic excitation probability is illustrated in Figure 5.4. The revivals become less frequent as δ is increased, and disappear completely for $\delta=\pi/2$; at this point the excitation probability shows continuous small-amplitude oscillations (see Fig. 5.5.)

5.1.4 Motional state Q function

We saw in §4.3.1 that finding the Q function amounts to calculating the magnitude of the matrix element $\langle\alpha|e^{-i\hat{H}_i t/\hbar}|\alpha_0\rangle$. We begin by using Eq. (5.10) to write

$$\begin{aligned} \langle\alpha|e^{-i\hat{H}_i t/\hbar}|\alpha_0\rangle = {} & \langle\alpha|D^\dagger(\kappa_i)S^\dagger(\xi_i)\,e^{-i\omega_i t(\hat{a}^\dagger\hat{a}+\frac{1}{2})}S(\xi_i)D(\kappa_i)|\alpha_0\rangle \\ & \times\exp\left[\frac{it}{2}\left(\frac{\chi\Omega^2\sin^2\delta}{\omega_T\mp 2\chi\Omega\cos\delta}\mp\Omega\cos\delta\right)\right]. \end{aligned} \tag{5.19}$$

The displacement operators can now be acted on the states in the manner outlined in Eq. (5.17) above. We find

$$\begin{aligned} \langle\alpha|e^{-i\hat{H}_i t/\hbar}|\alpha_0\rangle = {} & \langle\alpha+\kappa_i|S^\dagger(\xi_i)\,e^{-i\omega_i t(\hat{a}^\dagger\hat{a}+\frac{1}{2})}S(\xi_i)|\alpha_0+\kappa_i\rangle \\ & \times\exp\left[\frac{it}{2}\left(\frac{\chi\Omega^2\sin^2\delta}{\omega_T\mp 2\chi\Omega\cos\delta}\mp\Omega\cos\delta\right)\right]. \end{aligned} \tag{5.20}$$

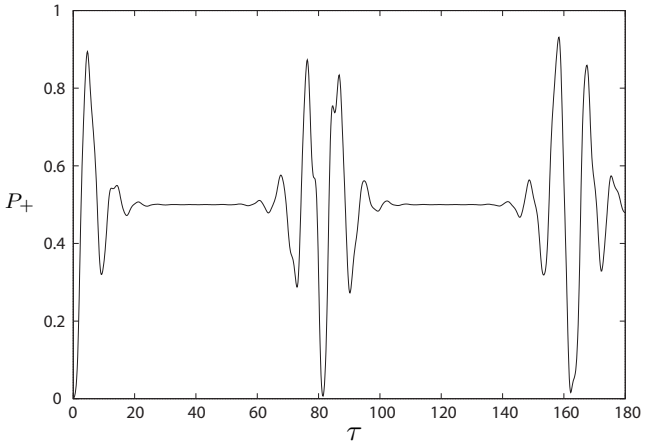

(a) $\delta = \pi/12$

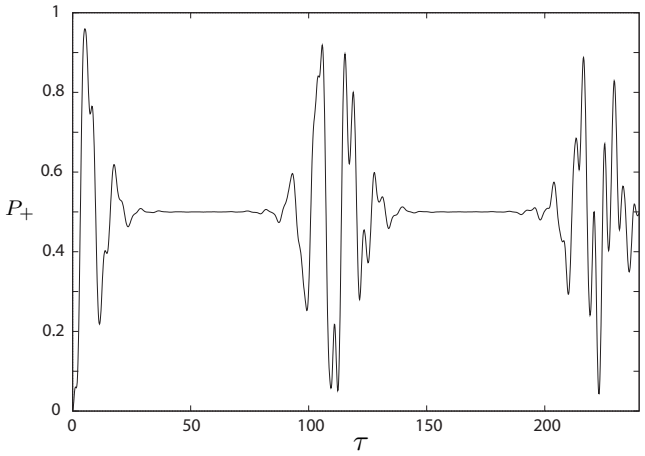

(b) $\delta = \pi/4$

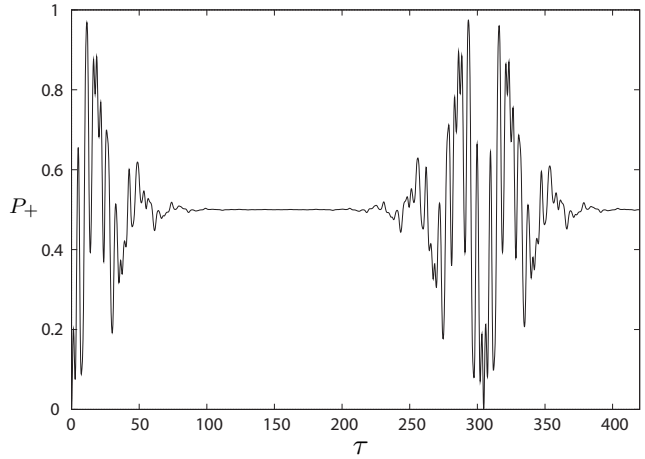

(c) $\delta = 5\pi/12$

Figure 5.4: Plots of the atomic excitation probability for different values of δ. The parameters are $\chi = 0.04$, $\Omega/\omega_T = 1$.

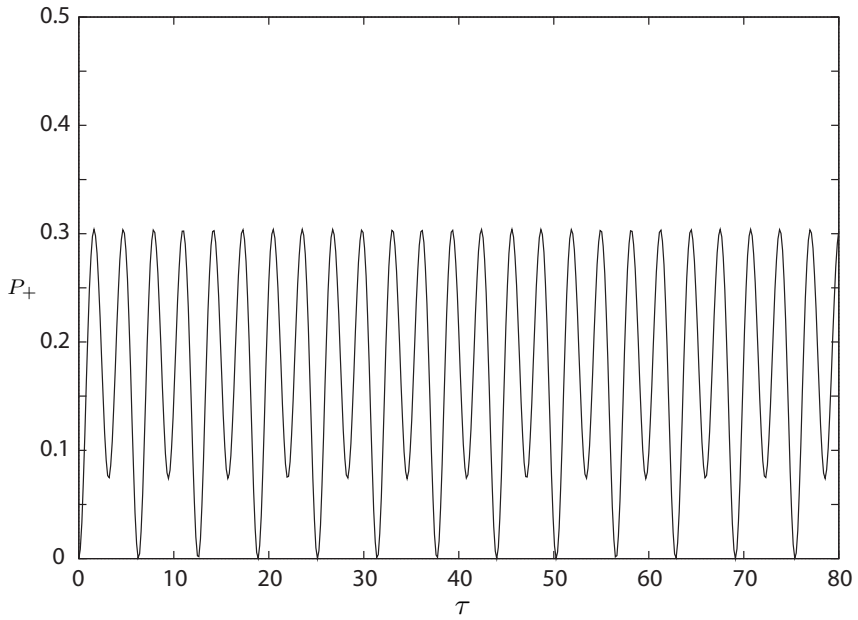

Figure 5.5: A plot of the the atomic excitation probability for $\delta = \pi/2$, with $\chi = 0.04$, $\Omega/\omega_T = 1$. The collapse and revival behaviour has been replaced by a regular small-amplitude oscillation.

This expression can be evaluated by an identical procedure to that used in §4.3.1; in fact, the sole difference is that the coherent states have amplitude $\alpha+\kappa_i$ and $\alpha_0+\kappa_i$ instead of α and α_0. We arrive at

$$Q^i_{\mathrm{CM}}(\alpha,\alpha^*) = e^{-|\alpha-\alpha_0|^2}|q_i|^2 \tag{5.21}$$

with

$$\begin{aligned} q_i = \sqrt{\frac{1-\eta_i^2}{e^{2i\omega_i t}-\eta_i^2}}\ \exp\left[(\alpha^*+\kappa_i)^2\frac{\eta_i}{2}\left(1-\frac{1-\eta_i^2}{e^{2i\omega_i t}-\eta_i^2}\right)\right] \\ \times \exp\left[-(\alpha^*+\kappa_i)(\alpha_0+\kappa_i)\left(1-\frac{e^{i\omega_i t}(1-\eta_i^2)}{e^{2i\omega_i t}-\eta_i^2}\right)\right] \\ \times \exp\left[(\alpha_0+\kappa_i)^2\frac{\eta_i}{2}\left(1-\frac{1-\eta_i^2}{e^{2i\omega_i t}-\eta_i^2}\right)\right]. \end{aligned} \tag{5.22}$$

As δ is increased from zero, the rotation of the two peaks of the Q-function slows down and the bounces they trace out become more pronounced. If we move to the interaction picture and set $\delta = \pi/2$, we find that the peaks no longer rotate about the origin, but instead move in circles of radius κ about the points $\alpha_0 \pm \kappa$. This is consistent with the behaviour of $\langle\hat{a}\rangle_U$ and $\langle\hat{a}\rangle_L$ described in §5.1.1.

5.1.5 Motional state Wigner function

The Wigner function can be evaluated by the same method as that outlined in §4.3.2. To evaluate the integral in Eq. (4.48), we write the matrix element as

$$\begin{aligned}\langle\phi_i(t)|e^{iz^*\hat{a}^\dagger+iz\hat{a}}|\phi_i(t)\rangle = e^{-\frac{1}{2}|z|^2}\langle\alpha_0|D^\dagger(\kappa_i)S^\dagger(\xi_i)e^{i\omega_i t(\hat{a}^\dagger\hat{a}+\frac{1}{2})}S(\xi_i)D(\kappa_i)e^{iz^*\hat{a}^\dagger}\\ \times\ e^{iz\hat{a}}D^\dagger(\kappa_i)S^\dagger(\xi_i)e^{-i\omega_i t(\hat{a}^\dagger\hat{a}+\frac{1}{2})}S(\xi_i)D(\kappa_i)|\alpha_0\rangle.\end{aligned}$$

The displacement operators can be removed from this expression by acting the outer two on the coherent states and using the inner two to transform the exponentials of $\hat{a}$ and $\hat{a}^\dagger$ according to Eq. (2.58). The remaining expression can be evaluated by an identical method to that used previously; we eventually arrive at

$$W^i_{\mathrm{CM}}(\alpha,\alpha^*) = \frac{1}{\pi\sqrt{ab}}\exp\left[\frac{d^2}{4a}\right]\exp\left[\frac{c^2}{4b}\right]$$

with

$$\begin{aligned}a &= \frac{1}{2(1-\eta_i^2)^2}\left[(1-\eta_i^2)^2 - 4\eta_i(1-\eta_i)^2\sin^2\omega_i t\right]\\ b &= \frac{1}{2(1-\eta_i^2)^2}\left[(1-\eta_i^2)^2 + 4\eta_i(1+\eta_i)^2\sin^2\omega_i t\right]\\ &\quad - \frac{2\eta_i^2\sin^2 2\omega_i t}{(1-\eta_i^2)^2 - 4\eta_i(1-\eta_i)^2\sin^2\omega_i t}\end{aligned}$$

and

$$\begin{aligned}c = {}& 2i\kappa_i(\cos\omega_i t - 1) - i(\alpha+\alpha^*) + \frac{i\alpha_0}{1-\eta_i^2}\left(e^{-i\omega_i t} - \eta_i^2 e^{i\omega_i t} - 2i\eta_i\sin\omega_i t\right)\\ &+ \frac{i\alpha_0^*}{1-\eta_i^2}\left(e^{i\omega_i t} - \eta_i^2 e^{-i\omega_i t} + 2i\eta_i\sin\omega_i t\right)\\ &+ \frac{2\eta_i\sin(2\omega_i t)(1-\eta_i^2)}{(1-\eta_i^2)^2 - 4\eta_i(1-\eta_i)^2\sin^2\omega_i t}\left\{\frac{\alpha_0^*}{1-\eta_i^2}\left(e^{i\omega_i t} - \eta_i^2 e^{-i\omega_i t} - 2i\eta_i\sin\omega_i t\right)\right.\\ &\left.+\ \alpha - \alpha^* - \frac{\alpha_0}{1-\eta_i^2}\left(e^{-i\omega_i t} - \eta_i^2 e^{i\omega_i t} + 2i\eta_i\sin\omega_i t\right) + 2i\kappa_i\sin\omega_i t\left(\frac{1-\eta_i}{1+\eta_i}\right)\right\},\end{aligned}$$

and

$$\begin{aligned}d = {}& \alpha - \alpha^* + \frac{\alpha_0^*}{1-\eta_i^2}\left[e^{i\omega_i t} - \eta_i^2 e^{-i\omega_i t} - 2i\eta_i\sin\omega_i t\right] + \kappa_i\left(\frac{1-\eta_i}{1+\eta_i}\right)2i\sin\omega_i t\\ &- \frac{\alpha_0}{1-\eta_i^2}\left[e^{-i\omega_i t} - \eta_i^2 e^{i\omega_i t} + 2i\eta_i\sin\omega_i t\right].\end{aligned}$$

The behaviour of the Wigner function is essentially identical to that of the Q function, consistent with the fact that for a coherent state the Q function is simply a broadened version of the Wigner function.

5.1.6 Comparison with the Jaynes-Cummings model

It has been known for some time that under certain conditions, a trapped ion with quantised motion interacting with an incident electromagnetic field is mathematically equivalent to the Jaynes-Cummings model [26, 70]. In both cases, the formal description is that of a two-level atom coupled to a quantised harmonic oscillator; the only point of difference is the physical meaning assigned to the oscillator. In the Jaynes-Cummings model, it represents a single mode of the quantised radiation field, while in the case of a trapped ion it corresponds to the mechanical motion of the centre of mass.

Although there is little to be gained from a lengthy discussion of this formal equivalence and the connection between the fields of cavity QED and trapped ions it entails, it is worthwhile demonstrating how the Jaynes-Cummings Hamiltonian can be obtained from the current system, if only for the sake of interest. Our starting point is the system Hamiltonian

$$\hat{H} = \hbar\omega_T(\hat{a}^\dagger\hat{a} + \tfrac{1}{2}) + \frac{\hbar\omega_A}{2}\hat{\sigma}_z + \frac{\hbar\Omega}{2}\left(\hat{\sigma}_+ e^{-i\omega_L t} + \hat{\sigma}_- e^{i\omega_L t}\right)\cos(k\hat{x} + \delta). \tag{5.23}$$

Aligning the trap with a node of the standing wave by setting $\delta = \pi/2$ and making the approximation $\sin k\hat{x} \approx k\hat{x}$ gives

$$\hat{H} = \hbar\omega_T(\hat{a}^\dagger\hat{a} + \tfrac{1}{2}) + \frac{\hbar\omega_A}{2}\hat{\sigma}_z + \hbar\Omega\sqrt{\frac{\chi}{2}}\left(\hat{\sigma}_+ e^{-i\omega_L t} + \hat{\sigma}_- e^{i\omega_L t}\right)(\hat{a} + \hat{a}^\dagger). \tag{5.24}$$

Let us now move into the interaction picture by making the transformation

$$\tilde{H} = e^{i\hat{H}_0 t/\hbar}\,\hat{H}\,e^{-i\hat{H}_0 t/\hbar} - \hat{H}_0 \tag{5.25}$$

where $\hat{H}_0 = \hat{H}_A + \hat{H}_T$ is the free Hamiltonian for the system. We find

$$\tilde{H} = \hbar\Omega\sqrt{\frac{\chi}{2}}\left(\hat{\sigma}_+ e^{-i\Delta t} + \hat{\sigma}_- e^{i\Delta t}\right)\left(\hat{a}e^{-i\omega_T t} + \hat{a}^\dagger e^{i\omega_T t}\right), \tag{5.26}$$

where $\Delta \equiv \omega_L - \omega_A$ is the detuning of the laser from the atomic transition frequency. Expanding the brackets, we arrive at

$$\begin{aligned}\tilde{H} = \hbar\Omega\sqrt{\frac{\chi}{2}}\,\big(&\hat{\sigma}_+\hat{a}\,e^{-i(\omega_T+\Delta)t} + \hat{\sigma}_+\hat{a}^\dagger e^{i(\omega_T-\Delta)t} \\ &+ \hat{\sigma}_-\hat{a}\,e^{-i(\omega_T-\Delta)t} + \hat{\sigma}_-\hat{a}^\dagger e^{i(\omega_T+\Delta)t}\big).\end{aligned} \tag{5.27}$$

The treatment up to this point is reminiscent of the development of the dipole interaction Hamiltonian presented in §2.3.2 and §2.3.3, and it should come as no surprise that the next step is to discard two of the terms appearing in Eq. (5.27) on the grounds that they are rapidly oscillating. Precisely which two terms to discard, however, is the key question, and it is here that the treatments diverge.

In contrast to the circumstances motivating the rotating-wave approximation, the form of the oscillation frequencies coupled with the fact that Δ is an experimentally controllable parameter means that we have the power to choose which terms are resonant. Different choices of detuning lead to different Hamiltonians, raising the possibility of engineering the Hamiltonian to suit our needs.

The Jaynes-Cummings model.

Consider the case of $\Delta = -\omega_T$; that is, the laser is detuned to the red side of the atomic transition by an amount equal to the trap frequency. The Hamiltonian becomes

$$\tilde{H} = \hbar\Omega\sqrt{\frac{\chi}{2}}\left(\hat{\sigma}_+\hat{a} + \hat{\sigma}_-\hat{a}^\dagger + \hat{\sigma}_+\hat{a}^\dagger e^{i2\omega_T t} + \hat{\sigma}_-\hat{a}e^{-i2\omega_T t}\right). \tag{5.28}$$

Discarding the oscillatory terms, we are left with a Hamiltonian of precisely the same form as that of the Jaynes-Cummings model (Eq. (2.98)):

$$\tilde{H} = \hbar\Omega\sqrt{\frac{\chi}{2}}\left(\hat{\sigma}_+\hat{a} + \hat{\sigma}_-\hat{a}^\dagger\right). \tag{5.29}$$

Just as the Jaynes-Cummings Hamiltonian describes the absorption and emission of photons by the atom, the terms appearing in this expression represent the excitation of the atom with the simultaneous destruction of a phonon (i.e. a lowering of the motional state of the atom in the trap) and the de-excitation of the atom with the creation of a phonon. This Hamiltonian gives rise to transitions of the form

$$|-\rangle|n\rangle \leftrightarrow |+\rangle|n-1\rangle$$

which are the type of transitions required for the sideband cooling of a trapped ion [39].

The 'anti-Jaynes-Cummings' model.

If we instead detune the laser to the blue side of the atomic transition such that $\Delta = \omega_T$, the Hamiltonian becomes

$$\tilde{H} = \hbar\Omega\sqrt{\frac{\chi}{2}}\left(\hat{\sigma}_+\hat{a}^\dagger + \hat{\sigma}_-\hat{a}\right). \tag{5.30}$$

The terms appearing here represent the excitation of the atom with the simultaneous *creation* of a phonon and the de-excitation of the atom with the *destruction* of a phonon. They describe transitions of the form

$$|-\rangle|n\rangle \leftrightarrow |+\rangle|n+1\rangle$$

and have thus been christened 'anti-Jaynes-Cummings' terms. Although this coupling is realisable in a trapped ion system, the fact that the corresponding atom-photon processes would violate energy conservation means that the anti-Jaynes-Cummings model has no analogue in cavity QED.

5.2 Exact solutions

The extent to which the solutions presented in the previous chapters describe what takes place in the real physical system depends on the validity of the approximations made in moving from the system to the mathematical model used to describe it.

Of the approximations made in the theoretical treatment presented here, most are well justified and need not be given a second thought. However, one which is deserving of further scrutiny is the neglect of higher-order terms in the expansion of $\cos k\hat{x}$ and $\sin k\hat{x}$ – the key question being, does the system exhibit the same behaviour if the higher-order terms in η_{LD} are retained?

Since keeping the trigonometric expressions in their entirety precludes the analytic solution of the Hamiltonian, the impact these terms have on the system must be investigated numerically. This section presents an analytic derivation of the exact matrix elements which appear in the equations of motion for the state expansion coefficients, and compares these results with the expressions that have been used to approximate them. The solutions for operator moments which result from these 'exact' equations are investigated, and compared with the 'approximate' solutions of Chapter 3.

5.2.1 Exact equations of motion

In the dressed-state basis and allowing for an arbitrary trap position, the system Hamiltonian in the atomic interaction picture is

$$\tilde{H} = \hbar\omega_T(\hat{a}^\dagger\hat{a} + \tfrac{1}{2}) + \frac{\hbar\Omega}{2}\big(|U\rangle\langle U| - |L\rangle\langle L|\big)\cos(k\hat{x} + \delta). \tag{5.31}$$

We use the state expansion given by Eq. (4.4), where the dressed motional states $|\phi_i(t)\rangle$ can be expanded in the number state basis as

$$|\phi_i(t)\rangle = \sum_n c_n^i(t)|n\rangle. \tag{5.32}$$

Using the Schrödinger equation and the orthogonality of the dressed atomic basis states, we find

$$i\hbar\frac{dc_m^i(t)}{dt} = \langle i|\langle m|\tilde{H}|\psi(t)\rangle. \tag{5.33}$$

Inserting the Hamiltonian (Eq. (5.31)) and expanding the motional dressed state gives

$$\begin{aligned} i\hbar\frac{dc_m^i(t)}{dt} &= \sum_n c_n^i(t)\,\langle m|\left[\hbar\omega_T(\hat{a}^\dagger\hat{a} + \frac{1}{2}) \pm \frac{\hbar\Omega}{2}\cos(k\hat{x} + \delta)\right]|n\rangle \\ &= \hbar\omega_T(m + \tfrac{1}{2})\,c_m^i(t) + \frac{\hbar\Omega}{2}\sum_n c_n^i(t)\langle m|\big[\cos k\hat{x}\cos\delta - \sin k\hat{x}\sin\delta\big]|n\rangle \end{aligned} \tag{5.34}$$

where the orthogonality of the number states has been used.

It is clear from this expression that the exact equations of motion for the expansion coefficients involve matrix elements of the form

$$\langle m|\cos k\hat{x}|n\rangle \qquad \text{and} \qquad \langle m|\sin k\hat{x}|n\rangle \tag{5.35}$$

which have been approximated thus far by the matrix elements

$$\langle m|\left[1-\frac{(k\hat{x})^2}{2}\right]|n\rangle \qquad \text{and} \qquad \langle m|k\hat{x}|n\rangle \tag{5.36}$$

respectively. These, then, are the expressions we wish to compare.

5.2.2 Evaluation of $\langle m|\cos k\hat{x}|n\rangle$

We begin the evaluation of the matrix elements $\langle m|\cos k\hat{x}|n\rangle$ by inserting the identity as

$$\hat{1} = \int_{-\infty}^{\infty} dx'\,|x'\rangle\langle x'|. \tag{5.37}$$

This allows the cosine term to be evaluated, giving

$$\langle m|\cos k\hat{x}|n\rangle = \int_{-\infty}^{\infty} dx'\,\langle m|x'\rangle\langle x'|n\rangle\cos kx'. \tag{5.38}$$

The terms appearing in the integral are the position-space wavefunctions of the m^{th} and n^{th} number states, which are given by Eq. (2.41). Substituting for the wavefunctions and converting from x' to the dimensionless position variable $y \equiv x'\sqrt{m\omega_T/\hbar}$, we find

$$\langle m|\cos k\hat{x}|n\rangle = \frac{1}{\sqrt{\pi 2^{m+n}m!n!}}\int_{-\infty}^{\infty} dy\,\cos\left(k\sqrt{\frac{\hbar}{m\omega_T}}y\right)e^{-y^2}H_m(y)H_n(y). \tag{5.39}$$

This integral is only different from zero if the integrand is even. Since the parity of $H_k(y)$ is the same as that of k (see Eq. (A.3)), the matrix element vanishes unless n and m are either both even or both odd; that is

$$\langle m|\cos k\hat{x}|n\rangle = \begin{cases} \text{Eq. (5.39)} & n = m+2l, \quad l\in\mathbb{Z} \\ 0 & \text{else.} \end{cases} \tag{5.40}$$

The matrix representation of $\cos k\hat{x}$ thus has non-zero terms only on every *second* off-diagonal, reflecting the fact that the series expansion of $\cos k\hat{x}$ contains only even powers of $\hat{a}+\hat{a}^\dagger$. Each line of non-zero entries is produced by terms describing the creation (or annihilation) of an *even* number of phonons – for example, the second off-diagonal elements result from $\hat{a}^2$ and $\hat{a}^{\dagger 2}$ terms.

However, these terms are not the only ones which contribute to the second off-diagonal matrix elements. Continuing the expansion of $\cos k\hat{x}$, we come across many other operator combinations that result in a *net* gain or loss of two phonons: for example, $\hat{a}^{\dagger 3}\hat{a}$ and $\hat{a}^{\dagger 3}\hat{a}^5$. Since these terms are of order χ^3 and above, they are not included in the approximation used in previous chapters. It is these corrections arising from higher-order terms in the expansion of $\cos k\hat{x}$ that we wish to find.

Since x is an observable, the matrix representing $\cos k\hat{x}$ is Hermitian, and we lose nothing by restricting our analysis to the half of the matrix lying above the main diagonal. To evaluate Eq. (5.39) for this case we can use the integral [12]

$$\int_0^\infty \cos(bz)\, e^{-z^2} H_k(z)\, H_{k+2l}(z) = 2^k \frac{\sqrt{\pi}}{2} k!\, (-1)^l b^{2l} e^{-\frac{b^2}{4}} L_k^{(2l)}\left(\frac{b^2}{2}\right), \tag{5.41}$$

which holds for $k, l \geq 0$. Here $L_n^{(m)}(x)$ is an associated Laguerre polynomial.

After some algebra, we arrive at

$$\langle m|\cos k\hat{x}|m+2l\rangle = (-1)^l 2^l \sqrt{\frac{m!}{(m+2l)!}}\, \chi^l\, e^{-\chi} L_m^{(2l)}(2\chi) \quad l = 0, 1, 2, \ldots. \tag{5.42}$$

We could, if we wished, use this expression to find exact expressions for all the off-diagonal elements to all orders of χ. However, in order to make our comparison with the approximate solutions a valid one, we restrict ourselves to evaluating the diagonal ($l = 0$) and second off-diagonal ($l = 1$) terms, which describe processes resulting in a net change in phonon number of zero or two respectively.

Diagonal elements

Setting $l = 0$ in Eq. (5.42), we find that the diagonal matrix elements are given by

$$\langle m|\cos k\hat{x}|m\rangle = e^{-\chi} L_m(2\chi) \tag{5.43}$$

where $L_m(x) = L_m^{(0)}(x)$ is a Laguerre polynomial. We can now expand the Laguerre polynomial (see Eq. (A.13)) and the exponential in powers of χ:

$$e^{-\chi} = 1 - \chi + \frac{\chi^2}{2} - \frac{\chi^3}{6} + \ldots \tag{5.44}$$

$$\begin{aligned} L_m(2\chi) &= \sum_{i=0}^{m} \frac{1}{i!} \binom{m}{m-i} (-2\chi)^i \\ &= 1 - 2m\chi + \frac{1}{2}\binom{m}{m-2} 4\chi^2 - \frac{1}{6}\binom{m}{m-3} 8\chi^3 + \ldots, \end{aligned} \tag{5.45}$$

giving

$$\begin{aligned}\langle m|\cos k\hat{x}|m\rangle &= \left(1-\chi+\frac{\chi^2}{2}-\ldots\right)\left(1-2m\chi+m(m-1)\chi^2+\ldots\right)\\ &= 1-(2m+1)\chi+(m^2+m+\tfrac{1}{2})\chi^2+\mathcal{O}(\chi^3).\end{aligned} \tag{5.46}$$

The matrix element by which this has been approximated is

$$\langle m|\left[1-\chi(\hat{a}+\hat{a}^\dagger)^2\right]|m\rangle = 1-(2m+1)\chi. \tag{5.47}$$

The difference between the exact and approximate matrix elements is therefore of order $\chi^2 m^2$. The diagonal matrix elements are of order 1, and so the fractional error is also $\sim \chi^2 m^2$.

Off-diagonal elements

The matrix elements appearing on the second off-diagonal can be found by setting $l = 1$ in Eq. (5.42). We find

$$\langle m|\cos k\hat{x}|m+2\rangle = -2\chi\sqrt{\frac{m!}{(m+2)!}}\,e^{-\chi}L_m^{(2)}(2\chi). \tag{5.48}$$

Expanding the Laguerre polynomial and exponential as before yields

$$\begin{aligned}\langle m|\cos k\hat{x}|m+2\rangle = &\frac{-2\chi}{\sqrt{(m+1)(m+2)}}\left(1-\chi+\frac{\chi^2}{2}-\ldots\right)\\ &\times\left[\frac{(m+1)(m+2)}{2}-\frac{m(m+1)(m+2)}{3}\chi+\ldots\right]\end{aligned} \tag{5.49}$$

which can be simplified to give

$$\langle m|\cos k\hat{x}|m+2\rangle = -\sqrt{(m+1)(m+2)}\left[\chi-\left(1+\frac{2m}{3}\right)\chi^2+\mathcal{O}(\chi^3)\right]. \tag{5.50}$$

The approximate expression used for the second off-diagonal matrix elements is

$$\langle m|\left[1-\chi(\hat{a}+\hat{a}^\dagger)^2\right]|m+2\rangle = -\chi\sqrt{(m+1)(m+2)} \tag{5.51}$$

and so the difference between the two is again of order $\chi^2 m^2$. However, the matrix elements themselves are of order χm, and so the fractional error is $\sim \chi m$ – significantly larger than for the diagonal elements.

5.2.3 Evaluation of $\langle m|\sin k\hat{x}|n\rangle$

The matrix elements of $\sin k\hat{x}$ can be evaluated in an identical manner to that outlined above. We arrive at (cf. Eq. (5.39))

$$\langle m|\sin k\hat{x}|n\rangle = \frac{1}{\sqrt{\pi\,2^{m+n}\,m!\,n!}}\int_{-\infty}^{\infty}dy\,\sin\left(k\sqrt{\frac{\hbar}{m\omega_T}}\,y\right)e^{-y^2}H_m(y)\,H_n(y). \tag{5.52}$$

For the integrand of this expression to be even, precisely one of $H_m(y)$ and $H_n(y)$ must be odd; thus we can write

$$\langle m|\sin k\hat{x}|n\rangle = \begin{cases} \text{Eq. (5.52)} & n = m + 2l + 1, \quad l \in \mathbb{Z} \\ 0 & \text{else.} \end{cases} \tag{5.53}$$

To evaluate this expression we require the integral [13]

$$\int_0^\infty \sin(bz)\, e^{-z^2} H_k(z)\, H_{k+2l+1}(z) = (-1)^l 2^{k-1} \sqrt{\pi}\, k!\, b^{2l+1} e^{-\frac{b^2}{4}} L_k^{(2l+1)}\left(\frac{b^2}{2}\right). \tag{5.54}$$

We are only interested in the elements appearing on the first off-diagonal of the matrix. Setting $l = 0$ gives

$$\langle m|\sin k\hat{x}|m+1\rangle = \frac{1}{\sqrt{m+1}}\sqrt{2\chi}\, e^{-\chi} L_m^{(1)}(2\chi) \tag{5.55}$$

which can be expanded to give

$$\begin{aligned} \langle m|\sin k\hat{x}|m+1\rangle &= \frac{1}{\sqrt{m+1}}\sqrt{2\chi}\left(1 - \chi + \frac{\chi^2}{2} - \ldots\right) \\ &\quad \times \left[m + 1 - m(m+1)\chi + \frac{(m-1)m(m+1)}{3}\chi^2 - \ldots\right] \\ &= \sqrt{2\chi}\sqrt{m+1}\Big[1 - (m+1)\chi + \mathcal{O}(\chi^2)\Big]. \end{aligned} \tag{5.56}$$

This matrix element has been approximated by

$$\langle m|k\hat{x}|m+1\rangle = \sqrt{2\chi}\sqrt{m+1}. \tag{5.57}$$

Comparing the two expressions, we find that the difference is of order $(\chi m)^{3/2}$, while the matrix elements themselves are of order $(\chi m)^{1/2}$. The fractional error in the first off-diagonal matrix elements is therefore $\sim \chi m$.

5.2.4 Behaviour of operator moments

In order to determine the effect of the difference between the approximate and exact matrix elements on the numeric solutions, we now turn to a direct comparison of the behaviour of the operator moments for the two cases. Figures 5.6 – 5.8 show the exact and approximate solutions for $\langle\hat{a}\rangle$, $\langle\hat{a}^\dagger\hat{a}\rangle$ and P_+ for the case of $\delta = 0$.

For short times, the exact numeric solutions agree well with the approximate solutions presented in Chapter 3. For longer times, however, the movement of $\langle\hat{a}\rangle$ on the phase plane and the periodic oscillations seen in the average phonon number become progressively smaller, while the revivals in the atomic excitation probability decrease in amplitude, becoming partial rather than complete. Eventually, the

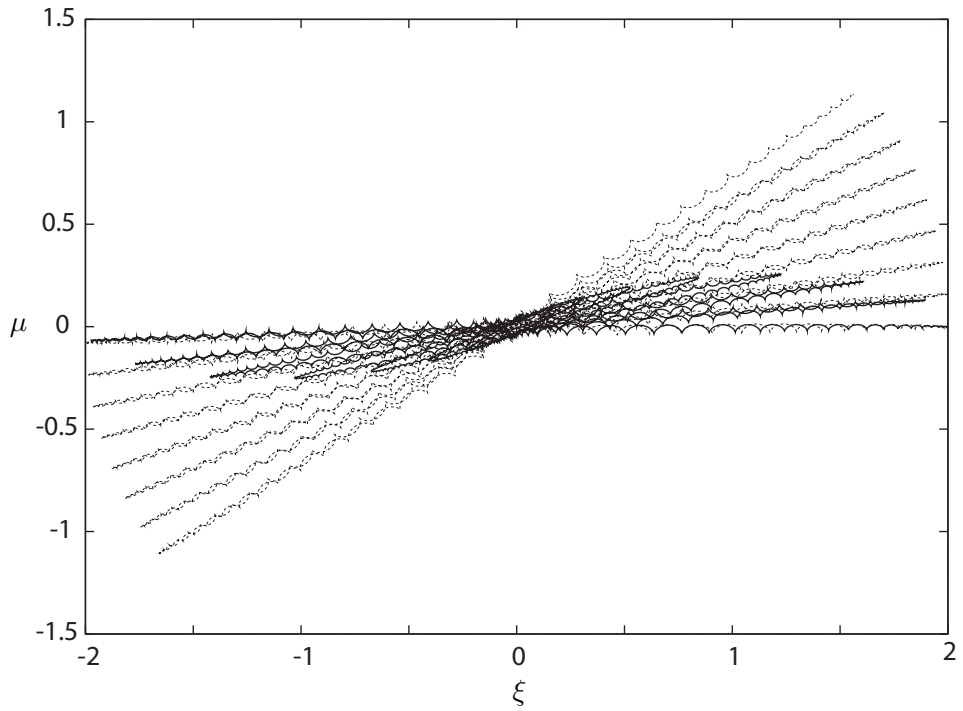

Figure 5.6: A comparison of the exact (solid) and approximate (dotted) solutions for the motion of $\langle \hat{a} \rangle$ on the phase plane. Parameters are $\chi = 0.025$, $\Omega/\omega_T = 1$, $\tau = 0 - 2000$.

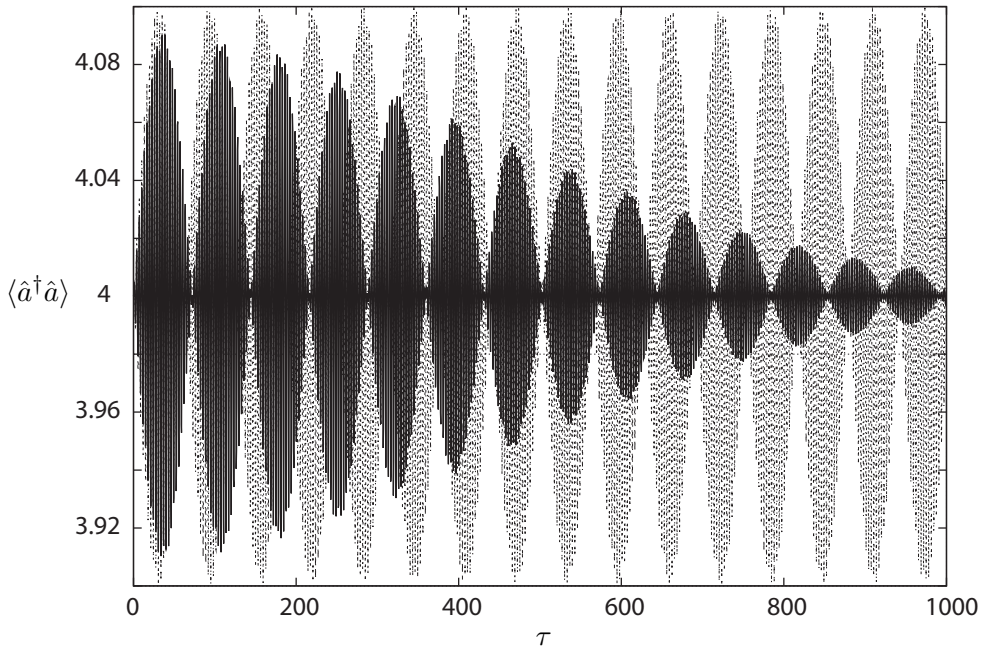

Figure 5.7: A comparison of the exact (solid) and approximate (dotted) solutions for the average phonon number. Parameters are $\chi = 0.025$, $\Omega/\omega_T = 1$.

motion of $\langle \hat{a} \rangle$ on phase plane ceases, the average phonon number stabilises at $|\alpha_0|^2$, and all traces of collapse and revival behaviour disappear from the atomic excitation probability, which instead shows complicated oscillations about the mean value of 0.5.

One approach to understanding this change in behaviour is to consider the Rabi oscillations of the individual number states. If we neglect the effect of the off-diagonal terms (which are smaller by a factor of $\chi\Omega$), we find that the state expansion coefficients $c_n^{\pm}$ execute Rabi oscillations with a frequency which depends on n. As seen earlier, the revivals in the atomic excitation probability can be understood as being caused by the periodic rephasing of the individual Rabi oscillations of the number states, and thus occur every time the difference between two neighbouring Rabi frequencies (i.e. $\chi\Omega$) is an integer multiple of 2π.

In the exact case, the difference between neighbouring diagonal matrix elements (and thus, the spacing of the individual Rabi frequencies) is given by the difference of two Laguerre polynomials multiplied by an exponential (see Eq. (5.43)). The exponential term means that – in contrast to the approximate case – the exact Rabi frequencies are irrational and therefore cannot completely rephase; the revivals seen in the atomic excitation probability thus gradually diminish in amplitude before disappearing altogether. The dynamics seen in the exact solution to the system

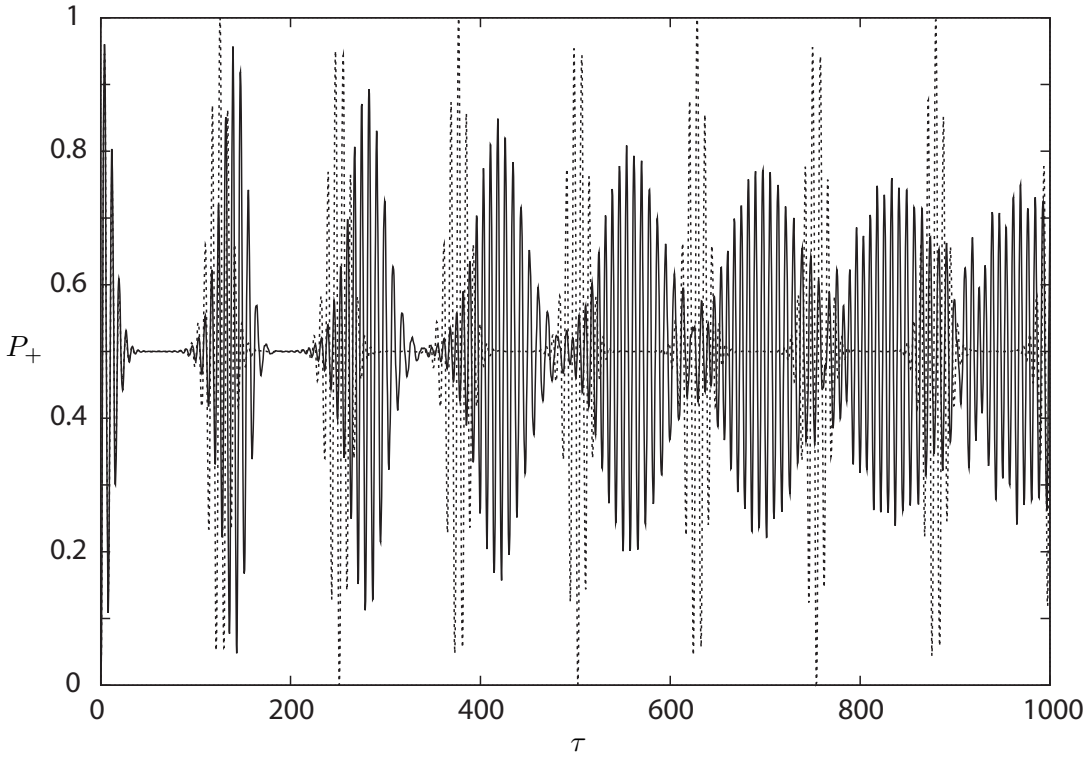

Figure 5.8: A comparison of the exact (solid) and approximate (dotted) solutions for the atomic excitation probability. Note that in the exact solution, the revivals are partial, becoming progressively smaller in amplitude. Parameters are $\chi = 0.025$, $\Omega/\omega_T = 1$.

are more closely related to the Jaynes-Cummings model than to the anharmonic oscillator.

Chapter 6

Conclusion

6.1 Summary

In this thesis we have presented the results of an investigation into the behaviour of a harmonically trapped two-level atom with quantised centre-of-mass motion interacting with a resonant standing wave electromagnetic field.

We investigated numerically the evolution of the motional and internal states of the atom. These numeric solutions showed that the atomic excitation probability exhibited collapse and revival behaviour. The revivals were found to be complete, bearing more resemblance to those appearing in the anharmonic oscillator than those of the Jaynes-Cummings model. We characterised the motional dynamics of the atom by constructing the Q function for the atomic centre-of-mass state and studying the behaviour of the mean atomic position. We found that the coupling of the atom to the electromagnetic field led to a modulation of the amplitude of oscillation of the atom in the trap. Empirical estimates showed that the frequency and amplitude of the modulation were both governed by the dimensionless parameter $\chi\Omega/\omega_T$, where χ is proportional to the Lamb-Dicke parameter, Ω is the Rabi frequency of the two-level atom, and ω_T is the frequency of the harmonic trap.

We then developed an analytic treatment of the system. A change in atomic basis from the energy eigenstates to the atomic dressed states led to the separation of the system Hamiltonian into two pieces, each of which governed the evolution of a single dressed motional state and had the form of a squeezing Hamiltonian. We showed that each piece could be put into a diagonal form by making a Bogoliubov transformation of the ladder operators for the harmonic trap $\hat{a}$ and $\hat{a}^\dagger$, then used these diagonal forms to derive analytic expressions for the operator moments, atomic excitation probability, and Q and Wigner functions for the atomic centre of mass state.

In addition to allowing the derivation of analytic solutions, the diagonalisation of the Hamiltonian proved to be a crucial step in the physical interpretation of the

effect of the atom-field interaction on the system. We used the diagonal form of the Hamiltonian to show that the interaction of the atom with the electromagnetic field produced a shift in the trap oscillation frequency which was dependent on the internal state of the atom. This state-dependent frequency shift was shown to be the root cause of the features seen in the system dynamics.

We then extended the analytic diagonalisation and solution of the system Hamiltonianto to include an arbitrary trap position on the standing wave. The results of this extension showed that as the trap was moved away from the antinode, the squeezing term gradually disappeared from the Hamiltonian and was replaced by a displacement term. Consequently, the state-dependent frequency shift was replaced by a state-dependent trap centre and oscillation amplitude, resulting in the disappearance of much of the interesting behaviour seen in the system dynamics.

We also investigated the effect of retaining some of the higher-order terms that were previously discarded from the Hamiltonian. We found that this 'exact' model initially exhibited qualitatively similar behaviour to the 'approximate' model; however, as time passed, the movement of $\langle \hat{a} \rangle$ on the phase plane ceased and the revivals in the atomic excitation probability became progressively smaller. We showed that this was a result of the higher-order terms making the individual Rabi frequencies irrational (and hence incommensurate) in a similar manner to the Jaynes-Cummings model.

6.2 Future directions

There are a number of directions in which the work presented in this thesis could be profitably extended. One such continuation is to consider the behaviour of the system outside the Lamb-Dicke regime. This was discussed in a limited way in Chapter 5, where we found that the inclusion of two-phonon terms to all orders in the Lamb-Dicke parameter changed the long-time behaviour of the system dynamics.

However, this particular extension is likely to be of interest more for the sake of completeness than for the possibility of discovering anything particularly novel about the system. Since the terms neglected in the treatment of §5.2 are of order η_{LD}^4 and higher, as long as η_{LD} is restricted to physically reasonable values we might expect that, at least for short- and medium- term dynamics, the effect of including further terms would be small and quantitative (for example, minor adjustments to the revival frequency) rather than qualitative.

Another extension of the current model is to allow for a non-zero detuning of the laser from resonance with the atom. In this case, the transformation that removed the time-dependence from the interaction term (cf. Eq. (4.1)) would be such that a

term in $\hat{\sigma}_z$ proportional to the detuning would remain in the Hamiltonian, i.e.

$$\tilde{H} = \hbar\Delta\,\hat{\sigma}_z + \hbar\omega_T\big(\hat{a}^\dagger\hat{a} + \tfrac{1}{2}\big) + \frac{\hbar\Omega}{2}(\hat{\sigma}_+ + \hat{\sigma}_-)\left[1 - \chi(\hat{a} + \hat{a}^\dagger)^2\right]. \tag{6.1}$$

This model could be solved numerically by a similar method to that used in this thesis. Alternatively, an analytical approach could be taken, although any attempt to apply an identical procedure to that used in this thesis is immediately faced with the difficulty that the dressed states (i.e. the interaction-picture eigenstates) of the atom are no longer simply $|U\rangle$ and $|L\rangle$. To find the atomic eigenstates for an arbitrary detuning requires solving the matrix equation

$$\begin{pmatrix} \hbar\omega_T\big(\hat{a}^\dagger\hat{a} + \frac{1}{2}\big) + \hbar\Delta & \frac{\hbar\Omega}{2}\left[1 - \chi(\hat{a} + \hat{a}^\dagger)^2\right] \\ \frac{\hbar\Omega}{2}\left[1 - \chi(\hat{a} + \hat{a}^\dagger)^2\right] & \hbar\omega_T\big(\hat{a}^\dagger\hat{a} + \frac{1}{2}\big) - \hbar\Delta \end{pmatrix} \begin{pmatrix} |\phi_+\rangle \\ |\phi_-\rangle \end{pmatrix} = E_{\text{atom}} \begin{pmatrix} |\phi_+\rangle \\ |\phi_-\rangle \end{pmatrix} \tag{6.2}$$

where the eigenstate has been expanded as $|\phi_+\rangle|+\rangle + |\phi_-\rangle|-\rangle$. Unfortunately, it is not clear from this expression that finding analytic solutions to the model is possible.

An extension which is certainly feasible, however, is to include spontaneous emission by the atom. This model is currently being investigated by our group at the University of Auckland. In this case the coherent evolution of the state vector is sporadically interrupted by 'measurements' corresponding to spontaneous emission events; the effect of each photon emission is to change the momentum of the atom by an amount equal to the photon recoil and reset the atom to the ground state. Since the timing of spontaneous emission events is inherently random, the mathematical language required to describe the system is that of stochastic processes. The system can be investigated numerically by use of a quantum trajectory method, the details of which are described in Ref. [24].

Appendix A

Special Functions

A.1 The Hermite polynomials

The Hermite polynomials are a set of orthogonal polynomials which are important in several areas of physics and mathematics [14]. They can be defined as

$$H_n(x) = (-1)^n e^{x^2} \frac{d^n}{dx^n} e^{-x^2} \tag{A.1}$$

and are orthogonal on the interval $(-\infty, \infty)$ with respect to the weighting function e^{-x^2}:

$$\int_{-\infty}^{\infty} H_m(x) H_n(x)\, e^{-x^2}\, dx = \delta_{m,n}\, 2^n\, n!\, \sqrt{\pi}. \tag{A.2}$$

They satisfy the symmetry condition

$$H_n(-x) = (-1)^n H_n(x) \tag{A.3}$$

and the recursion relation

$$H_{n+1}(x) = 2x\, H_n(x) - 2n\, H_{n-2}(x). \tag{A.4}$$

The first few Hermite polynomials are

$$H_0(x) = 1 \tag{A.5a}$$
$$H_1(x) = 2x \tag{A.5b}$$
$$H_2(x) = 4x^2 - 2 \tag{A.5c}$$
$$H_3(x) = 8x^3 - 12x \tag{A.5d}$$
$$H_4(x) = 16x^4 - 48x^2 + 12. \tag{A.5e}$$

A.2 The Laguerre polynomials

The Laguerre and associated Laguerre polynomials are useful in several areas of physics and appear, for example, in the solution of the Schrödinger equation for the hydrogen atom [15].

A.2.1 Laguerre polynomials

The Laguerre polynomials $L_n(x)$ are solutions to the Laguerre differential equation

$$x\frac{d^2y}{dx^2} + (1-x)\frac{dy}{dx} + ny = 0. \tag{A.6}$$

They can be defined as

$$L_n(x) = \frac{e^x}{n!}\frac{d^n}{dx^n}(x^n e^{-x}). \tag{A.7}$$

and satisfy the recurrence relation

$$(n+1)\,L_{n+1}(x) = (2n+1-x)\,L_n(x) - n\,L_{n-1}(x). \tag{A.8}$$

The first few Laguerre polynomials are

$$L_0(x) = 1 \tag{A.9a}$$
$$L_1(x) = 1 - x \tag{A.9b}$$
$$L_2(x) = \tfrac{1}{2}(2 - 4x + x^2) \tag{A.9c}$$
$$L_3(x) = \tfrac{1}{6}(6 - 18x + 9x^2 - x^3) \tag{A.9d}$$
$$L_4(x) = \tfrac{1}{24}(24 - 96x + 72x^2 - 16x^3 + x^4). \tag{A.9e}$$

A.2.2 Associated Laguerre polynomials

The Laguerre differential equation can be generalised to the *associated* Laguerre differential equation

$$x\frac{d^2y}{dx^2} + (\alpha+1-x)\frac{dy}{dx} + ny = 0. \tag{A.10}$$

The solutions to the associated Laguerre differential equation are known as the associated Laguerre polynomials, $L_n^{(\alpha)}(x)$. The Laguerre polynomials are thus related to the associated Laguerre polynomials by

$$L_n(x) = L_n^{(0)}(x). \tag{A.11}$$

The associated Laguerre polynomials can be defined as

$$L_n^{(\alpha)}(x) = \frac{e^x x^{-\alpha}}{n!}\frac{d^n}{dx^n}(e^{-x}x^{n+\alpha}) \tag{A.12}$$

and are given explicitly by

$$L_n^{(\alpha)}(x) = \sum_{i=0}^{n}\frac{1}{i!}\binom{n+\alpha}{n-i}(-x)^i, \tag{A.13}$$

where $\binom{n+\alpha}{n+i}$ is a binomial coefficient.

They satisfy the recurrence relations

$$L_n^{(\alpha-1)}(x) = L_n^{(\alpha)}(x) - L_{n-1}^{(\alpha)}(x) \tag{A.14a}$$

$$(n+\alpha)\, L_n^{(\alpha-1)}(x) = (n+1)\, L_{n+1}^{(\alpha)}(x) - (n+1-x)\, L_n^{(\alpha)}(x) \tag{A.14b}$$

which together imply

$$(n+1)\, L_{n+1}^{(\alpha)}(x) = (2n+1+\alpha-x)\, L_n^{(\alpha)}(x) - (n+\alpha)\, L_{n-1}^{(\alpha)}(x). \tag{A.14c}$$

The first few associated Laguerre polynomials are

$$L_0^{(\alpha)}(x) = 1 \tag{A.15a}$$

$$L_1^{(\alpha)}(x) = 1 + \alpha - x \tag{A.15b}$$

$$L_2^{(\alpha)}(x) = \tfrac{1}{2}\left[(\alpha+1)(\alpha+2) - 4x + x^2\right] \tag{A.15c}$$

$$L_3^{(\alpha)}(x) = \tfrac{1}{6}\left[(\alpha+1)(\alpha+2)(\alpha+3) - 3(\alpha+2)(\alpha+3)x + 3(\alpha+3)x^2 - x^3\right]. \tag{A.15d}$$

Appendix B

Operator Ordering Relations

In the course of finding analytic solutions for this system it has frequently been necessary to reorder various operator expressions. This section summarises some of the operator relations used in deriving the results presented in Chapter 4. For notational convenience, the operators will be written without hats.

B.1 Preliminaries

The starting point for any discussion of operator ordering is the Baker-Hausdorff expansion [44]:

$$e^{\lambda B} A\, e^{-\lambda B} = \sum_n \frac{\lambda^n}{n!}\, {}^{(n)}[B, A] \tag{B.1}$$

where ${}^{(n)}[B, A]$ denotes the n-fold-nested commutator of B and A. Let us assume the particular case of

$$[A, B] = kA \tag{B.2}$$

and consider the operator product

$$F \equiv e^{\lambda B} A\, e^{-\lambda B}. \tag{B.3}$$

We can apply the Baker-Hausdorff expansion directly, with the n-fold commutator being given by

$${}^{(n)}[B, A] = (-k)^n A; \tag{B.4}$$

thus

$$\begin{aligned} F &= A - \frac{\lambda k}{1!}A + \frac{\lambda^2 k^2}{2!}A - \frac{\lambda^3 k^3}{3!}A + \frac{\lambda^4 k^4}{4!}A - \dots \\ &= A\left(1 - \frac{\lambda k}{1!} + \frac{\lambda^2 k^2}{2!} - \frac{\lambda^3 k^3}{3!} + \frac{\lambda^4 k^4}{4!} - \dots\right) \\ &= A\, e^{-k\lambda}. \end{aligned} \tag{B.5}$$

This is the most direct way of evaluating an operator expression such as Eq. (B.3), and its success relies heavily on both the existence of a simple closed-form expression for the n-fold commutator and the recognition of the ensuing expression as the series representation of one or more common functions. Although in principle the procedure is applicable to the disentangling of any operator expression subject to arbitrary commutation relations, it is clear that in practice the algebra will render intractable all but the simplest cases. It is as well, therefore, to have in our repertoire a more powerful and general technique for evaluating operator expressions. To this end, let us return to the definition of F, Eq. (B.3) – from which it is clear that F is a function of λ – and find the form of this dependence by differentiating:

$$\begin{aligned}\frac{dF}{d\lambda} &= e^{\lambda B} B A\, e^{-\lambda B} - e^{\lambda B} A B\, e^{-\lambda B} \\ &= e^{\lambda B}[B, A] e^{-\lambda B} \\ &= -kF \end{aligned} \tag{B.6}$$

where we have used the commutation relation Eq. (B.2) and the definition of F. Straightforward integration of Eq. (B.6), coupled with the boundary condition $F|_{\lambda=0} = A$, gives the solution directly:

$$F = e^{\lambda B} A\, e^{-\lambda B} = A\, e^{-k\lambda}. \tag{B.7}$$

This technique of differentiation, rearrangement and re-integration is simple and powerful and will serve us well in our foray into the realm of operator disentangling.

B.2 Spin operator disentangling

Consider a set of operators $\sigma_\pm$, σ_z obeying spin commutation relations

$$[\sigma_+, \sigma_-] = \sigma_z \tag{B.8a}$$

$$[\sigma_z, \sigma_\pm] = \pm 2\, \sigma_\pm. \tag{B.8b}$$

These operators need not describe an actual spin system; it only matters that they satisfy the correct commutation relations. In particular, note that we can identify

$$\begin{aligned} -\frac{1}{2} a^2 &\longleftrightarrow \sigma_- \\ \frac{1}{2} a^{\dagger 2} &\longleftrightarrow \sigma_+ \\ a^\dagger a + \tfrac{1}{2} &\longleftrightarrow \sigma_z \end{aligned}$$

which provides the link between the proofs presented here and the operator disentangling relations stated in Chapter 4. Note that σ_z and $\sigma_\pm$ satisfy Eq. (B.2) with $k = \mp 2$, and so

$$e^{\beta\sigma_z} \sigma_\pm\, e^{-\beta\sigma_z} = \sigma_\pm\, e^{\pm 2\beta}. \tag{B.9}$$

Using the technique outlined above, it is simple to show that

$$e^{\alpha\sigma_\pm}\sigma_z\, e^{-\alpha\sigma_\pm} = \sigma_z \mp 2\alpha\sigma_\pm \tag{B.10a}$$

and in a similar fashion we can derive

$$e^{\beta\sigma_\mp}\sigma_\pm\, e^{-\beta\sigma_\mp} = \sigma_\pm \mp \beta\sigma_z - \beta^2\sigma_\mp \tag{B.10b}$$

$$e^{\kappa(\sigma_+ + \sigma_-)}\sigma_-\, e^{-\kappa(\sigma_+ + \sigma_-)} = \tfrac{1}{2}(\sigma_+ + \sigma_-) + \tfrac{1}{2}\sigma_z \sinh 2\kappa - \tfrac{1}{2}(\sigma_+ - \sigma_-)\cosh 2\kappa. \tag{B.10c}$$

The structure of the latter two operator products requires that the second and third derivatives, respectively, be taken. The only departure from the usual procedure imposed by this is the application of extra boundary conditions in order to find the constants of integration.

We are now in a position to prove the main results of this section.

B.2.1 First result

The first result that we have use of is

$$e^{\kappa(\sigma_+ + \sigma_-)} = e^{\sigma_\pm \tanh\kappa}(\cosh\kappa)^{\mp\sigma_z} e^{\sigma_\mp \tanh\kappa}. \tag{B.11}$$

Consider the operator expression $e^{\kappa(\sigma_+ + \sigma_-)}$. We wish to reorder this product so that the σ_+ operators appear to the left of the σ_- operators.[1] Due to the commutation relation given by Eq. (B.8a), this disentangling will produce some σ_z operators along the way; we can therefore write

$$e^{\kappa(\sigma_+ + \sigma_-)} = e^{f(\kappa)\sigma_+} e^{g(\kappa)\sigma_z} e^{h(\kappa)\sigma_-} \tag{B.12}$$

where $f(\kappa)$, $g(\kappa)$ and $h(\kappa)$ are unknown functions of κ. Our goal is to find the particular choice of f, g and h that makes Eq. (B.12) a true statement. We begin by rewriting it as

$$e^{\kappa(\sigma_+ + \sigma_-)} e^{-h(\kappa)\sigma_-} = e^{f(\kappa)\sigma_+} e^{g(\kappa)\sigma_z} \tag{B.13}$$

and differentiating with respect to κ :

$$\frac{d}{d\kappa}\,[\text{L.H.S}] = (\sigma_+ + \sigma_-) e^{\kappa(\sigma_+ + \sigma_-)} e^{-h(\kappa)\sigma_-} - h'(\kappa) e^{\kappa(\sigma_+ + \sigma_-)} \sigma_- e^{-h(\kappa)\sigma_-} \tag{B.14}$$

$$\frac{d}{d\kappa}\,[\text{R.H.S}] = f'(\kappa)\sigma_+ e^{f(\kappa)\sigma_+} e^{g(\kappa)\sigma_z} + g'(\kappa) e^{f(\kappa)\sigma_+} \sigma_z e^{g(\kappa)\sigma_z}. \tag{B.15}$$

[1] A largely identical procedure can, of course, be applied to derive the result for the opposite case.

Using Eq. (B.10) to move the exponentials to the right and gathering like terms yields

$$\frac{d}{d\kappa}\,[\text{L.H.S}] = \left[\sigma_+\left(1-\frac{h'(\kappa)(1-\cosh 2\kappa)}{2}\right)+\sigma_-\left(1-\frac{h'(\kappa)(1+\cosh 2\kappa)}{2}\right) -\sigma_z\frac{h'(\kappa)}{2}\sinh 2\kappa\right]\times e^{\kappa(\sigma_+ +\sigma_-)}e^{-h(\kappa)\sigma_-}$$

$$\frac{d}{d\kappa}\,[\text{R.H.S}] = \left[\sigma_+\big(f'(\kappa)-2g'(\kappa)f(\kappa)\big)+\sigma_z g'(\kappa)\right]\times e^{f(\kappa)\sigma_+}e^{g(\kappa)\sigma_z}$$

To make Eq. (B.12) true, the coefficients of σ_-, σ_+ and σ_z must be equal, implying

$$1-\frac{h'(\kappa)}{2}(1+\cosh 2\kappa)=0 \tag{B.16a}$$

$$1-\frac{h'(\kappa)}{2}(1-\cosh 2\kappa)=f'(\kappa)-2g'(\kappa)f(\kappa) \tag{B.16b}$$

$$-\sinh 2\kappa\frac{h'(\kappa)}{2}=g'(\kappa). \tag{B.16c}$$

With the help of the relation $\cosh 2\kappa + 1 = \operatorname{sech}^2\kappa$, Eq. (B.16a) is trivial to solve, giving

$$h(\kappa)=\tanh\kappa \tag{B.17}$$

where the boundary condition $h(0)=0$ (see Eq. (B.12)) has been applied. Substitution of this result into Eq. (B.16c) and application of the boundary condition $g(0)=0$ gives immediately

$$g(\kappa)=-\ln(\cosh\kappa). \tag{B.18}$$

The differential equation for $f(\kappa)$ is not as straightforward as the other two, but may be solved by the method of integrating factors [16]. Alternatively, a relationship between $f(\kappa)$ and $h(\kappa)$ can be deduced by considering the Hermitian conjugate of Eq. (B.12). Assuming for a moment that κ is real, the operator $e^{\kappa(\sigma_+ +\sigma_-)}$ is Hermitian; equating the right-hand side of Eq. (B.12) and its Hermitian conjugate gives $f(\kappa)=h^*(\kappa)$; thus we find

$$f(\kappa)=\tanh\kappa. \tag{B.19}$$

The assumption that κ is real can be lifted by applying a similar argument to the real and imaginary parts of κ independently, but we need not concern ourselves with this detail here.

B.2.2 Second result

The second result worthy of proof is

$$e^{\kappa\sigma_\pm}\,e^{\lambda\sigma_\mp}=e^{\lambda\sigma_\mp/(1+\kappa\lambda)}\,(1+\kappa\lambda)^{\pm\sigma_z}\,e^{\kappa\sigma_\pm/(1+\kappa\lambda)}. \tag{B.20}$$

Along the same lines as above, let us write

$$e^{\kappa\sigma_+}e^{\lambda\sigma_-} = e^{f(\kappa,\lambda)\sigma_-}e^{g(\kappa,\lambda)\sigma_z}e^{h(\kappa,\lambda)\sigma_+} \tag{B.21}$$

where f, g and h are now functions of both κ and λ. Treating λ as a constant parameter, differentiating with respect to κ and shuffling the exponentials to the right gives

$$\begin{aligned}\frac{d}{d\kappa}\left[\text{L.H.S}\right] &= \left[\sigma_+\left(1-(1+\kappa\lambda)^2\frac{dh}{d\kappa}\right)+\sigma_-\lambda^2\frac{dh}{d\kappa}+\sigma_z\left(\lambda(1+\kappa\lambda)\frac{dh}{d\kappa}\right)\right] \\ &\qquad \times e^{\kappa\sigma_+}e^{\lambda\sigma_-}e^{-h(\kappa,\lambda)\sigma_+} \\ \frac{d}{d\kappa}\left[\text{R.H.S}\right] &= \left[\sigma_-\left(\frac{df}{d\kappa}+2f\frac{dg}{d\kappa}\right)+\sigma_-\frac{dg}{d\kappa}\right]e^{f(\kappa,\lambda)\sigma_-}e^{g(\kappa,\lambda)\sigma_z}.\end{aligned}$$

Equating coefficients of σ_+, σ_- and σ_z gives

$$\frac{dh}{d\kappa} = \frac{1}{(1+\kappa\lambda)^2} \tag{B.22a}$$

$$\frac{dg}{d\kappa} = \lambda(1+\kappa\lambda)\frac{dh}{d\kappa} \tag{B.22b}$$

$$\frac{df}{d\kappa} = \lambda^2\frac{dh}{d\kappa} - 2f\frac{dg}{d\kappa} \tag{B.22c}$$

which, in conjunction with the boundary conditions $f(0,\lambda)=\lambda$, $g(0,\lambda)=h(0,\lambda)=0$, give the solutions

$$f(\kappa,\lambda) = \frac{\lambda}{1+\kappa\lambda} \tag{B.23a}$$

$$g(\kappa,\lambda) = \ln(1+\kappa\lambda) \tag{B.23b}$$

$$h(\kappa,\lambda) = \frac{\kappa}{1+\kappa\lambda}. \tag{B.23c}$$

B.2.3 Third result

The third operator relationship used was

$$\exp\left[\beta\,\hat{a}^\dagger\hat{a}\right] = :\exp\left[\left(e^\beta-1\right)\hat{a}^\dagger\hat{a}\right]: . \tag{B.24}$$

To prove this it is sufficient to show that the expectation value taken with respect to the coherent state $|\alpha\rangle$ is the same on each side. The expectation value of the quantity on the left-hand side is

$$\begin{aligned}\langle\alpha|\exp\left[\beta\,\hat{a}^\dagger\hat{a}\right]\rangle_\alpha &= e^{-|\alpha|^2}\sum_{m,n=0}^{\infty}\frac{\alpha^{*m}\alpha^n}{\sqrt{m!\,n!}}\langle m|\exp\left[\beta\hat{a}^\dagger\hat{a}\right]|n\rangle \\ &= e^{-|\alpha|^2}\sum_{n=0}^{\infty}\frac{|\alpha|^{2n}e^{\beta n}}{n!} \\ &= \exp\left[|\alpha|^2(e^\beta-1)\right].\end{aligned} \tag{B.25}$$

This is identical to the expectation value of the right-hand side of Eq. (B.24) with respect to a coherent state, which completes the proof.

Appendix C

Fourier Transforms

The Fourier transform plays an important role in many branches of science and mathematics and is an indispensable tool of the theoretical physicist, finding applications in areas ranging from optics and signal processing to quantum field theory. This section discusses and summarises some of the properties of the Fourier transform and its discrete counterpart.

The reader is assumed to be familiar with the basic theory of the continuous Fourier transform and only a brief summary of its key properties is given here. On the other hand, the discrete Fourier transform (DFT) is less commonly encountered, and so a derivation of the DFT which highlights its relationship to the continuous Fourier transform is included.

For a comprehensive development of the topics touched on here the reader is referred to the excellent books of Bracewell [22] and Briggs & Henson [23].

C.1 The Fourier transform

The Fourier transform $F(\nu)$ of a function $f(t)$ is defined as

$$F(\nu) = \int_{-\infty}^{\infty} f(t)\, e^{-i2\pi\nu t} dt \tag{C.1}$$

and exists as long as $f(t)$ is *absolutely integrable*, i.e.

$$\int_{-\infty}^{\infty} |f(t)|\, dt < \infty. \tag{C.2}$$

The further condition that $f(t)$ is of *bounded variation* allows $f(t)$ to be recovered via the inverse transform

$$f(t) = \frac{1}{2\pi} \int_{-\infty}^{\infty} F(\nu) e^{i2\pi\nu t} d\nu. \tag{C.3}$$

These conditions may be relaxed somewhat in order to extend the class of functions for which the Fourier transform exists; however the functions encountered in physics are almost invariably mathematically well-behaved and the current conditions will suffice for our purposes.

In the definition Eq. (C.1), t and ν are an example of a conjugate variable pair and show that the transform takes a function from the time domain into the frequency domain. They could equally well be replaced by $\lambda/(2\pi)$ and the wavenumber k, which would give a Fourier transform from the spatial domain into momentum space.

The Fourier transform has many useful properties, a full account of which can be found in Chapter 6 of Bracewell [22]. A selection of a few of the more important ones follows.

Linearity

$$af_1(t) + bf_2(t) \leftrightarrow aF_1(\nu) + bF_2(\nu) a, b \in \mathbb{C} \tag{C.4}$$

Scaling

$$f(at) \leftrightarrow \frac{1}{|a|} F\left(\frac{\nu}{a}\right) a \in \mathbb{R} \tag{C.5}$$

Shift theorem

$$f(t - t_0) \leftrightarrow \exp\left(-i2\pi\nu t_0\right) F(\nu) \tag{C.6}$$

Symmetry

$$\text{If } f(t) \text{ is } \left\{ \begin{array}{c} \text{even} \\ \text{odd} \\ \text{real} \\ \text{imaginary} \end{array} \right\}, \; F(\nu) \text{ is } \left\{ \begin{array}{c} \text{even} \\ \text{odd} \\ \text{hermitian} \\ \text{antihermitian} \end{array} \right\} \tag{C.7}$$

where (anti)hermitian means $F(-\nu) = (-)F^*(\nu)$.

C.2 The discrete Fourier Transform

Given the discrete nature of digital information storage, a numerical implementation of the Fourier transform must deal not with a continuous function $f(t)$, but with a vector consisting of a set of values of the function $f(t)$ at various instants of time. This motivates the definition of the discrete Fourier transform, which we shall explore here as an approximation to the continuous case.

For the purposes of computation, let us assume that $f(t)$ vanishes outside some interval, i.e. $f(t) = 0$ for $|t| > A/2$.[1] Then the Fourier transform of $f(t)$ is given by

$$F(\nu) = \int_{-\frac{A}{2}}^{\frac{A}{2}} f(t)\, e^{-i2\pi\nu t} dt. \tag{C.8}$$

We wish to approximate this integral in order to find a numerical implementation of the Fourier transform. Let us divide the interval of integration up into N pieces of length $\Delta t = A/N$; assuming N is even, this defines a grid of $N+1$ points in the time domain with values $t_n = n\Delta t$ ($n = -N/2, \ldots, N/2$). As long as $f(t)$ is known at the grid points, the integral contained in Eq. (C.8) can be approximated by the trapezoid rule. Defining the integrand

$$g(t) \equiv f(t) e^{-i2\pi\nu t} \tag{C.9}$$

we have

$$F(\nu) = \int_{-\frac{A}{2}}^{\frac{A}{2}} g(t)\, dt \approx \frac{\Delta t}{2} \left[g\left(-\frac{A}{2}\right) + 2 \sum_{n=-\frac{N}{2}+1}^{\frac{N}{2}-1} g(t_n) + g\left(\frac{A}{2}\right) \right]. \tag{C.10}$$

If we add the requirement that $g(-A/2) = g(A/2)$ – trivially fulfilled if we have chosen our interval A such that $f(t)$ vanishes at the boundaries – the approximated integral becomes

$$\begin{aligned} F(\nu) = \int_{-\frac{A}{2}}^{\frac{A}{2}} g(t)\, dt \;&\approx\; \Delta t \sum_{n=-\frac{N}{2}}^{\frac{N}{2}-1} g(t_n) \\ &= \frac{A}{N} \sum_{n=-\frac{N}{2}}^{\frac{N}{2}-1} f(t_n)\, e^{-i2\pi\nu t_n}. \end{aligned} \tag{C.11}$$

Although this approximation to the Fourier transform may be evaluated at any value of ν, the fact that we are working on a discrete grid leads us to choose a specific set of points at which to approximate $F(\nu)$. It makes sense to choose N values of ν, so that a vector of N samples in the time domain is mapped to a vector containing the Fourier transform evaluated at N points in the frequency domain. The question of *which* frequency values to use is intimately related to the structure of the grid on which our function $f(t)$ is defined — namely, a grid extending over $[-A/2, A/2]$ with grid spacing Δt and grid points $t_n = n\Delta t$. Associated with this is a similar grid in frequency space, denoted $[-\Omega/2, \Omega/2]$, with grid spacing $\Delta\nu$ and grid points $\nu_k = k\Delta\nu$, $k = -N/2, \ldots, N/2 - 1$. We wish to find the relationship between the four grid parameters $\Delta t, \Delta\nu, A$ and Ω.

[1] This is a reasonable assumption to make for most physically sensible functions, but see Chapter 2 of Briggs & Henson [23] for further discussion.

The reciprocity relations

Consider the family of sine and cosine waves which have an integer number of periods on $[-A/2, A/2]$ and so fit exactly on the interval in the time domain. The lowest frequency among these is that of the wave with a single period on the interval and a frequency $\nu_{\min} = 1/A$. The frequencies of the other waves will be integer multiples of this fundamental frequency, which makes it the logical choice for the grid spacing in the frequency domain:

$$\Delta\nu = \frac{1}{A}. \tag{C.12}$$

There are N grid points in frequency space, each separated by $\Delta\nu$, and so we find that

$$\Omega = N\Delta\nu = \frac{N}{A} \qquad \text{or} \qquad A\Omega = N. \tag{C.13}$$

We also know that the length of the interval in the time domain is related to the grid spacing by $A = N\Delta t$. Combining this with our knowledge of $\Delta\nu$ gives the relationship between grid spacings in the two domains:

$$\Delta t\Delta\nu = \frac{1}{N}. \tag{C.14}$$

Equations (C.13) and (C.14) constitute the *reciprocity relations*, which describe the inverse relationship between the grid parameters in time and frequency space.

Let us return to the approximation to the Fourier transform described by Eq. (C.11) and evaluate it at the grid points $\nu_k = k\Delta\nu = k/A$. Our new-found knowledge of the reciprocity relations allows us to write

$$t_n\nu_k = (n\Delta t)(k\Delta\nu) = \frac{nk}{N} \tag{C.15}$$

so that the approximation at the frequency grid points $\nu_k = k\Delta\nu$ is given by

$$F(\nu_k) = F\left(\frac{k}{A}\right) \approx \frac{A}{N}\sum_{n=-\frac{N}{2}}^{\frac{N}{2}-1} f(t_n)\, e^{-i2\pi nk/N}. \tag{C.16}$$

Denoting by f_n the sampled values $f(t_n)$, we now define the DFT to be

$$F_k \equiv \frac{1}{N}\sum_{n=-\frac{N}{2}}^{\frac{N}{2}-1} f_n\, e^{-i2\pi nk/N}. \tag{C.17}$$

Thus for any vector of N sampled time values f_n the DFT consists of the N coefficients F_k defined by Eq. (C.17). We can see from Eq. (C.16) that these coefficients are related to the Fourier transform at certain points; in fact

$$F(k\Delta\nu) \approx A\,F_k. \tag{C.18}$$

In general, the properties of the discrete Fourier transform (scaling, shifting, etc.) are of the same form as for the continuous case.

Appendix D

Bogoliubov Transformations

It is sometimes the case that a complicated Hamiltonian can be put into a simpler form by rewriting it in terms of a new set of operators, defined as linear combinations of the old ones. In the case of the harmonic oscillator operators $\hat{a}$ and $\hat{a}^\dagger$, the transformation linking the old and new operators is commonly known as a Bogoliubov transformation [21]. This section presents an outline of a generic Bogoliubov transformation and shows how it can be applied to diagonalise a squeezing Hamiltonian.

D.1 Formalism of the transformation

If we are transforming from $\hat{a}$ and $\hat{a}^\dagger$ to $\hat{b}$ and $\hat{b}^\dagger$, we could write

$$\begin{pmatrix} \hat{b} \\ \hat{b}^\dagger \end{pmatrix} = \begin{pmatrix} \mu & -\nu \\ -\nu^* & \mu^* \end{pmatrix} \begin{pmatrix} \hat{a} \\ \hat{a}^\dagger \end{pmatrix} \tag{D.1}$$

where the negative sign on ν has been included for later convenience. A restriction on μ and ν is enforced by the fact that the new operators must obey the same commutation rules as the old ones; i.e. that the transformation be canonical. This imposes the requirement that

$$\begin{aligned} |\mu|^2 - |\nu|^2 &= 1 \qquad \text{if } [\hat{a}, \hat{a}^\dagger] = 1, \text{ or} \\ |\mu|^2 + |\nu|^2 &= 1 \qquad \text{if } \{\hat{a}, \hat{a}^\dagger\} = 1. \end{aligned}$$

It would appear at first glance that with two complex parameters, each having a magnitude and a phase, we have four free variables. In reality, only two are independently specifiable: the overall phase of $\hat{b}$ and $\hat{b}^\dagger$ is arbitrary, meaning that one of μ or ν can be chosen to be real, while the requirement that the transformation be canonical means that the amplitudes of μ and ν cannot be specified independently. These restrictions can be taken into account by writing

$$\mu = \left\{ \begin{matrix} \cosh x \\ \cos x \end{matrix} \right\}, \qquad \nu = \left\{ \begin{matrix} e^{i\phi} \sinh x \\ e^{i\phi} \sin x \end{matrix} \right\} \tag{D.2}$$

where the top (bottom) line applies when $\hat{b}$ and $\hat{b}^\dagger$ are required to obey bosonic (fermionic) commutation relations. The two free variables are now the argument x of the trigonometric functions and the phase ϕ, and the transformation described by Eq. (D.1) can be written as

$$\begin{pmatrix} \hat{b} \\ \hat{b}^\dagger \end{pmatrix} = \frac{1}{\sqrt{1 \mp |\eta|^2}} \begin{pmatrix} 1 & -\eta \\ -\eta^* & 1 \end{pmatrix} \begin{pmatrix} \hat{a} \\ \hat{a}^\dagger \end{pmatrix} \tag{D.3}$$

where $\eta \equiv e^{i\phi} \tan(\mathrm{h})x$.

As well as simplifying the transformation somewhat, writing μ and ν in terms of trigonometric functions makes explicit the parallel between the squeezing transformation (Eq. (2.62)) and the bosonic case of Eq. (D.1). Comparison of the two gives

$$\hat{b}^{(\dagger)} = S^\dagger(x)\hat{a}^{(\dagger)}S(x); \tag{D.4}$$

in the bosonic case, Bogoliubov transformations are produced by the unitary squeezing operator.

D.2 Diagonalising a squeezing Hamiltonian

A squeezing Hamiltonian has the general form

$$\hat{H} = \hbar\omega(\hat{a}^\dagger\hat{a} + \tfrac{1}{2}) + \hbar g(\hat{a}^2 e^{2i\theta} + \hat{a}^{\dagger 2} e^{-2i\theta}) \tag{D.5}$$

where $\hat{a}$ and $\hat{a}^\dagger$ obey bosonic commutation relations. Since the θ dependence of this Hamiltonian can be removed by making a rotation of the phase space (i.e. by defining $\hat{a}' = \hat{a}\, e^{i\theta}$) we can restrict our solution to the case of $\theta = 0$.

We wish to find operators $\hat{b}$ and $\hat{b}^\dagger$ which make the squeezing Hamiltonian diagonal:

$$\hat{H} = \hbar\omega_b \left(\hat{b}^\dagger\hat{b} + \tfrac{1}{2}\right) \tag{D.6}$$

for some effective mode frequency ω_b. We begin by rescaling the Hamiltonian:

$$\hat{H}' \equiv \frac{\hat{H}}{\hbar\omega} = \hat{a}^\dagger\hat{a} + \tfrac{1}{2} + \lambda(\hat{a}^2 + \hat{a}^{\dagger 2}), \tag{D.7}$$

where $\lambda = g/\omega$. Next, we make use of the transformation relation given by Eq. (D.3) to write

$$\begin{pmatrix} \hat{a} \\ \hat{a}^\dagger \end{pmatrix} = \frac{1}{\sqrt{1 - |\eta|^2}} \begin{pmatrix} 1 & \eta \\ \eta^* & 1 \end{pmatrix} \begin{pmatrix} \hat{b} \\ \hat{b}^\dagger \end{pmatrix}$$

and substitute for $\hat{a}$ and $\hat{a}^\dagger$ in Eq. (D.7), giving

$$\hat{H}' = \frac{1}{1-|\eta|^2}\Big[\left(\hat{b}^\dagger\hat{b}+\tfrac{1}{2}\right)\left(|\eta|^2+2\lambda(\eta+\eta^*)+1\right) + \hat{b}^2\left(\lambda\eta^{*2}+\eta^*+\lambda\right)+\hat{b}^{\dagger 2}\left(\lambda\eta^2+\eta+\lambda\right)\Big]. \tag{D.8}$$

In order for this to be in the diagonal form of Eq. (D.6), we require the quadratic terms in $\hat{b}$ and $\hat{b}^\dagger$ to vanish. This is satisfied by choosing

$$\eta = \eta^* = \frac{-1\pm\chi}{2\lambda}, \tag{D.9}$$

where $\chi \equiv \sqrt{1-4\lambda^2}$. We can now evaluate the remaining term in Eq. (D.8) to find

$$\begin{aligned}\hat{H}' &= \pm\chi\left(\hat{b}^\dagger\hat{b}+\tfrac{1}{2}\right)\\ &= \pm\chi\, S^\dagger(x)\left(\hat{a}^\dagger\hat{a}+\tfrac{1}{2}\right)S(x)\end{aligned} \tag{D.10}$$

where $x = \tanh^{-1}\eta$. The requirement that the Hamiltonian return positive definite values for the energy means that only the upper sign in Eq. (D.9) is physically sensible. Converting back to the original Hamiltonian gives

$$\hat{H} = \sqrt{\omega^2-4g^2}\left(\hat{b}^\dagger\hat{b}+\tfrac{1}{2}\right) \tag{D.11}$$

which is the Hamiltonian for a single-mode harmonic oscillator with effective frequency $\omega_b = \sqrt{\omega^2-4g^2}$.

Appendix E

Aspects of the Numerical Solutions

The numerical solution of the system was carried out using FORTRAN 90. Here we comment on several features of the program used to solve the equations of motion.

E.1 Numerical considerations

Evaluation of exponential terms

Repeatedly calling the intrinsic exponential function is an inefficient way to calculate the values of the exponentials $e^{\pm 2i\tau}$ appearing in the equations of motion Eq. (3.19).These factors can be calculated more efficiently by writing

$$e^{\pm 2i\tau_n} = e^{\pm 2i\tau_{n-1}} \times e^{\pm 2i\Delta\tau},$$

where $\Delta\tau$ is the size of the time step used in the numerical integration, and $\tau_n \equiv n\Delta\tau$ are the discrete times at which the exponentials must be evaluated. The values of the exponentials at successive time steps are thus related by the constant factor $e^{\pm 2i\Delta\tau}$, which need only be calculated once at the beginning of the program. It can then be used to evolve the exponentials through time without calling the exponential function at each time step.

Evaluation of expansion cofficients of the state $|\alpha_0\rangle$

The appearance of $\sqrt{n!}$ in the evaluation of the coherent-state coefficients (see Eq. (3.20)) can pose a numerical problem if the coherent state is of sufficiently large amplitude that high number states are involved in its expansion. If the naïve approach of evaluating $n!$, then finding its square-root is taken, problems with the size of values able to be stored by FORTRAN data types can occur.

This problem can be avoided by defining quantities

$$A_{n,\alpha_0} = \ln\left(\frac{\alpha_0^n}{\sqrt{n!}}\right) \tag{E.1}$$

where $n = 0, 1, 2, \ldots$. These quantities obey the recursion relation

$$A_{n,\alpha_0} = A_{n-1,\alpha_0} + \ln \alpha_0 - \tfrac{1}{2} \ln n, \tag{E.2}$$

with initial condition $A_{0,\alpha_0} = 0$; the A_{n,α_0} can thus be constructed without ever explicitly evaluating the factorials they contain. The state expansion coefficients can then be found as

$$c_{n,\alpha_0} = e^{-\frac{1}{2}|\alpha_0|^2} \exp A_{n,\alpha_0}. \tag{E.3}$$

E.2 Exact matrix elements of $\cos k\hat{x}$ and $\sin k\hat{x}$

In the course of finding the 'exact' solutions presented in §5.2 it was necessary to numerically evaluate matrix elements containing Laguerre polynomials. This section outlines the procedure used to calculate these expressions; in all cases n denotes an integer which ranges from zero to a value determined by the highest number state included in the truncated Fock basis.

E.2.1 Elements of $\cos k\hat{x}$

Diagonal elements

Denoting by D_n the diagonal matrix elements of $\cos k\hat{x}$, we have from Eq. (5.43)

$$D_n = e^{-\chi} L_n(2\chi). \tag{E.4}$$

Since $L_n(2\chi)$ is related to $L_{n-1}(2\chi)$ and $L_{n-2}(2\chi)$ by way of Eq. (A.8), it is easy to show that the D_n are related by

$$D_{n+1} = \frac{2n+1-2\chi}{n+1} D_n - \frac{n}{n+1} D_{n-1}, \tag{E.5}$$

with initial conditions

$$D_0 = e^{-\chi} \tag{E.6a}$$

$$D_1 = (1-2\chi)\, e^{-\chi}. \tag{E.6b}$$

Second off-diagonal elements

Using U_n to denote the second off-diagonal matrix elements of the cosine, we have from Eq. (5.48)

$$U_n = \frac{2\chi}{\sqrt{(n+1)(n+2)}} e^{-\chi} L_n^{(2)}(2\chi). \tag{E.7}$$

By making use of the recursion relation for associated Laguerre polynomials (Eq. (A.14c)), it is easy to show that

$$U_{n+1} = \frac{2n+3-2\chi}{\sqrt{(n+1)(n+3)}} U_n - \sqrt{\frac{n(n+2)}{(n+1)(n+3)}}\, U_{n-1}, \tag{E.8}$$

with initial conditions

$$U_0 = \sqrt{2}\,\chi e^{-\chi} \tag{E.9a}$$

$$U_1 = \sqrt{\frac{2}{3}}\,\chi\, e^{-\chi}(3 - 2\chi). \tag{E.9b}$$

E.2.2 Elements of $\sin k\hat{x}$

We denote by S_n the elements appearing on the first off-diagonal of the matrix representation of $\sin k\hat{x}$. From Eq. (5.55) we have

$$S_n \equiv \sqrt{\frac{2\chi}{n+1}}\, e^{-\chi}\, L_n^{(1)}(2\chi). \tag{E.10}$$

Using the recursion relation given by Eq. (A.14c) we find that the elements S_n obey

$$S_{n+1} = \frac{2(n+1-\chi)}{\sqrt{(n+1)(n+2)}}\, S_n - \sqrt{\frac{n}{n+2}}\, S_{n-1} \tag{E.11}$$

with initial conditions

$$S_0 = \sqrt{2\chi}\, e^{-\chi} \tag{E.12a}$$

$$S_1 = \sqrt{\chi}\, e^{-\chi}(2 - 2\chi). \tag{E.12b}$$

E.3 Wigner function calculation

As mentioned in Chapter 3, the numerical evaluation of the Wigner function was carried out by a Fourier transform method. This method has not previously been used in our group at the University of Auckland, and it is worth summarising the procedure.

We wish to calculate expressions of the form (see Eq. (3.31))

$$W(\xi, \mu) = \int_{-\infty}^{\infty} e^{-i2\pi\mu\zeta}\, \psi^*(\xi - \pi\zeta/2)\, \psi(\xi + \pi\zeta/2)\, d\zeta \tag{E.13}$$

where $\psi(\xi)$ is the wave function of an arbitrary motional state, the expansion coefficients of which in the Fock state basis are known.

E.3.1 Motional state wave functions

The wave function of the motional state is given by

$$\psi(\xi) = \sum_n c_n \psi_n(\xi). \tag{E.14}$$

Here c_n is the expansion coefficient of the n^{th} number state, whose wave function $\psi_n(\xi)$ is given by (cf. Eq. (2.41))

$$\psi_n(\xi) = \frac{1}{\sqrt{2^n\, n!}} \left(\frac{2}{\pi}\right)^{\frac{1}{4}} e^{-\xi^2} H_n(\sqrt{2}\xi). \tag{E.15}$$

With the help of Eq. (A.4), it can be shown that these basis state wave functions satisfy

$$\psi_{n+1}(\xi) = \frac{2\xi}{\sqrt{n+1}}\, \psi_n(\xi) - \sqrt{\frac{n}{n+1}}\, \psi_{n-1}(\xi) \tag{E.16}$$

with initial conditions

$$\psi_0(\xi) = \left(\frac{2}{\pi}\right)^{\frac{1}{4}} e^{-\xi^2} \tag{E.17a}$$

$$\psi_1(\xi) = \left(\frac{2}{\pi}\right)^{\frac{1}{4}} 2\xi\, e^{-\xi^2}. \tag{E.17b}$$

Equations (E.14) and (E.16) can be used to calculate the wave function of the motional state.

E.3.2 Shifting the wave functions

The integrand in Eq. (E.13) contains the product of two wave functions that have been shifted in space. Let us now think about how to construct this product.

For the remainder of this appendix, alphabetical subscripts are to be understood as vector indices; for example, ξ_n means the n^{th} entry of the vector ξ.

We begin by defining vectors ξ, ζ and ψ such that

$$\xi_n = n\Delta\xi \tag{E.18a}$$

$$\zeta_n = n\Delta\zeta \tag{E.18b}$$

$$\psi_n = \psi(\xi)|_{\xi=\xi_n=n\Delta\xi}, \tag{E.18c}$$

where $\psi(\xi)$ is the motional state wave function, and $n = [-N/2, \ldots, N/2-1]$, with N a power of two.

With this discretisation of ξ and ζ, we may write the shifted wave functions appearing in Eq. (E.13) as

$$\psi\left(\xi + \frac{\pi}{2}\zeta\right) = \psi\left(k\Delta\xi + \frac{\pi}{2}n\Delta\zeta\right) \tag{E.19a}$$

$$\psi^*\left(\xi - \frac{\pi}{2}\zeta\right) = \psi^*\left(k\Delta\xi - \frac{\pi}{2}n\Delta\zeta\right) \tag{E.19b}$$

where k and n are varied over the range $[-N/2 : N/2 - 1]$.

Looking at these equations, it is clear that the arguments of the wave functions on the right hand side will not, in general, be a multiple of $\Delta\xi$. This presents a minor problem, as we only have information about the wave function evaluated at integer multiples of $\Delta\xi$; the vector ψ does not contain, for example, $\psi(\xi)|_{\xi=1.2\Delta\xi}$, or $\psi(\xi)|_{\xi=\pi\Delta\xi}$.

This problem may be solved in a number of ways, the simplest and most elegant of which is to impose a constraint on $\Delta\zeta$ that guarantees that the arguments of Eqs. (E.19) evaluate to an integer multiple of $\Delta\xi$. This is achieved by setting

$$\Delta\zeta = \frac{2}{\pi}\,\Delta\xi \tag{E.20}$$

so that

$$\psi\left(k\Delta\xi + \frac{\pi}{2}n\Delta\zeta\right) = \psi\big((k+n)\Delta\xi\big) = \psi_{k+n} \tag{E.21a}$$

$$\psi^*\left(k\Delta\xi - \frac{\pi}{2}n\Delta\zeta\right) = \psi^*\big((k-n)\Delta\xi\big) = \psi^*_{k-n}. \tag{E.21b}$$

When $\Delta\xi$ and $\Delta\zeta$ satisfy Eq. (E.20) the amount by which the wave functions are shifted is always an integer multiple of $\Delta\xi$, and so all the information we need about the shifted wave functions is present in the vector ψ.

E.3.3 The Wigner function as a DFT

Let us define a function $\phi(\xi, \zeta)$ such that

$$\phi(\xi, \zeta) = \psi^*(\xi - \pi\zeta/2)\,\psi(\xi + \pi\zeta/2) \tag{E.22}$$

where ξ and ζ are continuous variables. The Wigner function is the Fourier transform of this function with respect to ζ:

$$W(\xi, \mu) = \int_{-\infty}^{\infty} e^{-i2\pi\mu\zeta}\,\phi(\xi, \zeta)\,d\zeta. \tag{E.23}$$

After discretising ξ and μ, the function ϕ is represented by an $N \times N$ matrix with entries

$$\phi_{k,n} \equiv \phi(\xi, \zeta)|_{\xi=k\Delta\xi, \zeta=n\Delta\zeta}. \tag{E.24}$$

The Wigner function is proportional to the discrete Fourier transform (see §C.2) of this matrix:

$$W_{k,:} = (N\Delta\zeta)\,\mathrm{DFT}\left\{\phi_{k,:}\right\}, \tag{E.25}$$

where $\phi_{k,:}$ means the k^{th} row of ϕ. The Wigner function is an $N \times N$ matrix, with entries

$$W_{k,n} = W(\xi, \mu)|_{\xi=k\Delta\xi,\, \mu=n\Delta\mu} \tag{E.26}$$

where $\Delta\mu$ is given by

$$\Delta\mu = \frac{1}{N\Delta\zeta}. \tag{E.27}$$

E.3.4 Constructing the matrix ϕ

It follows from Eqs. (E.22) and (E.24) that the elements of ϕ are given by

$$\phi_{k,n} = \psi^*_{k-n}\, \psi_{k+n}, \tag{E.28}$$

and so ϕ can be constructed simply by multiplying pairs of elements from the vector ψ. In doing this, however, we must be careful not to overstep the ends of ψ. If we consider constructing ϕ in a row-by-row fashion by fixing k, then the range over which n can be varied is $[-n_{max}, n_{max}]$, with

$$n_{max} = \begin{cases} \frac{N}{2} - |k| & k < 0, \\ \frac{N}{2} - 1 - k & k \geq 0. \end{cases} \tag{E.29}$$

The asymmetry between $k < 0$ and $k \geq 0$ arises the fact that the vector ψ has $N/2$ points to the left of zero, but only $N/2 - 1$ to the right.

Note that this restriction on n means that we have no knowledge of the matrix ϕ outside a diamond-shaped region in the centre. However, this does not pose a problem in practice, since if ξ is chosen in such a way that the wave function ψ goes to zero long before the ends of the vector are reached, we can justifably set all unknown entries in ϕ to zero.

E.3.5 FORTRAN code

The calculation of the Wigner function was carried out by a FORTRAN subroutine, which we include here for completeness. The DFT itself is performed by a function taken from *Numerical Recipes in Fortran 90* [50] called `fourrow_dp`, which in turn requires the `nrtype` and `nrutil` modules.

The subroutine takes two wave functions `psi1` and `psi2`, which are assumed to be defined over `xivec`, and calculates the corresponding Wigner function for each.

```
SUBROUTINE CalculateWignerFn(xivec,muvec,range,psi1,psi2,NumPoints,filename,writerangeX,writerangeP,Wnorm1,Wnorm2)
    IMPLICIT NONE

    INTEGER, INTENT(IN) :: NumPoints
    COMPLEX*16, INTENT(IN), DIMENSION(-NumPoints/2:NumPoints/2-1) :: psi1,psi2
    REAL*8, INTENT(IN) :: writerangeX,writerangeP,range
    REAL*8, INTENT(IN), DIMENSION(-NumPoints/2:NumPoints/2-1) :: xivec,muvec
```

```
    CHARACTER(20), INTENT(IN) :: filename

    COMPLEX*16, DIMENSION(-NumPoints/2:NumPoints/2-1,-NumPoints/2:NumPoints/2-1):: WignerFunction1, WignerFunction2
    COMPLEX*16, DIMENSION(-NumPoints/2:NumPoints/2-1,-NumPoints/2:NumPoints/2-1):: phi11,phi22,swapper
    INTEGER :: k,b,limit
    REAL*8 :: Wnorm1,Wnorm2
    CHARACTER(15) :: fn2

    phi11=0;phi22=0;swapper=0; WignerFunction1=0;WignerFunction2=0; Wnorm1=0;Wnorm2=0;

    fn2=trim(filename)
3   format(100F15.9)
    open(40,status="replace",file=fn2)

    do k=-NumPoints/2,NumPoints/2-1
       if (k<0) then
          limit=NumPoints/2-abs(k)
       else
          limit=NumPoints/2-1-k
       end if

! construct the matrix phi
       do b=-limit,limit
          phi11(k,b)=psi1(k+b)*conjg(psi1(k-b))
          phi22(k,b)=psi2(k+b)*conjg(psi2(k-b))
       end do

    end do

! The NR implementation of the FFT means that to avoid a phase factor appearing
! on the transformed data we must shift out input functions
    swapper(:,-NumPoints/2:-1)=phi11(:,0:NumPoints/2-1)
    swapper(:,0:NumPoints/2-1)=phi11(:,-NumPoints/2:-1)
    phi11=swapper
    swapper(:,-NumPoints/2:-1)=phi22(:,0:NumPoints/2-1)
    swapper(:,0:NumPoints/2-1)=phi22(:,-NumPoints/2:-1)
    phi22=swapper

! Call the FFT algorithm
    CALL fourrow_dp(phi11,-1)
    CALL fourrow_dp(phi22,-1)


    swapper(:,-NumPoints/2:-1)=phi11(:,0:NumPoints/2-1)
    swapper(:,0:NumPoints/2-1)=phi11(:,-NumPoints/2:-1)
    WignerFunction1=swapper*real(range)/NumPoints                  ! Note the extra factor of 1/N appearing here

    swapper(:,-NumPoints/2:-1)=phi22(:,0:NumPoints/2-1)
    swapper(:,0:NumPoints/2-1)=phi22(:,-NumPoints/2:-1)
    WignerFunction2=swapper*real(range)/NumPoints

! Write the Wigner functions to a file
    do k=-NumPoints/2,NumPoints/2-1
       if (abs(xivec(k))<writerangeX) then
          do b=-NumPoints/2,NumPoints/2-1
             if (abs(muvec(b))<writerangeP) then
                write(40,3) xivec(k),muvec(b),WignerFunction1(k,b),WignerFunction2(k,b)
            end if
          end do
          write(40,*)
       end if
    end do

! Check the norm of each Wigner function
    do k=-NumPoints/2,NumPoints/2-1
       do b=-NumPoints/2,NumPoints/2-1
          Wnorm1=Wnorm1+WignerFunction1(k,b)*dxi*dmu
          Wnorm2=Wnorm2+WignerFunction2(k,b)*dxi*dmu
       end do
    end do

    close(40)
  END SUBROUTINE CalculateWignerFn
```

Bibliography

[1] The use of resonant electromagnetic radiation to cool free or trapped atoms is discussed in many places. See, for example, Ref. [69], Ref. [60], or §IV of Ref. [39] for theoretical discussions. References [30] and [46] contain examples of experimental achievements in this area.

[2] The Mathieu differential equation is discussed in §7.6 of Ref. [36].

[3] Floquet theory is discussed in, for example, Chapter IV, §6 of Ref. [35].

[4] This procedure is presented in more detail in, for example, §II.A of Ref. [39].

[5] See, for example, the discussion on p. 76 of Ref. [63].

[6] The Baker-Hausdorff relation can be found on p. 96 of Ref. [53].

[7] This procedure can be found in, for example, Chapter 14 of Ref. [54] or Chapter 5 of Ref. [56].

[8] See, for example, Ref. [54], Chapter 10.

[9] See Ref. [54], §3.1.

[10] The condition for sideband cooling is that the linewidth of the cooling transition be much smaller than the trap frequency [66] [69]. While using a quadrupole transition would relax the requirements on the trap strength, a dipole transition is preferred because each spontaneous emission cycle – and thus the cooling process as a whole – takes place on a much shorter time scale. Working in the Lamb-Dicke regime also substantially improves the selectivity of the transition and reduces the probability that higher motional states will be populated due to the recoil from spontaneous emission events.

[11] The issue of decoherence in quantum computers is discussed in a general context in Ref. [65] and in the context of the trapped ion implementation in Refs. [37] and [49].

[12] See Eq. 7.388.7, Ref. [34].

[13] See Eq. 7.388.6, Ref. [34], and subsequent correction in *Errata for Tables of Integrals, Series and Products, 6^{th} edition*, available in pdf format from http://www.mathtable.com/gr/. The relevant integral is item 242.

[14] See §13.1 of Ref. [17].

[15] See §13.2 of Ref. [17].

[16] See, for example, Ref. [61], §15.2.

[17] Arfken, G. B., and Weber, H. J. *Mathematical Methods for Physicists*, fifth ed. Harcourt/Academic Press, 2001.

[18] Bergquist, J. C., Hulet, R. G., Itano, W. M., and Wineland, D. J. Observation of quantum jumps in a single atom. *Phys. Rev. Lett. 57*, 14 (Oct 1986), 1699–1702.

[19] Bergquist, J. C., Itano, W. M., and Wineland, D. J. Recoilless optical absorption and doppler sidebands of a single trapped ion. *Phys. Rev. A 36*, 1 (Jul 1987), 428–430.

[20] Blatt, R., and Zoller, P. Quantum jumps in atomic systems. *Eur. J. Phys. 9* (1988), 250–256.

[21] Bogoliubov, N. On the theory of superfluidity. *J. Phys. USSR 11*, 1 (1947), 23 – 32. Reprinted in D. Pines, *The Many-Body Problem*, (W. A. Benjamin, New York, 1961), p. 292.

[22] Bracewell, R. N. *The Fourier Transform and Its Applications*, second ed. McGraw-Hill Book Company, 1978.

[23] Briggs, W. L., and Henson, V. E. *The DFT: An Owner's Manual for the Discrete Fourier Transform*. Society for Industrial and Applied Mathematics, 1995.

[24] Carmichael, H. *An Open Systems Approach to Quantum Optics*. Springer-Verlag, 1993.

[25] Cirac, J. I., Blatt, R., Parkins, A. S., and Zoller, P. Preparation of Fock states by observation of quantum jumps in an ion trap. *Phys. Rev. Lett. 70*, 6 (Feb 1993), 762–765.

[26] Cirac, J. I., Blatt, R., Parkins, A. S., and Zoller, P. Quantum collapse and revival in the motion of a single trapped ion. *Phys. Rev. A 49*, 2 (Feb 1994), 1202–1207.

[27] Cirac, J. I., Blatt, R., Zoller, P., and Phillips, W. D. Laser cooling of trapped ions in a standing wave. *Phys. Rev. A 46*, 5 (Sep 1992), 2668–2681.

[28] Cirac, J. I., and Zoller, P. Quantum computations with cold trapped ions. *Phys. Rev. Lett. 74*, 20 (May 1995), 4091–4094.

[29] Cirac, J. I., and Zoller, P. A scalable quantum computer with ions in an array of microtraps. *Nature 404* (2000), 579.

[30] Diedrich, F., Bergquist, J. C., Itano, W. M., and Wineland, D. J. Laser cooling to the zero-point energy of motion. *Phys. Rev. Lett. 62*, 4 (Jan 1989), 403–406.

[31] Gabrielse, G., Dehmelt, H., and Kells, W. Observation of a relativistic, bistable hysteresis in the cyclotron motion of a single electron. *Phys. Rev. Lett. 54*, 6 (Feb 1985), 537–539.

[32] Gerry, C. C., and Grobe, R. Statistical properties of squeezed Kerr states. *Phys. Rev. A 49*, 3 (Mar 1994), 2033–2039.

[33] Ghosh, P. K. *Ion Traps*. Oxford University Press, 1995.

[34] Gradshteyn, I. S., and Ryzhik, I. M. *Table of Integrals, Series and Products*, fourth ed. Academic Press, 1965.

[35] Hartman, P. *Ordinary Differential Equations*. John Wiley & Sons, 1964.

[36] Hille, E. *Lectures on Ordinary Differential Equations*. Addison-Wesley, 1969.

[37] Hughes, R. J., James, D. F. V., Knill, E. H., Laflamme, R., and Petschek, A. G. Decoherence bounds on quantum computation with trapped ions. *Phys. Rev. Lett. 77*, 15 (Oct 1996), 3240–3243.

[38] Klein, H. A., Barwod, G. P., Gill, P., and Huang, G. Single trapped ions for optical frequency standards. *Phys. Script. T86* (2000), 33–37.

[39] Leibfried, D., Blatt, R., Monroe, C., and Wineland, D. Quantum dynamics of single trapped ions. *Reviews of Modern Physics 75*, 1 (2003), 281.

[40] Li, L.-X., and Guo, G.-C. Preparation of motional cat states for trapped ions using a standing wave in strong excitation. *J. Opt. B: Quantum Semiclass Opt. 1* (1999), 339–340.

[41] Liebfried, D., Knill, E., Seidelin, S., Britton, J., Blakestad, R. B., Chiaverini, J., Hume, D. B., Itano, W. M., Jost, J. D., Langer, C., Ozeri, R., Reichle, R., and Wineland, D. J. Creation of a six-atom 'Schrödinger cat' state. *Nature 438* (2005), 639–642.

[42] Lorrain, P., Corson, D. R., and Lorrain, F. *Fundamentals of Electromagnetic Phenomena*. W.H. Freeman and Co., 2000.

[43] Loudon, R. *The Quantum Theory of Light*, second ed. Oxford University Press, Oxford, 1983.

[44] Louisell, W. H. *Quantum Statistical Properties of Radiation.* John Wiley & Sons, New York, 1973.

[45] Monroe, C., Meekhof, D. M., King, B. E., Itano, W. M., and Wineland, D. J. Demonstration of a fundamental quantum logic gate. *Phys. Rev. Lett. 75*, 25 (Dec 1995), 4714–4717.

[46] Monroe, C., Meekhof, D. M., King, B. E., Jefferts, S. R., Itano, W. M., Wineland, D. J., and Gould, P. Resolved-sideband raman cooling of a bound atom to the 3d zero-point energy. *Phys. Rev. Lett. 75*, 22 (Nov 1995), 4011–4014.

[47] Nagourney, W., Sandberg, J., and Dehmelt, H. Shelved optical electron amplifier: Observation of quantum jumps. *Phys. Rev. Lett. 56*, 26 (Jun 1986), 2797–2799.

[48] Paul, W. Electromagnetic traps for charged and neutral particles. *Rev. Mod. Phys. 62*, 3 (Jul 1990), 531–540.

[49] Plenio, M. B., and Knight, P. L. Realistic lower bounds for the factorization time of large numbers on a quantum computer. *Phys. Rev. A 53*, 5 (May 1996), 2986–2990.

[50] Press, W. H., Teukolsky, S. A., Vetterling, W. T., and Flannery, B. P. *Numerical Recipes in Fortran 90.* Cambridge University Press, 1996. `fourrow_dp` taken from Chapter B12; `nrtype` and `nrutil` modules taken from Appendix C1.

[51] Raab, E. L., Prentiss, M., Cable, A., Chu, S., and Pritchard, D. E. Trapping of neutral sodium atoms with radiation pressure. *Phys. Rev. Lett. 59*, 23 (Dec 1987), 2631–2634.

[52] Reichle*et al.*, R. Experimental purification of two-atom entanglement. *Nature 443* (2006), 838–841.

[53] Sakurai, J. J. *Modern Quantum Mechanics.* The Benjamin/Cummings Publishing Company, Inc., 1985.

[54] Schleich, W. P. *Quantum Optics in Phase Space.* Wiley-VCH Berlin, 2001.

[55] Schmidt-Kaler, F., Häffner, H., Riebe, M., Guide, S., Lancaster, G. P. T., Deuschle, T., Becher, C., Roos, C. F., Eschner, J., and Blatt, R. Realization of the Cirac-Zoller controlled-NOT quantum gate. *Nature 422* (2003), 408–411.

[56] Scully, M. O., and Zubairy, M. S. *Quantum Optics.* Cambridge University Press, 1997.

[57] Shore, B. W., and Knight, P. L. Topical review: The Jaynes-Cummings model. *J. Mod. Opt. 40*, 7 (1993), 1195–1238.

[58] Steane, A. The ion trap quantum information processor. *Appl. Phys. B 64* (1997), 623–642.

[59] Steane, A. M., and Lucas, D. M. Quantum computing with trapped ions, atoms and light. *Fortschr. Phys. 48* (2000), 839–858.

[60] Stenholm, S. The semiclassical theory of laser cooling. *Rev. Mod. Phys. 58*, 3 (Jul 1986), 699–739.

[61] Stewart, J. *Calculus*, third ed. Brooks/Cole Publishing Company, 1995.

[62] Thompson, R. Precision measurement aspects of ion traps. *Meas. Sci. Technol. 1*, 2 (1990), 93–105.

[63] Thompson, R. Spectroscopy of trapped ions. *Adv. At. Mol. Phys. 31* (1993), 63–136.

[64] Turchette, Q. A., Wood, C. S., King, B. E., Myatt, C. J., Leibfried, D., Itano, W. M., Monroe, C., and Wineland, D. J. Deterministic entanglement of two trapped ions. *Phys. Rev. Lett. 81*, 17 (Oct 1998), 3631–3634.

[65] Unruh, W. G. Maintaining coherence in quantum computers. *Phys. Rev. A 51*, 2 (Feb 1995), 992–997.

[66] Wineland, D., and Dehmelt, H. Proposed $10^{14}\Delta\nu < \nu$ laser fluorescence spectroscopy on Tl^+ mono-ion oscillator III. *Bull. Am. Phys. Soc. 20* (1975), 637.

[67] Wineland, D. J., Barrett, M., Britton, J., Chiaverini, J., DeMarco, B., Itano, W. M., Jelenković, B., Langer, C., Leibfried, D., Meyer, V., Rosenband, T., and Schätz, T. Quantum information processing with trapped ions. *Phil. Trans. R. Soc. Lond. A 361* (2003), 1349–1361.

[68] Wineland, D. J., Bergquist, J. C., Bollinger, J. J., and Itano, W. M. Quantum effects in measurements on trapped ions. *Phys. Script. T59* (1995), 286–293.

[69] Wineland, D. J., and Itano, W. M. Laser cooling of atoms. *Phys. Rev. A 20*, 4 (Oct 1979), 1521–1540.

[70] Wu, Y., and Yang, X. Jaynes-Cummings model for a trapped ion in any position of a standing wave. *Phys. Rev. Lett. 78*, 16 (Apr 1997), 3086–3088.

[71] Yu, N., Dehmelt, H., and Nagourney, W. Trapped individual ion at absolute zero temperature. *Proc. Natl. Acad. Sci. USA 86* (1989), 5671.

[72] Yurke, B., and Stoler, D. Generating quantum mechanical superpositions of macroscopically distinguishable states via amplitude dispersion. *Phys. Rev. Lett. 57*, 1 (Jul 1986), 13–16.

[73] Zheng, S.-B. A proposal for generating Schrödinger cat states of the motion of a trapped ion. *Phys. Lett. A 245* (1998), 11–13.